PhD-FSTM-2022-120

The Faculty of Science, Technology and Medicine

DISSERTATION

Presented on 21/10/2022 in Luxembourg

to obtain the degree of

DOCTEUR DE L'UNIVERSITE DU LUXEMBOURG
EN INFORMATIQUE

by

Puneeth JUBBA HONNAIAH
Born on 4 July 1990 in Bangalore, India

DEMAND-BASED OPTIMIZATION FOR ADAPTIVE MULTI-BEAM SATELLITE COMMUNICATION SYSTEMS

Dissertation defense committee

Dr. Symeon Chatzinotas, Dissertation Supervisor
Professor and Head of SIGCOM, SnT, University of Luxembourg
Dr. Bhavani Shankar Mysore Rama Rao, Chairman
Assistant Professor, SnT, University of Luxembourg
Dr. Björn Ottersten, Vice Chairman
Professor and Director of SnT, University of Luxembourg
Dr. Jens Krause, Member
Senior Manager, Systems Engineering, SES S.A., Luxembourg
Dr. Laura Cottatellucci, Member
Professor, Friedrich-Alexander Universität, Germany

Demand-based optimization for adaptive multi-beam satellite communication systems

Puneeth Jubba Honnaiah

Abstract

Satellite operators use multiple spot beams of high throughput satellite systems to provide internet services to broadband users. However, in recent years, new mobile broadband users with diverse demand requisites are growing, and satellite operators are obliged to provide services agreed in the Service Level Agreements(SLA) to remote rural locations, mid-air aeroplanes and mid-ocean ships. Furthermore, the expected demand is spatio-temporal which varies along the geographical location of the mobile users with time and hence, creating more dynamic, non uniformly distributed, and time sensitive demand profiles. However, the current satellite systems are only designed to perform similarly irrespective of the changes in demand profiles. Hence, a practical approach to meet such heterogeneous demand is to design adaptive systems by exploiting the advancements in recently developed technologies such as precoding, active antenna array, digital beamforming networks, digital transparent payload and onboard signal processing.

Accordingly, in this work, we investigate and develop advanced demand-based resource optimization modules that fit future payload capabilities and satisfy the satellite operators' interests. Furthermore, instead of boosting the satellite throughput (capacity maximization), the goal is to optimize the available resources such that the satellite offered capacity on the ground continuously matches the geographic distribution of the traffic demand and follows its variations in time. However, we can introduce adaptability at multiple levels of the transmission chain of the satellite system, either with long term flexibility (optimization over frequency, time, power, beam pattern and footprint) or short term flexibility (optimization over user scheduling). These techniques can be optimized as either standalone or in parallel or even jointly for maximum demand satisfaction. However, in the scope of this thesis, we have designed real time optimizations only for some of the radio resource schemes.

Firstly, we explore beam densification, where by increasing the number of beams, we improve the antenna gain values at the high demand hot-spot regions. However, such increase

in the number of beams also increase the interbeam interference and badly affects SINR performance. Hence, in the first part of Chapter 2 of this thesis, we focus on finding an optimal number of beams for given high demand hot-spot region of a demand distribution profile. Also, steering the beams towards high demand regions, further increase the demand satisfaction. However, the positioning of the beams need to be carefully planned. On one hand, closely placed beams result in poor SINR performance. On the other hand, beams that are placed far away will have poor antenna gain values for the users away from the beam centers. Hence, in the second part of Chapter 2, we focus on finding optimized beam positions for maximum demand satisfaction in high demand hot-spot regions. Also, we propose a dynamic frequency-color coding strategy for efficient spectrum and interference management in demand-driven adaptive systems.

Another solution is the proposed so-called Adaptive Multi-beam Pattern and Footprint (AMPF) design, where we fix the number of beams and based on the demand profile, we configure adaptive beam shapes and sizes along with their positions. Such an approach shall distribute the total demand across all the beams more evenly avoiding overloaded or underused beams. Such optimization was attempted in Chapter 3 using cluster analysis.

Furthermore, demand satisfaction at both beam and user level was achieved by carefully performing demand driven user scheduling. On one hand, scheduling most orthogonal users at the same time may yield better capacity but may not provide demand satisfaction. This is majorly because users with high demand need to be scheduled more often in comparison to users with low demand irrespective of channel orthogonality. On the other hand, scheduling users with high demand which are least orthogonal, create strong interbeam interference and affect precoding performance. Accordingly, two demand driven scheduling algorithms (Weighted Semi-orthogonal scheduling (WSOS) and Interference-aware demand-based user scheduling) are discussed in Chapter 4.

Lastly, in Chapter 5, we verified the impact of parallel implementation of two different demand based optimization techniques such as AMPF design and WSOS user scheduling. Evidently, numerical results presented throughout this thesis validate the effectiveness of the proposed demand based optimization techniques in terms of demand matching performance compared to the conventional non-demand based approaches.

Acknowledgements

First and foremost, I would like to begin by thanking all my supervisors and colleagues who have not only enriched me with their knowledge but also inspired me with humility and compassion. Apparently, my PhD journey (shown in Figure 1) resembles a wrongly interpreted curve of the "Dunning-Kruger effect". A special thanks to Dr Nicola Maturo for being patient with me when I was at the peak of "mount stupid". Also, my sincere gratitude to Dr Eva Lagunas, for her excellent guidance. Her continuous supervision and support helped me survive the "valley of despair". Furthermore, I am extremely grateful to my supervisor, Prof. Symeon Chatzinotas, for his excellent technical guidance and timely feedback on my research throughout the course of my PhD journey. Also, I would like to extend my gratitude to Dr. Jens Krause from SES, for his insightful technical guidance.

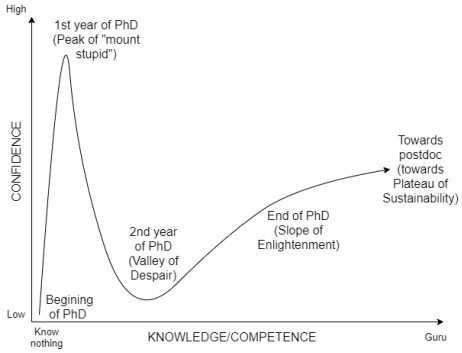

Figure 1: My PhD journey

I would also like to thank Luxembourg National Research Fund (FNR) and SES S.A. for funding my work. Furthermore, my gratitude to European Space Agency (ESA) who generously provided support during the course of my PhD. Last but not least, I would like to thank my family and friends.

Puneeth Jubba Honnaiah

Luxembourg, Sep 2022

Preface

This Ph.D. thesis has been carried out from January 2019 to October 2022, in part at the SIGCOM research group, SnT - Interdisciplinary Centre for Security, Reliability and Trust, University of Luxembourg, under supervision of Prof. Symeon Chatzinotas, Dr. Eva Lagunas, Dr Nicola Maturo and Dr. Jens Krause (SES S.A.). The time-to-time evaluation of the Ph.D. thesis was duly performed by the CET members constituting the supervisors and co-supervisors.

Contents

This Ph.D. thesis entitled "Demand-based optimization for adaptive multi-beam satellite communication systems" is divided into six chapters. In Chapter 1, introduction, background, motivation, dynamic resource management system architecture and contributions of this thesis are described. Chapter 2 provides adaptive dynamic beam densification technique, which discuss the advantages of increasing the number of beams over high demand hot-spot regions. Next, to evenly distribute the total demand among fixed number of beams, an adaptive dynamic beam footprint design methodology using cluster analysis is discussed in Chapters 3. Chapter 4 provides two dynamic user scheduling techniques, firstly the so called weighted semi-orthogonal scheduling (WSOS) and then the interference aware demand based user scheduling, and Chapter 5 discusses a work of parallel implementation of user scheduling and beam designing. Finally, Chapter 6 provides concluding remarks and future work.

Collaborations

This work was made possible from the generous support of European Space Agency (ESA) and SES S.A. However, the views expressed in this work are those of the author and do not reflect the views of European Space Agency (ESA) or of SES S.A.

Support of the Thesis

This work was supported by the Luxembourg National Research Fund (FNR) in the IS - Information and Communication Technologies domain under Industrial Fellowship Scheme (AFR PPP) with industrial partner SES S.A., project title "REGAL- Resource Allocation and IntErference MitiGation for demand based capAcity adaptabiLity in Satellite Communication System," grant FNR14147087. The effort of collaborators and dissemination costs were supported by other projects, namely, the FNR FlexSAT (C19/IS/13696663) and, DISBuS. Additionally, the substantial support from SIGCOM is also gratefully acknowledged.

Declaration

Except where acknowledged in the customary manner, the material presented in this thesis is, to the best of the authors knowledge, original and has not been submitted in whole or part for a degree in any university.

Publication List

Journals

[I] P. J. Honnaiah, N. Maturo, S. Chatzinotas, S. Kisseleff and J. Krause, "Demand-Based Adaptive Multi-Beam Pattern and Footprint Planning for High Throughput GEO Satellite Systems," *in IEEE Open Journal of the Communications Society,* vol. 2, pp. 1526-1540, 2021, doi: 10.1109/OJCOMS.2021.3093106.

[II] P. J. Honnaiah, E. Lagunas, S. Chatzinotas and J. Krause, "Interference-Aware Demand-Based User Scheduling in Precoded High Throughput Satellite Systems," in *IEEE Open Journal of Vehicular Technology,* vol. 3, pp. 120-137, 2022, doi: 10.1109/OJVT.2022.3161621.

[III] P. J. Honnaiah, E. Lagunas, S. Chatzinotas and J. Krause, "Opportunistic beam densification in Multi-Beam Satellite Communication Systems," *IEEE Transactions on Aerospace and Electronic Systems* - submitted

Conference/Workshop Papers

[IV] P. J. Honnaiah, E. Lagunas, D. Spano, N. Maturo and S. Chatzinotas, "Demand-based Scheduling for Precoded Multibeam High-Throughput Satellite Systems," *2021 IEEE Wireless Communications and Networking Conference (WCNC),* 2021, pp. 1-6, doi: 10.1109/WCNC49053.2021.9417300.

[V] P. J. Honnaiah, E. Lagunas, N. Maturo and S. Chatzinotas, "Demand-Aware Beam Design and User Scheduling for Precoded Multibeam GEO Satellite Systems," *WSA 2021; 25th International ITG Workshop on Smart Antennas,* 2021, pp. 1-6. doi: https://ieeexplore.ieee.org/document/9739195

[VI] P. Jubba Honnaiah, E. Lagunas, N. Maturo and S. Chatzinotas, "Clustering-based Adaptive Beam Footprint Design for 5G Urban Macro-Cell," *2021 IEEE 4th 5G World Forum (5GWF)*, 2021, pp. 24-29, doi: 10.1109/5GWF52925.2021.00012.

[VII] P. J. Honnaiah, N. Maturo and S. Chatzinotas, "Foreseeing Semi-Persistent Scheduling in Mode-4 for 5G enhanced V2X communication," *2020 IEEE 17th Annual Consumer Communications & Networking Conference (CCNC)*, 2020, pp. 1-2, doi: 10.1109/CCNC46108.2020.9045276.

[VIII] P. J. Honnaiah, E. Lagunas, S. Chatzinotas and J. Krause, "Satellite Beam Densification for High-Demand Areas," *11th Advanced Satellite Multimedia Systems Conference and the 17th Signal Processing for Space Communications Workshop*, 2022.

Contents

1 Introduction **1**

1.1 Background . . . 2

1.2 Motivation . . . 4

1.3 Satellite Dynamic Resource Management systems . . . 6

1.3.1 Protocol stack Architecture . . . 7

1.3.2 Key enabling technologies for demand driven adaptability . . . 7

1.4 Demand driven adaptability using real time optimization modules . . . 9

1.4.1 Long term flexibility . . . 9

1.4.2 Short term flexibility . . . 13

1.5 Contributions . . . 13

2 Demand driven beam densification **17**

2.1 Introduction . . . 17

2.1.1 Trends in On-board Antenna Architectures . . . 19

2.1.2 Related works . . . 19

2.1.3 Contributions . . . 21

2.2 System Model . . . 23

2.3 Opportunistic Regular Beam Densification . . . 26

2.4 Dynamic beam densification . . . 29

2.4.1 Determining the number of beams . . . 29

2.4.2 Determining beam placement . . . 31

2.5 Dynamic frequency reusing scheme . . . 33

2.5.1 Graph construction . . . 33

2.5.2 Optimized color coding . . . 35

2.6 Simulation parameters and results . . . 37

2.6.1 Beam pattern analysis . . . 38
2.6.2 Impact of densification with 4 color frequency reuse . . . 40
2.6.3 Impact of densification with full frequency reuse and precoding . . . 41
2.6.4 Impact of densification with Dynamic frequency reuse . . . 46
2.6.5 Performance evaluation neighbouring beams of densification . . . 49
2.7 Conclusion . . . 50
2.8 Acknowledgement . . . 51

3 Clustering based beam footprint design **52**
3.1 Introduction . . . 52
3.1.1 Literature Review . . . 52
3.1.2 Contribution . . . 54
3.2 System Model . . . 56
3.2.1 Multi-beam Satellite System . . . 56
3.2.2 Beam Footprint and Beam Pattern . . . 56
3.2.3 Multi-beam Satellite Channel . . . 58
3.3 Problem Statement . . . 58
3.4 Proposed Solution . . . 62
3.4.1 Domain Transformation . . . 63
3.4.2 Clustering of distributed users . . . 65
3.4.3 Voronoi Tessellation . . . 68
3.4.4 Elliptic approximation . . . 69
3.4.5 Antenna gain calculation . . . 72
3.5 Simulation and Results . . . 75
3.5.1 Data Set Model and link budget . . . 75
3.5.2 Numerical Results . . . 76
3.6 Conclusion . . . 82

4 Demand Driven Adaptive User Scheduling **83**
4.1 Weighted Semi-orthogonal Scheduling . . . 83
4.1.1 Introduction . . . 83
4.1.2 System Model . . . 85
4.1.3 Proposed Demand-based Scheduling . . . 88

4.1.4 Simulation and result analysis . . . 90
4.1.5 Conclusions and Future Work . . . 94
4.2 Interference-aware Demand-based User Scheduling . . . 95
4.2.1 Introduction . . . 95
4.2.2 System Model . . . 100
4.2.3 Generalized Scheduling Problem Statement . . . 107
4.2.4 Interference-aware demand-based user scheduling . . . 108
4.2.5 Simulation and Results . . . 116
4.2.6 Conclusion . . . 126

5 Parallel implementation of beam design and user scheduling 127
5.1 Introduction . . . 127
5.2 System Model . . . 128
5.3 Problem Statement and Proposed Solution . . . 130
5.3.1 Demand-Aware Beam Design . . . 130
5.3.2 Demand-Aware User Scheduling . . . 133
5.4 Numerical Evaluation . . . 136
5.4.1 Simulation Parameters . . . 136
5.4.2 Beam level Demand Satisfaction . . . 136
5.4.3 User level Demand Satisfaction . . . 137
5.5 Conclusion . . . 139

6 Conclusion and Further Work 140
6.1 Conclusion . . . 140
6.2 Future work . . . 141

Bibliography 144

List of Figures

1 My PhD journey vii

1.1 Typical end to end satellite communication system 2
1.2 Satellite frequency bands 3
1.3 (a)conventional contoured beam antenna, and (b) multiple beam antennas (X-axis: Azimuth & Y-axis: Elevation) [16]. 4
1.4 Demand profile at 00:00 hr 5
1.5 Demand profile at 04:00 hr 5
1.6 Demand profile at 17:00 hr 5
1.7 Demand profile at 20:00 hr 5
1.8 Adaptive multibeam satellite system Architecture with Satellite Dynamic Resource Management (SDRM) system 6
1.9 Satellite protocol stack with real time optimization techniques 8
1.10 dynamic beam densification 11
1.11 dynamic beam footprint design 11

2.1 Demand distribution at 12 PM EST. 18
2.2 Beam densification in terrestrial network and satellite network 18
2.3 Regular Beam Densification in the high demand region by replacing one beam with four beams increases inter-beam interference. 27
2.4 Beams 3, 7, 6 and 10 are the beams in the centre of Europe and with high demand 27
2.5 Regular beam densification, where 4 beams are replaced by 16 beams 28
2.6 Demand driven beam densification where the 4 beams are replaced by 13 beams 28
2.7 Uneven demand distribution at the densified region 29
2.8 Finding optimal number of beams 32

2.9 Non densified 14 beams to the left and densified 26 beams to the right 34
2.10 Graph representing non densified 14 beams on the left and graph representing densified 26 beams on the right 34
2.11 Graph obtained from the adjacency matrix to the beams in Figure 1. 36
2.12 Antenna Gain of non densified beams 38
2.13 Improved antenna gain by regularly densified 16 beams 39
2.14 Improved antenna gain by demand driven densified 13 beams 39
2.15 Beam Pattern gain after densification 39
2.16 SINR performance at densified area for 4CR frequency reuse 41
2.17 SINR performance at densified area for 4CR frequency reuse 42
2.18 Capacity performance based on DVB-S2X at densified area for 4CR frequency reuse 42
2.19 Mean capacity performance based on DVB-S2X at densified area for 4CR frequency reuse 42
2.20 System (sum) capacity performance based on DVB-S2X at densified area for 4CR frequency reuse 43
2.21 Demand satisfaction with 4CR frequency reuse 43
2.22 SINR performance of Precoding with FFR 43
2.23 SINR performance at densified area for full frequency reuse 44
2.24 Capacity performance based on DVB-S2X at densified area for full frequency reuse 44
2.25 Mean capacity performance based on DVB-S2X at densified area for full frequency reuse 44
2.26 System (sum) capacity performance based on DVB-S2X at densified area for full frequency reuse 45
2.27 Demand satisfaction with full frequency reuse 45
2.28 SINR performance at densified area for DFR frequency reuse 45
2.29 SINR performance at densified area for DFR frequency reuse 46
2.30 Capacity performance based on DVB-S2X at densified area for Dynamic frequency reuse 47
2.31 Mean capacity performance based on DVB-S2X at densified area for dynamic frequency reuse 47

2.32 System (sum) capacity performance based on DVB-S2X at densified area for dynamic frequency reuse 47
2.33 Demand satisfaction with dynamic frequency reuse 48
2.34 CDF plots of per beam avg SNIR on neighbouring beams 49
2.35 Average user SINR on neighbouring beams 49
2.36 Average user SINR on neighbouring beams 50

3.1 High throughput Multi-beam Satellite System architecture using four colour scheme. 55
3.2 Two-dimensional Gaussian function approximation to define the beam pattern 57
3.3 Benchmark FMPF plan beam footprint over Europe using 71 Fixed Beams showing flight user locations in blue, ship user locations in red and FSS user locations in beige. 59
3.4 Sampled coverage area of the benchmark FMPF beams (shown in blue) and the user positions (shown in red) on the surface of the Earth. 63
3.5 Difference between Earth's latitude-longitude domain and satellite angular domain. Latitude, longitude, elevation and azimuth angles are in degrees. 64
3.6 Sampled coverage area of the benchmark FMPF beams (shown in blue) and the user positions (shown in red) in satellite angular domain 66
3.7 Beam boundaries (shown using green convex polygons) defined by Voronoi Tessellations in satellite angular domain. Sampled coverage area is shown in blue and the user positions are shown in red 68
3.8 Beam Footprint as ellipses (shown using green) over Europe using 71 Adaptive Beams in satellite angular domain. Sampled coverage area is shown in blue and the user positions are shown in red 70
3.9 Projection of 71 ellipses (shown in red) on the surface of the Earth over Europe 72
3.10 Antenna pattern of FMPF plan where the colour bar represents Antenna gain values on the surface of the Earth. 72
3.11 Antenna pattern of FMPF plan where the colour bar represents Antenna gain values on the satellite angular domain. 73
3.12 Antenna pattern of proposed AMPF plan where the colour bar represents Antenna gain values on the satellite angular domain. 73

3.13 Antenna pattern of proposed AMPF plan where the colour bar represents Antenna gain values on the surface of the Earth. 74
3.14 Empirical Cumulative Distribution Function (CDF) showing the system demand distribution across all the beams 77
3.15 Jain's Fairness Index ($\mathfrak{J}$) at different time stamps of a day. 78
3.16 Throughput demand requested and offered throughput to any user in the benchmark FMPF plan beams. 79
3.17 Throughput demand requested and offered throughput to any user in the proposed AMPF plan beams. 80
3.18 Normalized Capacity Deviation (NCD) in percentage at different time stamps of a day. 81

4.1 System Architecture: Multibeam High Throughput-Satellite System with four colour scheme 85
4.2 System Architecture: Precoded Multibeam High Throughput-Satellite System 86
4.3 Considered beam cluster, with users' positions considered for scheduling. . . . 91
4.4 Per-beam Average User Rate vs. Average Demand 93
4.5 Per-user Rate vs. Demand 93
4.6 High throughput multi-beam satellite high-level system architecture. 98
4.7 Footprint over Europe using 71 Fixed Beams showing flight user locations in blue, ship user locations in red and FSS user locations in beige. 101
4.8 Different user-beam association scenarios 104
4.9 Shared user at overlapping region of two beams can be scheduled more often by either of the two beams 104
4.10 Scheduling model 105
4.11 Steps involved in interference-aware demand-based user scheduling. 109
4.12 System model of 6 beams, where each beam is divided into 6 sectors. 110
4.13 Graph Model of the system model in Figure 4.12 111
4.14 Example of edge pruning 112
4.15 Class scheduling model 114
4.16 Comparison between different demand distribution profiles 119
4.17 Results for moderately uniform demand distribution 121
4.18 Results for nonuniform demand distribution 123

4.19 Empirical Cumulative Distribution Function (eCDF) for 100 different demand distribution profiles . . . 124
4.20 Run-time complexity Analysis. . . . 125
4.21 Shared user positions. . . . 125
4.22 Improved demand satisfaction of shared users. . . . 125

5.1 GEO multibeam system architecture including beam design, user scheduling and precoding. . . . 128
5.2 Fixed Beam Footprint . . . 131
5.3 Demand-Aware Adaptive Beam Footprint . . . 134
5.4 Beam-level Demand Satisfaction . . . 137
5.5 Demand Distribution across all 6 beams . . . 138
5.6 User-level Demand Satisfaction . . . 138

List of Tables

2.1 Simulation Parameters 38
2.2 Power and Bandwidth allocation for 4CR frequency reuse 40
2.3 Power and Bandwidth allocation for dynamic frequency reuse 48

3.1 Table Of Acronyms 53
3.2 Simulation Parameters 75

4.1 Simulation Parameters 92
4.2 Sum rate and Jain's fairness index of users' satisfaction for the considered scheduling schemes, with Priority update based on average offered rate. . . . 94
4.3 Class Definition using sectors 111
4.4 Simulation Parameters 117

5.1 Cases evaluated 135
5.2 Simulation Parameters 136

Abbreviations

4CR	Four color Reuse
5G	Fifth Generation of Mobile Communications
AMPF	Adaptive Multi-beam Pattern and Footprint
ACM	Adaptive Coding and Modulation
ACTS	Advanced Communications Technology Satellite
AFR	Array-Fed Reflector
AFR	Array Fed Reflector
ADCs	Analog to Digital Converters
AG	Antenna Gain
BH	Beam Hopping
CLARA	ClusteringLARge Applications
CDF	Cumulative Distribution Function
CH	Calinski-Harabasz
CPA	Carrier and Power Allocation
CSI	Channel State Information
CA	Carrier Aggregation,
CDF	Cumulative Distribution Function
DRA	Direct Radiating Antenna
DTP	Digital Transparent Payload
DBN	Digital Beamforming Networks
DM	Distance Metric
DBS	Demand Based Scheduling
DL	Deep Learning
DACs	Digital to Analog Converters
DVB	Digital Video Broadcasting

DPC	Dirty Paper Coding
ESA	European Space Agency
FD	Flux Density
FMPF	Fixed Multi-beam Pattern and Footprint
FSS	Fixed Satellite Sevices
FSPL	Free-Space Path Loss
FDMA	Frequency Division Multiple Access
FFR	Full Frequency Reuse
FAFRs	Focal Array Fed Reflectors
GEO	Geostationary Earth Orbit
GPS	Global Positioning System
HTS	High Throughput Satellite
IoT	Internet of Things
LHCP	Left-Handed Circular Polarization
LEO	Low Earth Orbit
LOS	Line of Sight
MEO	Medium Earth Orbit
MMSE	Minimum Mean Square Error
MFPB	Multi-Feed Per beam
NOC	Network Operational Cente
NCD	Normalized Capacity Deviation
NGSO	Non-geostationary Orbit
ODP	Onboard Digital Processing
PAM	Partitioning Around Medoids
QoS	Quality of service
RHCP	Right-Handed Circular Polarization
SCIP	Solving Constraint Integer Programs
SatCom	Satellite Communications
SFPB	Single-Feed Per Beam
SLA	Service Level Agreement
SOS	Semi-Orthogonal Scheduling
SDMA	Space Division Multiple Access

SOC	Satellite Operational Center
SINR	Signal-to-Interference-plus-Noise Ratio
SDRM	Satellite Dynamic Resource Management
SMAC	Satellite Medium Access Control
SOTA	State Of The Art
TT&C	Tracking, Telemetry, and Command system
TDMA	Time Division Multiple Access
TRU	Total Resource Utilization
VHTS	Very High Throughput Satellite
WCH	Weighted Calinski-Harabasz
WED	Weighted Euclidean Distance
WSOS	Weighted Semi-Orthogonal Scheduling

Notations

$\log(z)$	The natural logarithm of z.
e^z	Exponential function of z.
$\mathbb{E}[\cdot]$	Expected value.
$\boldsymbol{b}^{\mathbf{T}}, \boldsymbol{B}^{\mathbf{T}}$	Transpose of vector $\boldsymbol{b}$, transpose of matrix $\boldsymbol{B}$.
$\boldsymbol{b}^{\mathbf{H}}, \boldsymbol{B}^{\mathbf{H}}$	Conjugate transpose of vector $\boldsymbol{b}$, Conjugate transpose of matrix $\boldsymbol{B}$.
$\text{diag}(\boldsymbol{b})$	Diagonal matrix of vector $\boldsymbol{b}$.
$\text{Trace}\{\boldsymbol{B}\}$	The sum of elements on the main diagonal of the square matrix $\boldsymbol{B}$.
$\lvert z\rvert$, $\lvert\mathcal{Z}\rvert$	The absolute value of z, cardinality of set $\mathcal{Z}$.
$\lVert\boldsymbol{b}\rVert$	The norm of vector $\boldsymbol{b}$.
max	Maximum operation.
min	Minimum operation.
$z \in \mathcal{Z}$	Element z belongs to set $\mathcal{Z}$.
$\mathcal{Z} \setminus \mathcal{Q}$	Set $\mathcal{Z}$ excluding elements in $\mathcal{Q}$.
$\mathcal{Z} \cup \mathcal{Q}$	Union of set $\mathcal{Z}$ and set $\mathcal{Q}$.
$\mathbb{C}, \mathbb{C}^{n\times m}$	Set of complex values, set of $n \times m$ matrices with complex-valued entries.
$\circ$	Element-wise Hadamard operations
$(\cdot)^T$	Transpose of $(\cdot)$
$\mathcal{Z} \subseteq \mathcal{Q}$	Set $\mathcal{Z}$ is a subset of $\mathcal{Q}$.
$P(.)$	Power set

Chapter 1

Introduction

For over five decades, satellite companies such as SES S.A. have generated major revenue from television broadcasting using communication satellites. However, since the introduction of the internet, social media interactive technologies have enabled people to create, interact and share information in virtual communities leading to the shift in demand from television broadcast to internet broadband services. Furthermore, the on-demand entertainment industry further declined the popularity of television broadcasting. Hence, satellite companies are moving from broadcast to broadband services and thus have enabled internet using the multi-beam high throughput satellite systems [1].

Furthermore, the demand for broadband services is evolving dynamically such that the user demand is spatio-temporal with more mobile users [2, 3]. On one hand, this results in non-uniformly distributed demand profiles with high and low demand spot regions with different demand requirements [4]. On the other hand, due to mobile nature of the users, the demand profiles continue to change rapidly [5].

However, the previous generation multi-beam high throughput satellite systems, were only designed to provide same performance across the coverage region for the whole life cycle of the satellite. Hence, to introduce adaptability, efforts have been made to develop Satellite Dynamic Resource Management (SDRM) systems [6]. Effectively, flexible active antenna techniques are used to implement Digital Beamforming Networks (DBN) which enables to implement digitally steerable beams. Also, re-programmable and flexible telecommunication payloads with high speed processing capabilities are used to develop Digital Transparent Payloads (DTP) [7]. Furthermore, precoding acts as an effective interference mitigation tool [8]. Hence, such key enabling technologies have provided a platform to implement real

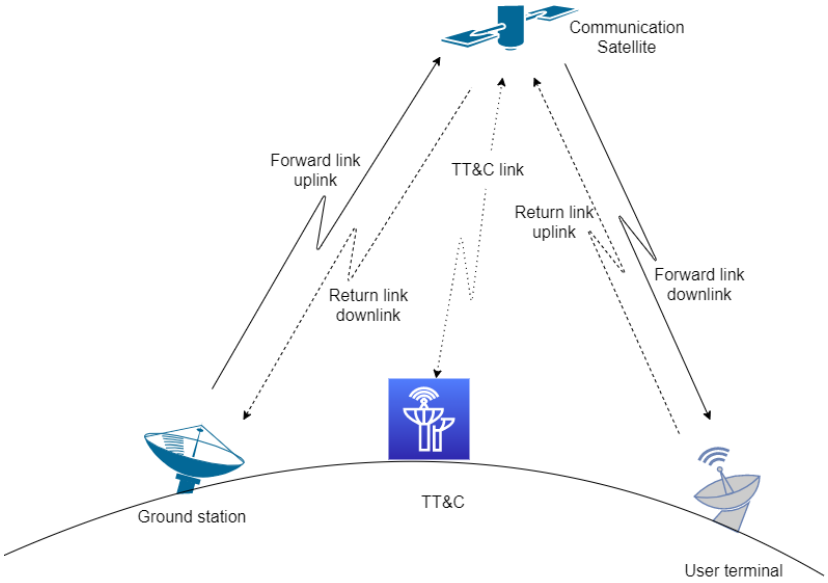

Figure 1.1: Typical end to end satellite communication system

time optimization modules in satellite communication mainly to obtain demand satisfaction.

1.1 Background

A communication satellite receives radio telecommunication signals from a transmitter (source) and relays it to receiver (destination) on a satellite communication channel. Such satellites are of great importance as they make it possible to connect terminals separated by large distances on the surface of the earth. Since its invention, communication satellites are widely used in television broadcasting, telephone, radio broadcasting, internet broadband, and military applications [9].

A typical end to end satellite communication system is shown in the Figure 1.1 includes a large ground station (gateway), communication satellite (space segment) and user terminals [10]. Ground stations are terrestrial radio stations typically connected to local area network or to the internet and are typically operated by satellite service providers. The space segment or satellites are placed in specified orbits. Based on the distance from the surface of the Earth, the orbits are named as geostationary orbit (GEO), Medium Earth Orbit (MEO) or Low Earth Orbit (LEO). The user terminals typically consists of an outdoor unit (satellite dish) and indoor unit (processing unit). Forward link indicate that the direction of transmission is from gateway to user terminals and return link indicate that the direction of transmission is

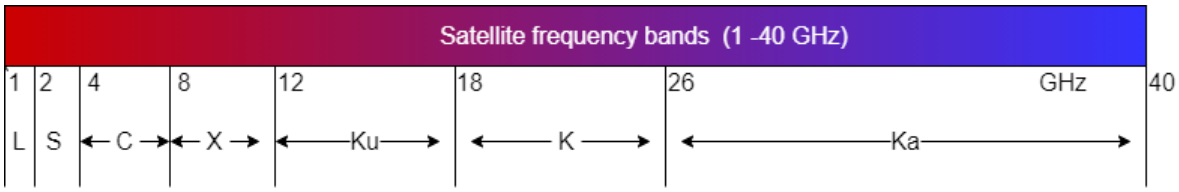

Figure 1.2: Satellite frequency bands

from user terminals to gateway. Often times telemetry, tracking and commanding (TT&C) operations are carried by the gateway. However, in multiple other occasions, a separate TT&C stations are used. The link connecting the TT&C stations and the satellite is termed as TT&C link. The physical and data link layer of terminal and space segments, along with the air interface consisting of forward, return and TT&C links are standardized by a set of international open standards for digital television known as DVB [11].

The satellite systems transmit radio telecommunication signals using frequencies from the satellite frequency bands shown in Figure 1.2 and at which both the radio transmitters and receivers operate [12]. The higher frequency bands have wider bandwidth. However, the transmission in the higher frequency bands experience signal degradation due absorption of radio signals by atmospheric rain. The lower frequency bands have smaller bandwidth but signal degradation due to rain fade is relatively less.

Single beam broadband satellites communicate on X band (8–12 GHz) or Ku band (12–18 GHz) frequencies, typically using wide-beam technology to cover a large geographical regions as shown in the Figure 1.3.a. Multiple access is achieved either by sharing time (TDMA [13]) or frequency (FDMA [14]) and lets multiple users share the allotted spectrum in the most effective manner. However, this technology does not support high throughput and not suitable for broadband communication.

Accordingly, to address the high broadband demand, High Throughput Satellites (HTS) with multi-beam technology was introduced [15]. In this case, the total geographical region is covered using multiple narrow-beams as shown in the Figure 1.3.b. Generally, the total available bandwidth is divided into number of smaller frequency bands. This division of bandwidth is called as the so-called frequency reuse scheme, where while the adjacent beams operate at different frequencies, non-adjacent beams can operate at same frequencies. Naturally, lower the frequency reuse, greater is the available bandwidth. However, careful planning has to be done to ensure frequency orthogonality between adjacent beams [16, 17].

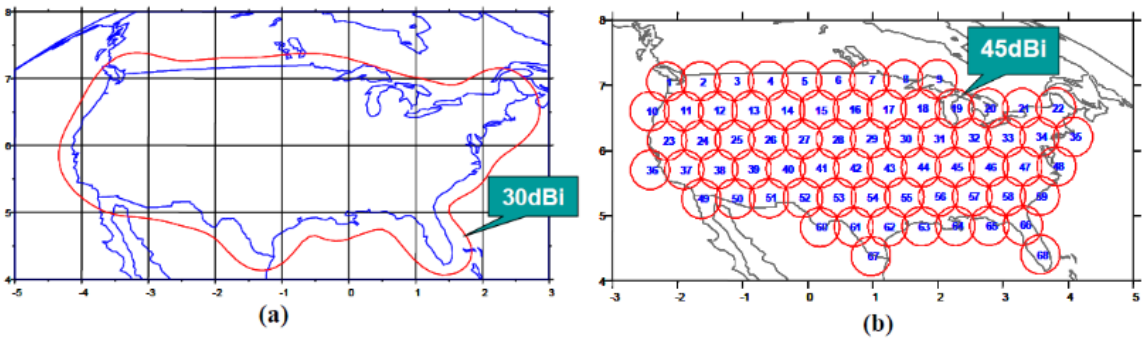

Figure 1.3: (a)conventional contoured beam antenna, and (b) multiple beam antennas (X-axis: Azimuth & Y-axis: Elevation) [16].

1.2 Motivation

By the end of 2020, 43 million broadband users were connected using communication satellites. Furthermore, this number is expected to be increased to 110 million by the end of 2029. Also with advancements in very high throughput satellite systems, it is estimated that the satellite connectivity can be provided to more than 697 million broadband users across the globe [18].

Furthermore, the current satellite broadband users are diverse and have unique demand and latency requisites. For example, Fixed Satellite Service (FSS) terminal users including home broadband terminals require web browsing and video streaming traffic. Governmental terminal users require secure communications with ultra reliable traffic. Vehicle to everything (V2X) communication users require low latency ultra reliable traffic. Mobile terrestrial users, broadband aeronautical users and broadband maritime users require continuity in traffic, irrespective of the frequent changes in location/user positions. Accordingly, such mobile users with unevenly distributed users will result in not only non uniformly distributed demand profiles but also in time sensitive dynamically changing demand profiles. For example, Figures 1.4, 1.5, 1.6 and 1.7 shows different demand profiles from the data provided by traffic simulator for multibeam satellite communication systems [2–5]. Evidently, the total demand is not uniformly distributed in any of the demand profiles. Also, the demand profiles vary with time.

Furthermore, satellite operators and service providers agree upon a legal contract named Service-Level Agreement (SLA) that involves volume-based guaranteed broadband rate with availability constraint. Such SLAs will evolve with more sophisticated definitions, including

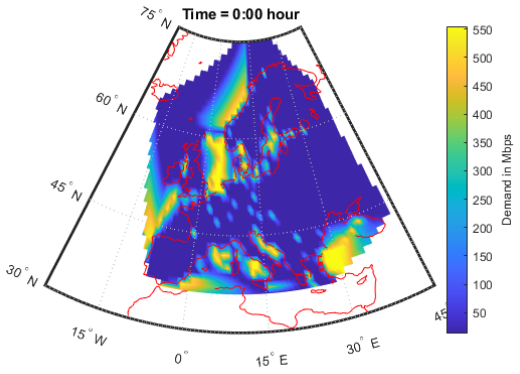

Figure 1.4: Demand profile at 00:00 hr

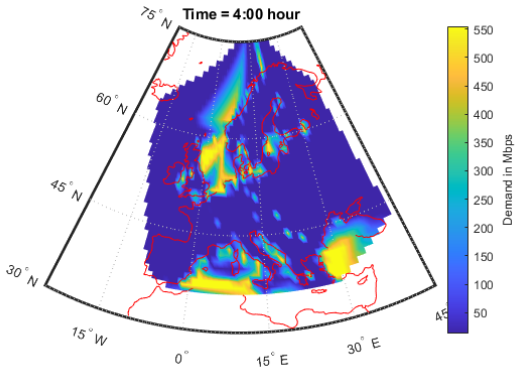

Figure 1.5: Demand profile at 04:00 hr

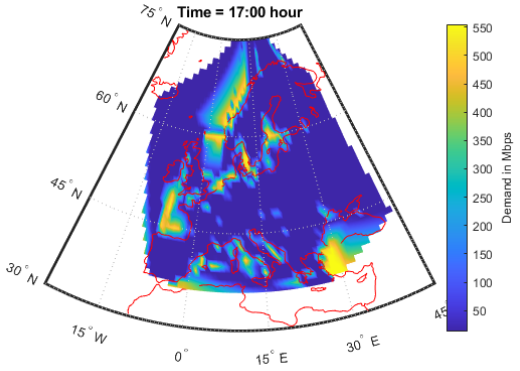

Figure 1.6: Demand profile at 17:00 hr

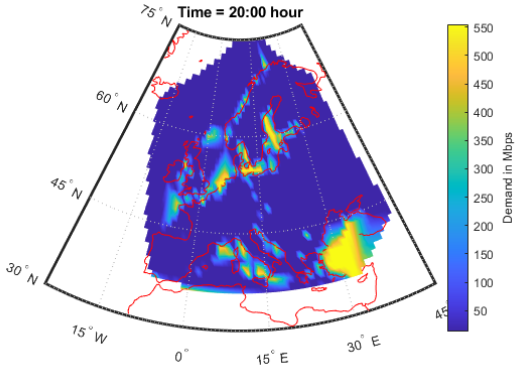

Figure 1.7: Demand profile at 20:00 hr

minimum/average achievable throughput, packet loss due to ACM error during configuration changes and failure to meet the latency constraints [19].

Hence, to provide every broadband user with the agreed levels of all the metrics defined in the SLA, especially for non uniformly distributed demand profiles that are also dynamically changing, is a challenging job for the satellite operators. Hence, there is a need for conventional rigid high throughput multi-beam satellite systems to adapt to the beam profiles. Accordingly, in this work, to make optimum use of the available resources, we aim to deliver capacity where it is required the most. Also, unlike regular capacity maximization approach, we consider demand satisfaction as a key metric. Such an approach intends to ensure that we minimize unused and unmet capacity by various demand driven optimization schemes. Conclusively, the main aim of demand driven systems is to dynamically adapt the beam layout, beam power, bandwidth and user scheduling in coherence to the demand profiles. Also, adapting the beam layout to serve the scheduled users means that the satellite power can

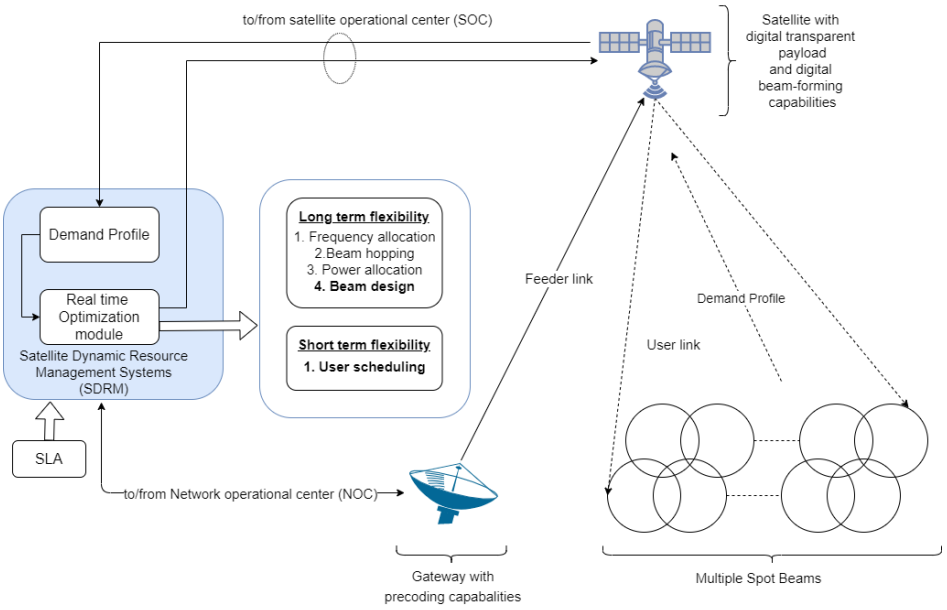

Figure 1.8: Adaptive multibeam satellite system Architecture with Satellite Dynamic Resource Management (SDRM) system

be better focused on the areas of interest and the available bandwidth can be intelligently reused.

1.3 Satellite Dynamic Resource Management systems

An adaptive multi-beam satellite system architecture is shown in Figure 1.8 with Satellite Dynamic Resource Management System (SDRM) [19] implementation. SDRM is an intelligent unit that achieve a traffic and link condition based automated network resources optimization. SDRM interconnects Network Operational Center (NOC) and Satellite Operational Center (SOC). Ideally, SDRM systems can be implemented in either at the ground segment or in the space segment. However, in current implementation, it is considered to be implemented on ground. Furthermore, in the near future, with the advancement in the digital transparent payload with onboard processing capabilities, we can assume the SDRM system in the space segment.

Throughout this thesis, we assume single ground segment or single gateway with ideal feeder link. Also, the space segment is capable of digital beamforming capabilities that enables SDRM system to implement dynamic beam footprints.

The SDRM system includes demand profile and real time optimization module. To eval-

uate the demand profile, the SDRM systems evaluate the long term user demand trends both for return and forward links (10 min time frame). Also, demand predictors can be used to predict future demands to avoid error in real time optimization modules. Furthermore, real time demand profile from the reverse user link serves as an input to the SDRM systems. Various real time optimization modules (for both long and short term flexibility) can be used to achieve demand satisfaction of the satellite broadband users using multiple spot beams. In the scope of this thesis, we evaluate only dynamic beam design and demand-driven dynamic user scheduling.

1.3.1 Protocol stack Architecture

The satellite protocol stack is shown in Figure 1.9 with the implementation of real time optimization techniques. The upper layers such as application, TCP/UDP and IP layers are satellite independent and termed as transparent layers with the space segment. However, satellite radio link control (SLC), satellite medium access control (SMAC) and satellite physical layer (SPHY) are satellite dependent layers.

Real time optimization techniques can be implemented in the satellite dependent layers. In the scope of this thesis, while the user scheduling is implemented in the SMAC layer, beam design and beam densification is implemented in the SPHY layer.

1.3.2 Key enabling technologies for demand driven adaptability

Precoding

Enabling the spatial interference mitigation methodology, precoding increases the system capacity by reusing the same frequency in multiple beams. Hence, full frequency reuse can be achieved in multibeam satellite systems. Accordingly, many authors in literature [20–22] have explored this topic. The Annex E of DVB-S2X [11] standard enables the usage of interference mitigation techniques using precoding in satellite communication systems. This standard proposes the superframe structure to overcome the issues of aligning pilot fields among the different beams. Also, a Channel State Information (CSI) feedback framework is proposed in the standard, where each user can report estimated values for up to 32 beams. However, due to practical impairments, commercial deployment of the precoding techniques in satellite payloads or even at gateways is still work in progress. Nevertheless, it is envisaged

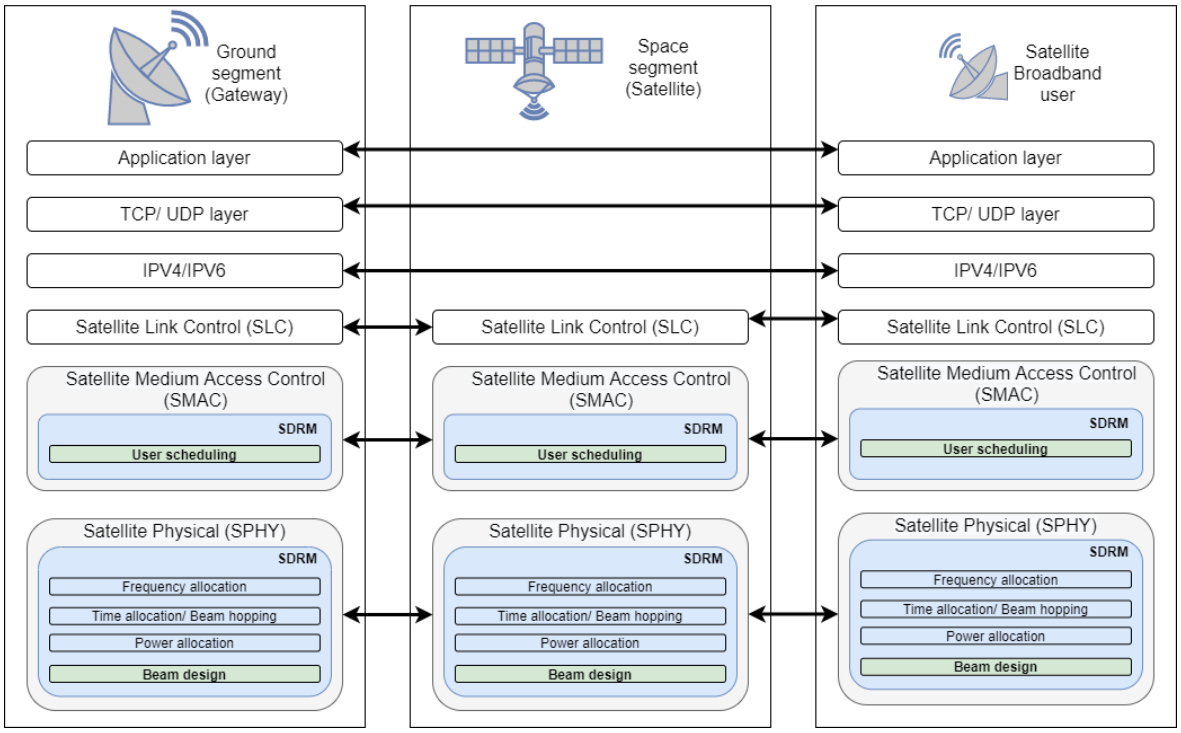

Figure 1.9: Satellite protocol stack with real time optimization techniques

that precoding along with user scheduling, power and bandwidth allocation will be the game changer in future demand driven multibeam satellite systems [23, 24].

Digital Beamforming Network (DBN)

In the current satellites, conventional analog beamforming networks are used to perform fixed beamforming, where weights are designed in advance and kept constant, resulting in fixed beam patterns and footprints. However, flexibility in coverage is a must for future generation satellite systems and hence, active antenna arrays powered by digital beamforming network (DBN) became a relevant technical solution [25–27].

Accordingly, DBN generates reconfigurable beams on Earth, such that the array beam pattern is automatically optimized by adaptively calculating complex weighting coefficients until a certain optimization is achieved. The optimization criteria can be demand satisfaction, maximization of the signal-to-interference-and-noise ratio, minimization of the mean square error (MSE), linear constraint minimum variance (LCMV) and so on. These array beam pattern can also be changed quite significantly from time-slot to time-slot based on the demand profiles [28].

Digital Transparent Payload (DTP)

In conventional satellite systems, the payloads do not have digital channelization such that the feeder link signal is simply converted in frequency, amplified and forwarded preventing any possibility for flexible channelization and load balancing. However, satellite manufacturers and operators such as SES S.A. are currently deploying advanced Digital Transparent Payload DTP as the de facto platform for future missions [7]. DTP enables digital synthesis of narrow-band user/beam specific carriers from the incoming wideband stream using filter banks and programmable routing of such carriers to end users, offering flexibility in terms of connectivity, channelization and frequency plan [29–32].

1.4 Demand driven adaptability using real time optimization modules

Exploiting the benefits of the key enabling technologies such as precoding, DBN and DTP, the optimization modules of the SDRM systems can enable the future demand driven satellite systems. Accordingly, using real time optimization modules, demand driven adaptability can be implemented for many techniques of the satellite transmission chain. Such an approach provides various degrees of flexibility, majorly categorized as long term flexibility and short term flexibility.

1.4.1 Long term flexibility

Long term scheduling involves optimization modules that should be used only during the change of the demand profile. The time frame can be once in few hours to once in few days.

Frequency Flexibility

Transmission frequencies are a limited radio resource and have to be used optimally. In conventional approach, the total available system bandwidth will be split equally for all the carriers. The assignment problem is solved using frequency reuse methodology. The so-called four color frequency reuse method is a sub-optimal solution that assigns same frequencies to the beams that are separated by considerable distance and are orthogonal.

However, demand satisfaction can be better obtained by carefully adjusting the bandwidth of each beam according to the demand requisites. Nevertheless, such flexible bandwidth

allocation is a trade-off between the maximizing the system capacity and fairness among the beams with different traffic demand. While the authors of [33–35] have worked on this approach, other have gone a step further to jointly optimize power and bandwidth [36, 37].

Time flexibility (Beam hopping)

The on-board resources on the satellite payload can be time-shared for better or even for optimal usability. Such approach has given raise to techniques such as beam hopping (BH) which is used to determine (a) the beams to be simultaneously activated which is known as beam illumination pattern and (b) how long should these beam illumination pattern can be used.

In literature, while the authors of [38–40] propose a heuristic iterative algorithm to generate a beam illumination design, other authors such as [41, 42] discuss joint beam hopping designs with either power or spectrum assignments. However, even though most of the related works concentrate on capacity maximization, they open up the possibilities for future works to optimize with an objective of demand satisfaction.

Power flexibility

In conventional mutibeam satellite systems, the total power is divided equally among all the beams. However, dynamic power allocation (i.e assigning beams with different power in coherence with different objective functions) is not a new topic but has been very broadly discussed in early works to perform load balancing [43–45]. However, recent works in [36, 46, 47] consider to optimize power along with other degrees of freedom, to further exploit the benefits of dynamic power allocation.

Beam Pattern Flexibility

The beamforming design or simply beam design is based on geometrical information, such as direction of transmission and direction of reception. Such information can be reliably estimated through the satellite ephemeris and geographical coordinates of the user terminal population. This geospatial information along with the actual rate demand per user across the coverage area can be effectively used to design the number and shape of the beams.

1. **Beam densification**: It is a process of increasing the number of beams only at high demand hotspot regions and is explained in Figure 1.10. However, the beam directivity

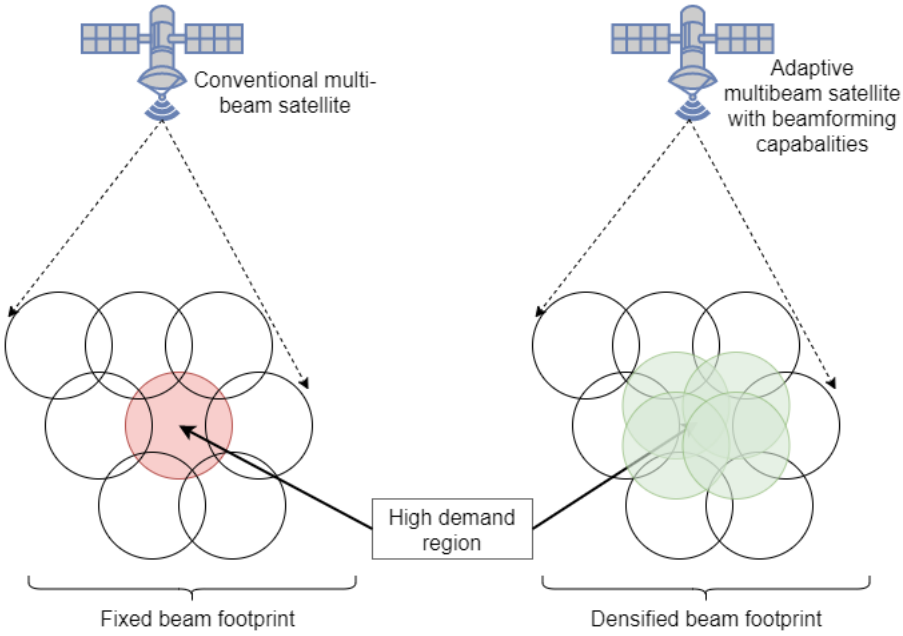

Figure 1.10: dynamic beam densification

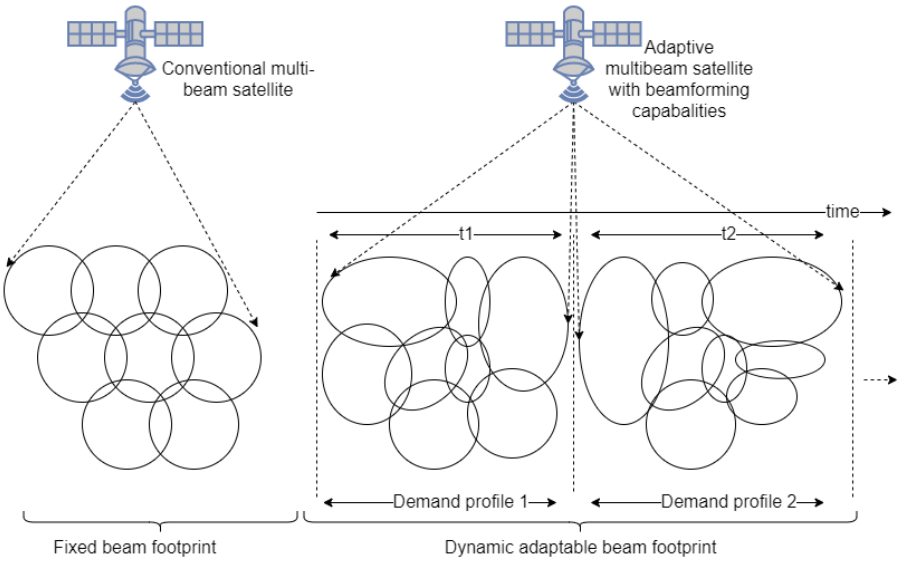

Figure 1.11: dynamic beam footprint design

of the increased number of beams remains similar before and after densification and hence, beam overlap increases upon densification. Nevertheless, by increasing the beams overlap, we reduce the beam gain gap between users in beam center and users in beam edge, which typically suffer from a -3dB loss in the antenna pattern when considering regular beam grid. Evidently, upon densification, antenna gain around the beam edges are significantly improved as the beam edges are now at lower loss in the antenna pattern. Furthermore, by retaining the same beam size (directivity), we do not increase the complexity of the payload architecture even after densification. The example shown in Figure 1.10 is termed as fixed or regular beam densification where, the densification factor and the beam position was arbitrarily chosen. The chapter 2 of this thesis, presents advanced demand driven beam densification.

2. **Dynamic or adaptive footprint design**: The conventional beam footprint design is limited to predefined beam layouts with regular beams of mostly same diameters. The shapes of the beam footprints are often approximated to hexagonal grid like structure to cover the region of coverage. The major problem with such beam design is that, it may lead to overload some beams in urban areas with high demand and underuse some beams in rural areas with low demand. Hence, dynamic footprint design need to optimize the beam shape and size to distribute the beam demands more evenly among all the beams of the multibeam system. In that attempt, the beam design reduces to a clustering problem where the targeted users have to be grouped based on proximity measures in a number of clusters equal to the number of desired beams. Even though, the actual capacity per beam largely depends on the allocated power and bandwidth, it would be wise to form the beams in a way that the aggregate demand per cluster does not present very large deviations. The adaptive beam footprint design are shown in Figure 1.11. As expected, hotspots are covered with smaller beams, whereas cold-spots with wider beams. However, when the beam demand profile changes, we can update the beam footprint again for even distribution of demand amoung the beams of a multibeam system. The chapter 3 of this thesis, presents this work more in detail. Also, as an extension of this thesis, practical constraints are verified in [48].

1.4.2 Short term flexibility

Short term flexibility involves optimization modules that are used at every scheduling period (mS) range.

User scheduling

The air interface suggested in DVB-S2 [11] is able to adapt the Code and Modulation (ACM) to the propagation conditions so that the spectral efficiency maximized. This is done by providing to each user with the most suitable modulation and code (ModCod) value according to the measured signal-to-noise-plus-interference ratio (SNIR). In this context, user scheduling plays a key role to guarantee an efficient resource management, since they can play with the time dimension to distribute satellite resources among different beams and receivers based on the channel conditions and QoS requirements [49–51].

More specifically, in traditional unicast packet scheduling, for every scheduling period, a scheduler selects one user per beam such that the total selected users (equal to the number of beams) are as orthogonal as possible. This ensures higher SINR and in turn better spectrum efficiency results. However, for demand driven adaptability, demand of individual users also affect the scheduling decisions. For example, in the first section of chapter 4, we present weighted semiorthogonal scheduling that considers both user demand and channel orthogonality. Furthermore, in the second part of the chapter 4, we discuss interference aware user scheduling, where the scheduler first groups users as interfering and non interfering classes and finally schedules users in the non interfering classes together based on demand.

1.5 Contributions

The total contribution of this PhD thesis is distributed among the chapters 2, 3, 4 and 5 and are as listed below:

1. **Chapter 2 :** Traditional multi-beam Geostationary (GEO) satellite communication systems provide broad- band coverage using a regular grid of fixed spot-beams with uniform 4-colour frequency (4CR) reuse scheme. However, user distribution is non-uniform on ground and, consequently, the demand distribution varies geographically. One potential solution to address high-demand regions is to enhance the satellite beam gain only in those areas. In this paper, we propose the so-called opportunistic beam

densification approach, which leverages the recent advances in on-board active antenna technologies to generate a higher number of beams over high demand hot-spot areas. Increasing the number of beams result in higher beam overlapping which needs to be carefully considered within the beam frequency planning. In this context, we propose a combination of beam densification, where the number of beams and beam placement is optimized targeting the demand satisfaction objective, followed by frequency-color coding strategy for efficient spectrum and interference management. Supporting results based on numerical simulations show the benefits of the proposed opportunistic beam densification in terms of demand matching performance compared with non-densified schemes and regular densification schemes.

2. **Chapter 3 :** The current broadband coverage area requisites and the expected user demand is satisfied by the state of the art satellite industry by using multiple spot beams of high throughput satellites with fixed multi-beam pattern and footprint planning. However, in recent years, new mobile broadband users with dynamic traffic demand are requesting for services in remote geographical locations such as air (aeroplanes) and water (ships). Furthermore, the expected demand varies with time and geographical location of the users. Hence, a practical approach to meet such heterogeneous demand is to plan adaptive beams to the satellites equipped with beamforming capabilities. In this paper, we study the state of the art fixed multi-beam pattern and footprint plan and show its drawbacks to support the non-uniformly distributed user terminals and varying traffic demands. To end this, we propose an adaptive multi-beam pattern and footprint plan where we design spot beams with flexible size and position based on the spatial clustering of the users in order to increase the flexibility of the high throughput satellite system. Numerical simulations demonstrate the high system performance of the proposed methodology.

3. **Chapter 4.1 :** The growing demand for broadband applications has driven the satellite communication service providers to investigate High Throughput Satellite (HTS) solutions. While precoding has been identified as the most promising technique to boost the satellite spectral efficiency, new advanced solutions focus on re-configurable demand-driven systems, where throughput delivered aligns with the time and geographical variations of the traffic demand. For such goal, conventional user scheduling algo-

rithms fail to meet the uneven user traffic demand. In this paper, we propose a novel unicast scheduling algorithm that takes into account both the channel orthogonality required for precoding along with the particular user demands. We name such technique as Weighted Semi-Orthogonal Scheduling (WSOS) methodology. Supporting numerical results are provided that validate the effectiveness of the proposed scheduling and quantify the benefits over conventional scheduling techniques.

Chapter 4.2 : In recent years, dynamic traffic demand requisites have driven the satellite communication service providers to implement reconfigurable demand-driven features to align the delivered throughput with the temporal and geographical variations of the traffic demand. Also, in current interference-limited High Throughput Satellite (HTS) systems, the resulting inter-beam co-channel interference can be mitigated by carefully performing precoding and user scheduling. Unfortunately, the conventional user scheduling algorithms fail to provide demand satisfaction for dynamic traffic demand requisites. Hence, in this paper, we focus on the user scheduling design for precoded satellite systems where both co-channel interference and user demands are taken into account. In particular, we first classify the sectors in each beam according to the interference they may cause to neighboring beams. Next, we formulate the scheduling problem such as the activation of neighboring beam sectors is avoided while proportionally dwelling on the sectors based on their traffic demands. The supporting numerical results for different demand distribution profiles validate the effectiveness of proposed interference-aware demand-based user scheduling over conventional scheduling techniques.

4. **Chapter 5 :** For many years, satellite footprints have been fixed from the design phase until the last day of the satellite operational life. Flexibility in coverage by means of reconfigurable beams is becoming increasingly popular thanks to the recent developments in active antenna systems. On the other hand, spatial frequency reuse combined with precoding has been shown to boost the spectral efficiency while lowering the cost per bit. In this context, and motivated by the unbalanced demand requests of the satellite users, we propose a shift from the traditional system-throughput maximization design towards a demand-Aware design, where a new beam shaping technique and user scheduling are combined to satisfy the users' demands. Supporting numerical results are provided that validate the effectiveness of the proposed beam planning and

scheduling and quantify the benefits over conventional rigid techniques.

Chapter 2

Demand driven beam densification

2.1 Introduction

Reusing the spectral resources across sufficiently separated geographical areas has been considered as the baseline design to ensure high spectral efficiency in broadband multi-beam GEO satellite communication systems [52, 53]. Conventional GEO satellite beam-pattern considers a regular spot-beam grid over the targeted coverage area where the so-called 4-color frequency reuse is applied [54, 55]. In other words, satellite communications systems allow using two polarizations concurrently and hence the overall available spectrum is divided into 2 orthogonal blocks and each block is used either with one or the other of orthogonal polarizations, resulting in 4 non-interfering frequency resources.

Due to rapid population growth and its spatial distribution, the communication traffic is highly non-uniform over the Earth. This has let to hot-spot regions with high capacity requirement over Europe, Eastern and Western United States and South East Asia [56]. For illustration purposes, an example of such high demand hot-spot region generated with the SnT Satellite Traffic Emulator [57] is shown in Figure 2.1. Accordingly, traditional method of regular spot-beam grid with spectral reuse of 4 non-interfering frequency resources fails to provide demand satisfaction at these so called high demand hot-spot regions [32, 58–61]. This is because the traditional regular beam grid is designed to provide the same capacity to all beams.

Future high-throughput satellites (HTS) will count with different degrees of freedom to dynamically adapt the supplied capacity to the on-ground demand [62]. Flexibility is typically enabled by two different technologies: (i) frequency flexibility, enabled by on-board

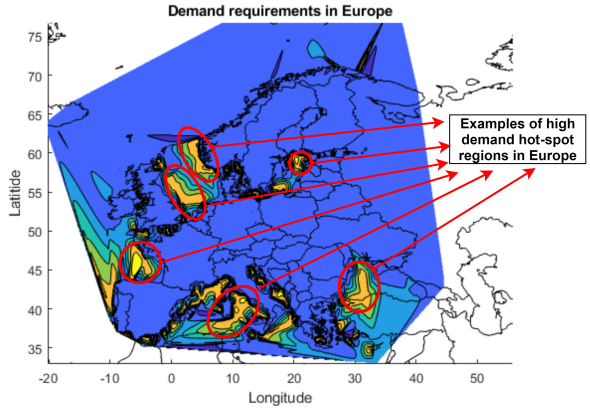

Figure 2.1: Demand distribution at 12 PM EST.

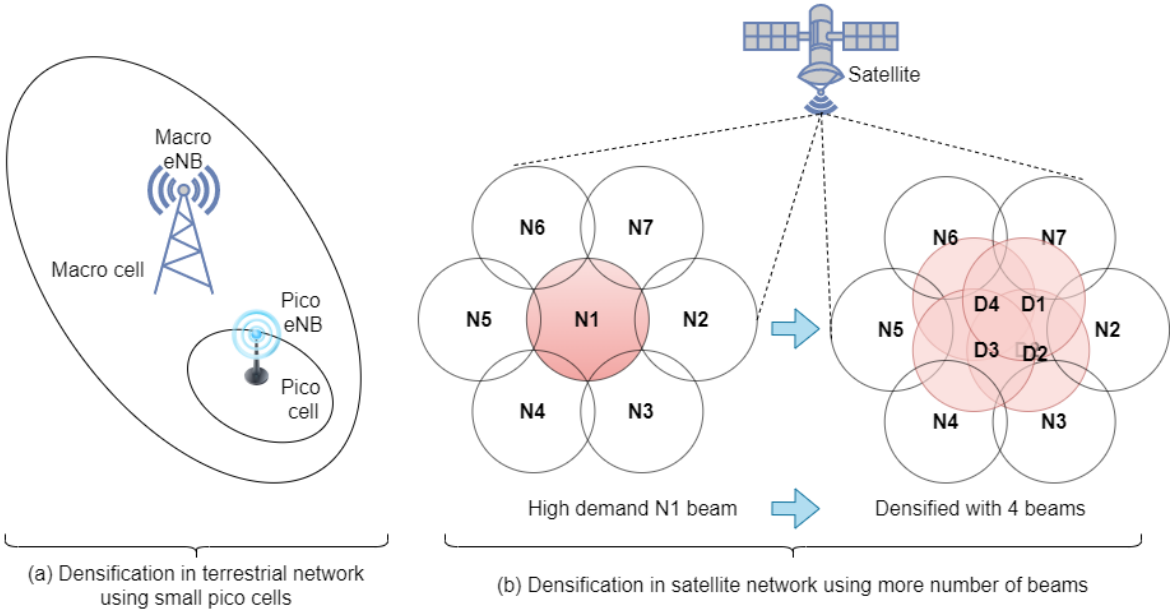

Figure 2.2: Beam densification in terrestrial network and satellite network

channelization of the different beams [63, 64]; and (ii) time flexibility, most commonly known with Beam Hopping (BH), where the same spectral resource is shared by a sub-set of beams that is active for a certain period of time [38, 65]. Power control can also play a role [66, 67], although has minor impact than the frequency/time domain optimization.

Recently, the current state-of-the-art satellite communications see a trend towards the deployment of on-board active antenna systems [68–70]. As highlighted in the recent review paper of de Gaudenzi et al. [71], the adoption of active antennas with large number of radiating elements and digital beam-forming will open the door to the exploitation of advanced beam

pattern design in telecommunication satellites.

2.1.1 Trends in On-board Antenna Architectures

The conventional regular beam grid is typically obtained from a Single-Feed Per beam (SFPB) architecture, where each spot beam on the ground is generated by using a single antenna feed element, typically a feed horn. The SFPB architecture is simplistic in terms of hardware but it scales in an unsustainable manner when the number of beams increases [72]. Furthermore, SFPB requires generally 4 reflectors to generate beams adjacent to each other.

Array antennas are very well established solutions in the general wireless communication domain and it was a question of time that they will break into the satellite architecture. Array antennas can generate customized radiating patterns with high directivity by using a large number of radiating elements. The latter is known as Multi-Feed Per beam (MFPB) architecture [73], because a sub-set of feeds is used to generate one beam. The main advantages of the MFPB architecture is that (i) it requires only 2 reflectors, one for transmission and one for reception; and (ii) combined with a Beam-Forming Network (BFN), it allows to reconfigure the desired beam pattern [74].

Large Array Fed Reflector (AFR), either employing direct center-fed or offset-fed architectures/ focal or defocussed architectures, have been shown promising performance in the satellite communications domain [75]. The offset design is frequently preferred as it has no blockage [76]. Such rapid development of on-board active antenna systems has made it feasible to implement more advanced beam pattern solutions when facing non-uniform geographical demand patters and is the key enabler for beam densification.

2.1.2 Related works

Beam densification is a new concept in satellite communication. Nevertheless, a similar concept was introduced in terrestrial communications with the advent of the 5th Generation (5G) of cellular networks [77,78], where the network is densified by placing smaller pico cells in the coverage region of macro cells (Figure 2.2(a)). Related works include, for example, [79], where the authors discuss industry perspectives of cell densification and the challenges of small cell backhaul, or [80], where the authors explain the benefits of spacial densification in 5G systems.

However, the cell densification of 5G differs in some aspects from the beam densification

proposed herein. On one hand, the densification in 5G was imposed by the use of higher frequency bands (from sub-6 GHz to mmWave) [80], which intrinsically provide shorter coverage range. Therefore, the signal loss between the cell center and the cell edge should remain approximately the same as for the non-densified case (in case we keep the same antenna design). On the other hand, shorter wavelengths due to higher frequencies have empowered the design of antenna arrays antennas and unleashed their beamforming capabilities [81,82]. The latter allows to steer the signal towards specific directions, thus compensating the signal loss with beam pattern gain.

In the case of HTS systems (Figure 2.2(b)), they have been for a long time operating on the Ka-band for the user link but only recently they are making the technology shift to advanced antenna systems (AAS) [83]. Conventional GEO HTS beam patterns (i.e. without AAS) consider $>$ 100 spot-beams distributed in a regular manner over the coverage area, and with a typical coverage (between beam center and the half-power or -3 dB point of the main lobe) of $\sim$ 300 Km. One of the main disadvantages of such beam planning is the fact that all geographical regions from the coverage region are treated in the same manner. For high demand areas (so-called hot-spots), it may occur that some users are located in the edge of a beam, where they suffer the -3 dB beam pattern loss. Ideally, the beam pattern shall provide similar beam gain over the whole hot-spot area. Hence, the opportunistic beam densification emerges as a potential solution to reduce the beam gain difference between user terminal in high demand areas.

The satellite beam densification as described above is relatively new, although some previous works have studied the beam pattern design from different perspective. In particular, the authors of [84,85] propose an adaptive multi-beam pattern and footprint plan where they design spot beams with flexible size and position based on the spatial clustering of the users in order to increase the demand satisfaction of the users and flexibility of the high throughput satellite system. Furthermore, the authors of [62] use fixed payload and optimize irregular beams coverage and beam pattern to minimize the error between offered and required capacity. Also, the authors of [86] obtain significant gains by increasing or reducing the overlap of signals from adjacent beams at beam edge by adjusting transmission power.

In conventional regular grid of fixed spot beams, 4-colour frequency reuse coding is used for spectrum management, which divides the total available bandwidth into four sub-frequencies and avoids interference between adjacent beams by not allocating the same sub-frequency

to any adjacent beams [32, 58]. However, recent studies in demand driven dynamic beam footprint design [84] and furthermore, beam densification discussed in this paper has given raise to non-regular and overlapping beams. Hence, in such scenarios, the current 4-color coding (spectral reuse of 4 non-interfering frequency resources) will not be able to preclude the inter-beam interference and consequently, affects the capacity performance of the system [59–61].

Hence, in irregular and overlapping beams, we must increase color coding factor to reduce the inter-beam interference. However, having high number of colors will result in lower bandwidth availability per beam and reduces the spectral efficiency. On the other hand, having fewer colors will results in higher inter-beam interference. Hence, in this paper, in order to color code with highest spectral efficiency and least inter-beam interference in irregular and overlapped beam footprints, we focus on graph theory based color coding scheme, which on one hand improves the spectral efficiency by choosing least number of colors and on the other, assigns colors to beams for least inter-beam interference.

Furthermore, the beams used for densification herein will retain the shape and size of the non-densified beams with same beam width/antenna gain. This is majorly because, the deployed beams are already as directive as possible (based on the state of the art technologies) and any further attempt to reduce the narrow the beams will increases the complexity of the payload architecture.

2.1.3 Contributions

In this work, we focus on frequency and beam pattern flexibility. In particular, we carry out a design trade-off analysis to evaluate the performance of opportunistic beam densification which involves increasing the number of beams at high demand hot-spot regions for demand satisfaction. In our design, the power and frequency resources are limited, and the increase in number of beams does not translate into an increase of available resources. While on one hand, beam densification allows to schedule a higher number of users at the same time, it also facilitates the scheduled users to experience better transmit antenna gain. However, the resources per user may diminish with densification, revealing a trade-off design. Furthermore, we study the impact of beam densification on the neighbouring non-densified beams. Also, we focus on employing demand-driven system adaptability by proposing demand driven beam densification and lastly, we propose a novel demand driven frequency reuse strategy using

dynamic color coding. The detailed contributions of the paper can be listed as follows:

1. **Regular beam densification**: First of all, we propose and evaluate the potential of a regular beam densification over the target hot-spot area. The latter does not involve any optimization procedure but rather a systematic densification regardless of the particularities of the scenario. For this, we present a system design trade-off analysis of a specific regular densified beam configuration for different frequency coloring / reuse (including full frequency reuse with and without linear precoding). With this preliminary study, we not only identify the main benefits that can be reached with beam densification but also enumerate the design challenges such as determining the number of beams for the densified area and determining the appropriate frequency reuse scheme. These two points motivate the next contributions listed below, which propose an optimization-based design targeting end-user demand-matching.

2. **Number of beams**: Beam densification involves increasing the number of beams over a certain high demand coverage, while considering the same system power and bandwidth. However, selecting the right number of beams is a challenging task. Choosing too many beams may cause the undesirable effect of increasing the beam overlap (subsequently, the inter-beam interference) and reduction in bandwidth per beam (when higher order frequency reuse is implemented). In this work, we propose a methodology to determine the right number beams for beam densification in accordance to the demand requisites.

3. **Beam Placement**: After the determination of the right number of beams, it is very important to choose the positions of the beams in the high demand coverage region. Traditionally, beams are always chosen equidistant from each other on a grid-like structure (i.e. regular beam grid). In this work, the beam placement is driven by the spatial demand distribution. In particular, we proposed a methodology to find the best beam position by minimizing the error between the demand and offered capacity.

4. **Dynamic frequency reusing scheme**: With the increased number of beams and irregular beam distribution, the frequency plan has to be carefully designed to avoid harmful inter-beam interference. Therefore, the last contribution of our work targets the appropriate beam color coding scheme after densification. Having less "colors" will result in higher bandwidth availability per beam, but may lead to higher inter-beam

interference. In this work, we propose a novel graph theory based methodology to both minimize the number of colors and to obtain an optimal frequency plan strategy.

The rest of the paper is organised as follows: In Section 2.2, the system model employing multi-beam high throughput satellite channel is described. In Section 2.3, regular beam densification is explained. Dynamic beam densification to define number of beams and beam positions is explained in Section 2.4. In Section 2.5, dynamic frequency reuse scheme is discussed. Section 2.6 provides the simulation results, and section 2.7 concludes the paper.

Notation: We use upper-case and lower-case bold-faced letters to denote matrices and vectors, respectively. $\circ$ denotes the element-wise Hadamard operations. $(\cdot)^T$ denotes the transpose of $(\cdot)$. $|\,.\,|$ and $\|.\|$ depict the amplitude and Euclidean norm, respectively.

2.2 System Model

We consider a GEO multi-beam HTS system, where the ground segment is assumed to be a single gateway with ideal feeder link. In the forward link, the multi-beam satellite system provides service to N single-antenna users using K spot beams where $N >> K$, which are distributed across the coverage area of the satellite. The user distribution on-ground is typically non-uniform, e.g. airport surrounding areas are typically more congested than residential low-populated areas. In addition, the demand requests of users depend on the final service, e.g. satellite backhauling terminals tend to aggregate traffic of many cell phone users resulting in high demand, while residential broadband VSAT terminals typically requests lower traffic.

In this paper, for comparison purposes, we will assume (for some cases) that the satellite system performs precoding on the transmitted signals [8]. In such cases, the precoding is calculated and implemented on ground at the gateway. After that, the precoded signals are transmitted through the feeder link to the satellite and the satellite performs a frequency shift, amplifies and forwards the precoded signals to the final users on ground. Low-complexity linear precoding techniques are considered to alleviate the complexity burden of the gateway [87].

The forward link air interface is assumed to be based on DVB-S2(X) [11], which considers Adaptive Coding and Modulation (ACM) allowing real-time adaptation of transmission parameters according to the link conditions.

For the methodology presented in this work, it does not matter if the beams are conformed with a single-feed-per-beam (SFPB) architecture or a multiple-feed-per-beam (MFPB)[1]. The users on each beam are served following a Time-Division Multiplex (TDM) scheme, i.e. the entire forward link spectrum is used by one user at a time on each beam. Therefore, in the following, we make use of the same index to indicate served user and beam. The received signal of user n is y_n and is expressed as,

$$y_n = \mathbf{h}_n^T \mathbf{x} + \mathfrak{N}_n, \tag{2.1}$$

where $\mathbf{h}_n \in \mathbb{C}^{K\times 1}$ is the channel vector and includes the channel coefficients seen by user n from all K beams; $\mathbf{x}$ represents the vector of K symbols and $\mathfrak{N}_n$ is the zero-mean thermal noise seen by the user n. By rearranging all the users' received signals in a vector $\mathbf{y} = [y_1 \dots y_K]^T \in \mathbb{C}^{K\times 1}$, and $\mathbf{H} = [\mathbf{h}_1 \dots \mathbf{h}_K]^T \in \mathbb{C}^{K\times K}$, the above model can also be expressed as,

$$\mathbf{y} = \mathbf{H}\mathbf{x} + \boldsymbol{N}, \tag{2.2}$$

where $\boldsymbol{N} \in \mathbb{C}^{K\times 1}$ is the concatenation of noise samples $\mathfrak{N}_n$.

The channel is defined as $\mathbf{H} = \mathbf{\Phi}^{\mathrm{LNB}}\mathbf{\Phi}^{(prop)}\mathbf{B} \in \mathbb{C}^{K\times K}$, where $\mathbf{B} = [\mathbf{b}_1 \dots \mathbf{b}_N]^T \in \mathbb{R}^{K\times K}$ is the system channel matrix whose $(n,k)^{th}$ component is given by,

$$[\mathbf{b}]_{n,k} = \frac{\sqrt{G_{Rn}G_{kn}}}{(4\pi\frac{\mathfrak{D}_n}{\lambda})}, \tag{2.3}$$

where λ is the wavelength of the transmission, G_{kn} is the gain of beam k in the direction of user n, G_{Rn} is the user's receive antenna gain and $\mathfrak{D}_n$ is the distance between the satellite and the n-th user.

Our channel has two phase terms introduced by the diagonal matrices $\mathbf{\Phi}^{LNB}$ and $\mathbf{\Phi}^{(prop)}$. The phase noise introduced by the user's Low-Noise Block (LNB) downconverter, whose diagonal elements ϕ_n^{LNB} are modelled as Gaussian random variable with zero mean and standard deviation of $\sigma_{RX} = 0.24°$ [88]. The diagonal elements of the phase due to RF propagation, ϕ_n^{prop}, depend on the user-to-satellite distance and are modelled as,

$$\phi_n^{prop} = \frac{2\pi}{\lambda}\mathfrak{D}_n \text{ [rad]}. \tag{2.4}$$

[1]The numerical simulations have been obtained with a SW-emulated Defocused Phased AFR.

The received signal-to interference-plus-noise ratio (SINR) of the n-th user is given by,

$$\gamma_n = \frac{g_{n,n}p_n}{\sum\limits_{k=1,k\neq n}^{K} g_{n,k}p_k + N_o B_n}, \tag{2.5}$$

where B_n is the per-user occupied bandwidth which in the case of unicast systems are equal to per-beam occupied bandwidth B_k. Furthermore, the total system bandwidth is a function of frequency reuse factor. For example, in 4CR frequency reuse generic case, the total system bandwidth is divided into 4 parts : $B_n = B_k = \frac{B_{total}}{4}$. However, considering the benifits of orthogonality introduced by polarization, in this paper, for 4CR frequency reuse, $B_n = B_k = \frac{B_{total}}{2}$. In general, $B_n = B_k = \frac{B_{total}}{\frac{1}{2}\times(number-of-colors)}$. Hence, having higher number of colors will result in lower bandwidth availability per beam.

Also, N_o is the noise spectral density and $g_{n,k} = |h_{n,k}|^2$ is the channel power gain. Furthermore, the Shannon offered capacity for user n is given by,

$$C_n = B_n \log_2(1 + \gamma_n). \tag{2.6}$$

However, based on the values of modulation and coding schemes (ACM), DVB-S2X [11] defines a table to map SINR to Spectral Efficiency. Thus, the offered capacity obtained using spectral efficiency (ζ) in DVB-S2X defined table, can be analysed for more practical systems. Hence, in this work, we consider the system capacity based on DVB-S2X and is defined using,

$$C_n = B_n \times \zeta(\gamma_n). \tag{2.7}$$

As mentioned earlier, sometimes in this work we evaluate full frequency reuse and, as a consequence, we assume that the transmitted symbols are precoded. In that case, $\mathbf{x}$ represents the precoded signal and is given by,

$$\mathbf{x} = \mathbf{W}\mathbf{s}. \tag{2.8}$$

where $\mathbf{W}$ is the precoding matrix and $\mathbf{s}$ denoted the vector of raw symbols that satisfies $\mathbb{E}[\mathbf{s}\mathbf{s}^H] = \mathbf{I}$. The precoding matrix $\mathbf{W}$ is obtained with the well-known Minimum Mean Square Error (MMSE) design (denoted sometimes as regularized zero-forcing) [89], which can be expressed as,

$$\mathbf{W}_{RZF} = \eta \boldsymbol{H}^{\boldsymbol{H}}(\boldsymbol{H}\boldsymbol{H}^{\boldsymbol{H}} + \alpha_r \boldsymbol{I})^{-1}, \tag{2.9}$$

where α_r is a predefined regularisation factor and η is the power allocation factor that, in our case is defined to comply with the total satellite power constraints,

$$\eta = \sqrt{\frac{P_{tot}}{\text{Trace}(\mathbf{W}\mathbf{W}^{\dagger})}}, \tag{2.10}$$

with P_{tot} being the total available power at the satellite.

2.3 Opportunistic Regular Beam Densification

In high demand hot-spot region, beam densification involves increasing the beam pattern gain at edge of the original beam by increasing the number of beams. However, while increasing the number of beams, topological packing and geometrical tractability is a key challenge. Topological packing can be defined as the way the densified beams are placed/packed in the high demand hot-spot region. Furthermore, geometrical tractability is important to keep the operational complexity to minimal.

Inspired by the regular grid beam footprint design of the conventional GEO satellite system, densification can be carried out in a regular fashion. For example, in the Figure 2.2.B, the high densified N1 beam is replaced by 4 densified beams such that the 4 densified beams (D1, D2, D3 and D4) are placed in a regular fashion around N1 and also equidistant from each other. Such design, on one hand have a high topological packing for its regularity and on the other hand, have good geometrical tractability for its low complexity.

Generally, the beam pattern gain at the beam edge of the non-densified beams (N1 to N7) are at -3dB to -4dB from the beam center. Accordingly, any user scheduled at the beam edge, will suffer from poor beam pattern gain. Furthermore, as the densified beams are not narrow beams or directed beams, and densified beams (D1 to D4) follows the shape and size of the non-densified beams. However, from the Figure 2.3.A, after beam densification, the scheduled user will now have better beam pattern gain, in comparison to the non-densified case.

Notwithstanding, from the Figure 2.3.B, 4 color frequency reuse scheme fails. D3 and N5 (D4 and N4/ D2 and N3) are adjacent beams sharing the same frequency resources and hence cause strong inter-beam interference. Accordingly, in this work, we first evaluate the regular beam densification with 4CR frequency reuse and later with 16CR frequency reuse.

For evaluation purposes, this paper assumes a GEO satellite located at 13 degrees East

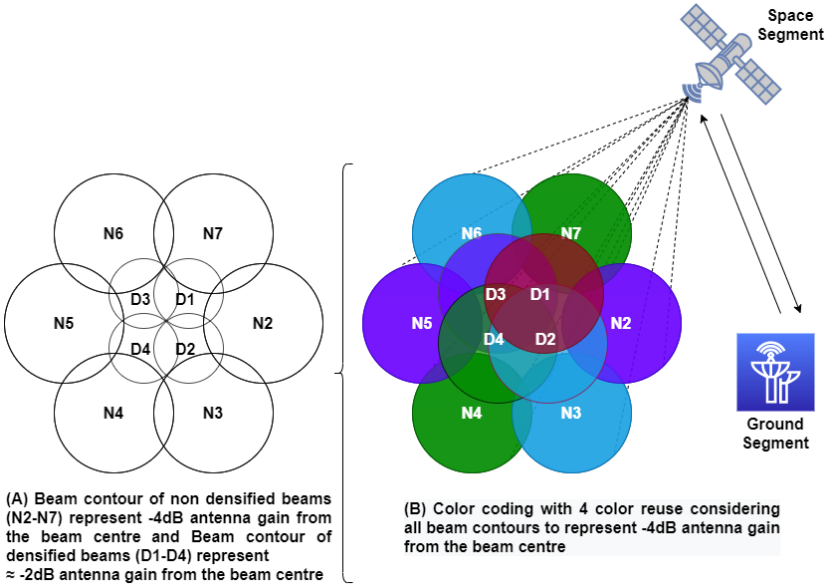

Figure 2.3: Regular Beam Densification in the high demand region by replacing one beam with four beams increases inter-beam interference.

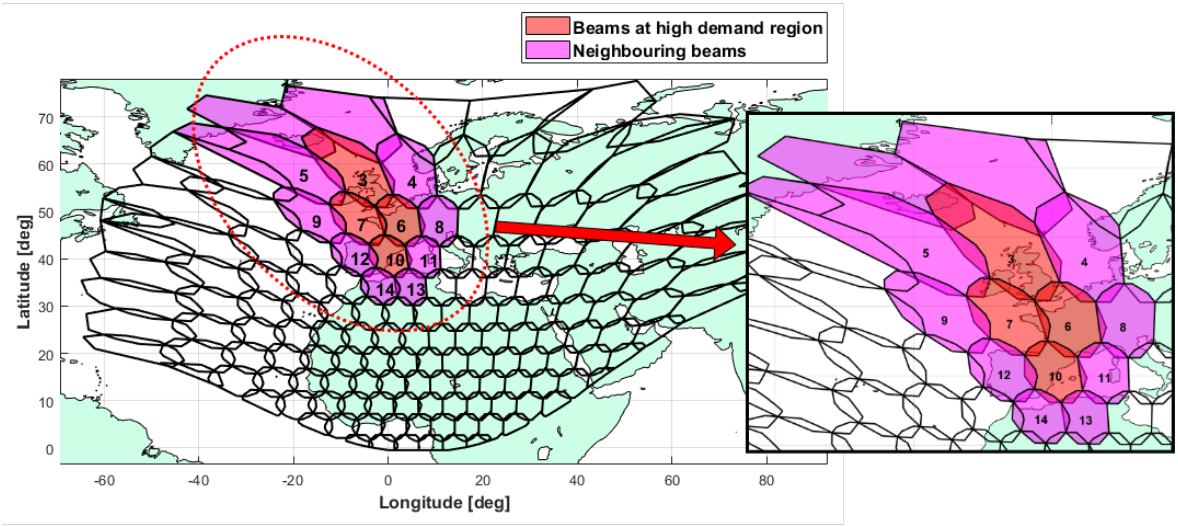

Figure 2.4: Beams 3, 7, 6 and 10 are the beams in the centre of Europe and with high demand

with a beam pattern obtained with a dedicated software from the European Space Agency (ESA), which has been programmed to model a defocused phased Array-Fed Reflector (AFR). The reflector size is of 2.2m and an array diameter of roughly 1.2m. The antenna array before the reflector is a circular array with 2λ spacing and 511 elements. The pattern has been generated assuming a slight radial amplitude tapering of the array elements. ESA kindly provided the beam pattern to the authors to carry out this study.

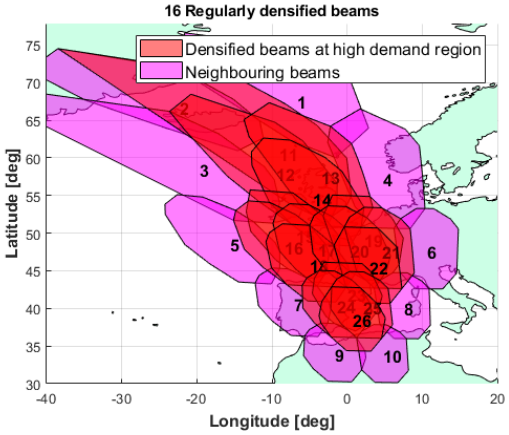

Figure 2.5: Regular beam densification, where 4 beams are replaced by 16 beams

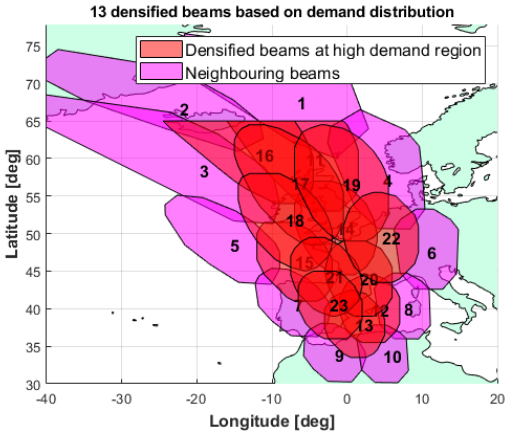

Figure 2.6: Demand driven beam densification where the 4 beams are replaced by 13 beams

As noted in Figure 2.4, we select 14 beams out of the ESA beam pattern. Beams 3, 6, 7 and 10 are beams with high demand and we call them as parent beams. The shapes and size of the beams in Figure 2.4 appears to be different for different beams due to the curvature of the Earth and the map projection. Nevertheless, it should be noted that all the beams have same size and shape.

Figure 2.5, provides the regularly densified beam densification, where the 4 parent beams are replaced by 16 child beams. Furthermore, upon densification of parent beams, the performance of child beams (those beams that replace the parent beams) and the beams around the child beams may be impacted in terms of performance. Therefore, beams around the high-demand area (i.e. the neighbouring beams) will be also considered in our analysis.

2.4 Dynamic beam densification

The homogeneous beam densification, presented as an example in the previous section, can be advantageous when the demand of hot-spot regions is itself homogeneously distributed. However, when demand also varies unevenly over the high demand region as shown in Figure 2.7, it is beneficial to adapt the beam densification scheme for better demand satisfaction.

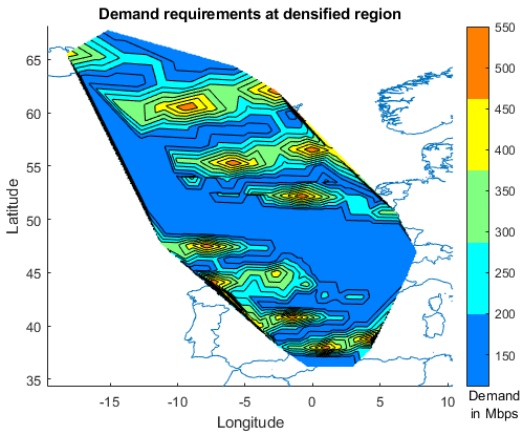

Figure 2.7: Uneven demand distribution at the densified region

Also, in the previous densification example, the demand of the hot-spot region was not considered in determining both the number of beams and beam placement. Hence, for dynamic demand requisites, beam densification can be further enhanced by considering demand as a determining factor to decide the number of beams and beam positions.

2.4.1 Determining the number of beams

Densifying the high demand hot-spot from 4 beams to 16 beams as shown in Section 2.3, was an arbitrary choice. Determining the number of beams for densification is not an easy task, as it comes with the following trade-off: With same system power and bandwidth, selecting fewer number of beams may not mitigate enough the beam pattern gain loss between users in beam center and users in beam edge but may reduce the beam overlap between adjacent beams; on the other hand, selecting too many beams may be beneficial in terms of offering good beam pattern gain to all users but may result in higher inter-beam interference. Hence there is a need for effective algorithm to define optimal number of beams as a function of demand. Accordingly, we define the optimal number of beams as K and formulate an optimization problem as below,

$$\min_{K} \sum_{k=1}^{K} (D_k - C_k)^2; \tag{2.11a}$$

$$s.t. \quad C_k = B_k \times \zeta(\gamma_k) \tag{2.11b}$$

where the objective function is to reduce the error between the overall beam demand $D_k = \sum_{n \in \mathcal{G}^k} d_n$, $\mathcal{G}^k$ denoting the set of users belonging to beam k, and beam offered capacity C_k. In unicast systems, $C_k = C_n$, $B_k = B_n$ and $\zeta(\gamma_k) = \zeta(\gamma_n)$ and is defined in Equation (2.7).

However, by its virtue, the objective function chooses highest number of beams that best satisfy the beam demand. Furthermore, the constraint having interference signal in the denominator limits the choice of the number of beams to a realistic value. Nevertheless, the problem (2.11a) is NP hard problem because of the interference signal in the denominator of the constraint (as it is a function of the number of beams). Hence, we make use of cluster analysis [90, 91].

In cluster analysis, increasing the number of clusters will reduce the error in user clustering. Accordingly, when we consider each cluster element as a cluster, we can obtain zero clustering error which is not an ideal or practical approach as such huge number of beams will have strong inter-beam interference. Hence the optimal decision of K is a balance between the highest compression of the cluster elements using a single cluster, and the highest efficiency by assigning each user to its own cluster.

Authors of [92–94] have focused on finding the ideal number of clusters for a given data set. In particular, Variance Ratio Criterion (VRC) or Calinski-Harabasz(CH) index is used, i.e. the ratio of the sum of between-clusters dispersion and of inter-cluster dispersion for all clusters. The higher the CH index, the better the clustering.

However, the CH index does not assign weights to its cluster point and hence, will not be an ideal scheme for demand satisfaction. Accordingly, to adapt the CH index to our particular problem (2.11a), we define spatially distributed demand grid of J points with d_j indicating the demand of the j^{th} grid point. Then we define beam demand as $D_k = \sum_{j=1}^{J} d_j$. Furthermore, we define the overall system demand defined as, $D_{sys} = \sum_{k=1}^{K} D_k$.

Later, we update the regular CH index to account for the users' demand in the form of

Weighted Calinski-Harabasz (WCH) index, defined by,

$$WCH(K) = \frac{\sum_{k=1}^{K} n_k \|\mathfrak{M}_k - \mathfrak{M}\|^2}{\sum_{k=1}^{K} \sum_{j \in \mathcal{G}_j} \|\Theta_j - \mathfrak{M}_k\|^2 \times \frac{D_k}{D_{sys}}} \frac{(J-K)}{(K-1)} \tag{2.12}$$

where n_k is the number of spatially distributed demand grid points in a cluster k, $\mathfrak{M}_k$ is the centroid of the cluster k, $\mathfrak{M}$ is the geographical mean of the spatially distributed demand grid points, $\|\mathfrak{M}_k - \mathfrak{M}\|$ is the Euclidean distance between the two vectors and Θ_j is the position of the spatially distributed demand grid point j.

The proposed procedure to determine the optimal number of beam based on Equation (2.12) is given in Algorithm 1, where high demand hot-spot region is divided into different values of K clusters using weighted k-means clustering [84] and then WCH index for the K cluster is computed. Any value for K that maximizes CH index is considered as good number of cluster.

Algorithm 1: Evaluate cluster size using WCH criteria

Input : X, K_{min}, K_{max}
Output : K

for $K = K_{min}$ **to** K_{max} **do**
  1. Obtain K clusters using weighted k-means algorithm [84].
  2. Evaluate WCH index for the K clusters using,
  $WCH(K) = \frac{\sum_{k=1}^{K} n_k \|\mathfrak{M}_k - \mathfrak{M}\|^2}{\sum_{k=1}^{K} \sum_{j \in \mathcal{G}_j} \|\Theta_j - \mathfrak{M}_k\|^2 \times \frac{D_k}{D_{sys}}} \frac{(J-K)}{(K-1)}$
end
3. Evaluate ideal value of K using $K = \max(CH(k))$

As illustrative example, we have executed Procedure 1 with $K_{min} = 4$ and $K_{max} = 16$ and considering the high-demand area indicated in Figure 2.7, which was originally covered in Figure 2.4 by beams 3, 6, 7 and 10. The results are shown in Figure 2.8, where it can be observed that $K = 13$ maximizes the WCH value and hence is considered as optimal number of beams for this particular example.

2.4.2 Determining beam placement

After determining the number of beams for densification, the next crucial step is to determine the beam center position. In regular densification, the densified child beams were positioned regularly equidistant from each other. However, in this section, by considering the demand requisites, we propose a novel beam positioning scheme that provides the most demand

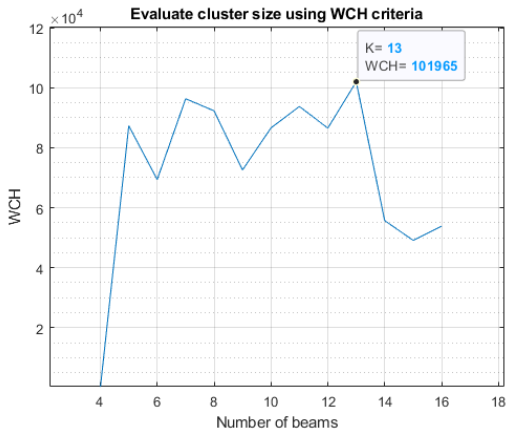

Figure 2.8: Finding optimal number of beams

satisfaction.

Once the optimal number of beams is identified, the reader may note that a possible beam placement solution can be obtain simply by executing step 1 of Procedure 1.

In this section, we provide a generalization of Step 1, by considering a grid of possible beam center locations different than the grid points considered by the weighted K-means proposed in [28]. In particular, assuming that the user-to-beam assignment is extracted from Procedure 1, we can address the beam center positioning problem independently for each beam[2].

Let us assume that the spatially distributed demand is represented into a grid of J points, with d_j indicating the demand of the j^{th} grid point. Also, we define $\theta_i = \{\theta_1, \theta_1, ...\theta_I,\}$ as possible beam center location. Furthermore, to obtain maximum demand satisfaction $\forall j$ in every beam k, we need to find θ_i as below,

$$\min_{\theta_i} \sum_{j=1}^{J} d_j - c_{j,\theta_i} \tag{2.13}$$

and place the beam k at position of θ_i. Accordingly, Figure 2.6 provides the demand driven beam densification where the 4 beams are replaced by 13 beams for the demand profile shown in Figure 2.7.

[2]Note that the interference issues will be addressed in the frequency planning section

2.5 Dynamic frequency reusing scheme

In conventional regular grid of fixed spot beams, 4-colour frequency reuse coding is used for spectrum management, which divides the total available bandwidth into four sub-frequencies and avoids interference between adjacent beams by not allocating the same sub-frequency to any adjacent beams. However, recent studies in demand driven dynamic beam footprint design and furthermore, beam densification discussed in this paper has given raise to non-regular and overlapping beams. Hence, in such scenarios, the current 4-color coding (spectral reuse of 4 non-interfering frequency resources) will not be able to preclude the inter-beam interference and consequently, affects the capacity performance of the system [32, 58–61].

Hence, in irregular and overlapping beams, we must increase color coding factor to reduce the inter-beam interference. However, having high number of colors will result in lower bandwidth availability per beam and reduces the spectral efficiency. On the other hand, having fewer colors will results in higher inter-beam interference. Hence, in this paper, in order to color code with highest spectral efficiency and least inter-beam interference in irregular and overlapped beam footprints, we focus on graph theory based color coding scheme, which on one hand improves the spectral efficiency by choosing least number of colors and on the other, assigns colors to beams for least inter-beam interference.

2.5.1 Graph construction

Upon densification, to reduce inter-beam interference, we can use color code of higher order. For example, in Figure 2.3.B, upon densification, one beam is densified by four beams, 4CR frequency reuse will not be efficient to reduce the inter-beam interference and accordingly, beams can be coded with 7 colors such that no two adjacent beams have the same color.

However, increasing the number of colours will decrease the offered channel bandwidth and consequently affects the offered capacity. Hence, it is important to color code with minimum number of colors. In this case of Figure 2.3.B, we could compute the colors manually because the number of colors and the beams are few. However, as shown in Figure 2.9, when multiple adjacent beams are densified, color coding is not a straightforward approach. Hence, we propose the use of graph theory to compute the optimal number of colours and colouring strategy.

The 14 beams of Figure 2.9 can be represented using graph theory by the graph $G = (V, e)$,

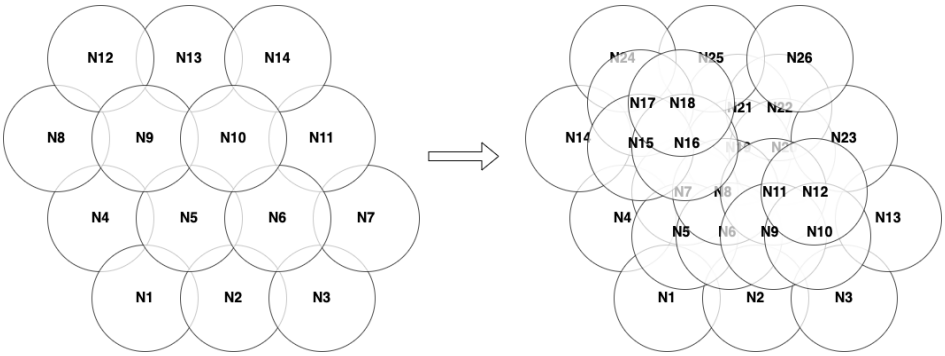

Figure 2.9: Non densified 14 beams to the left and densified 26 beams to the right

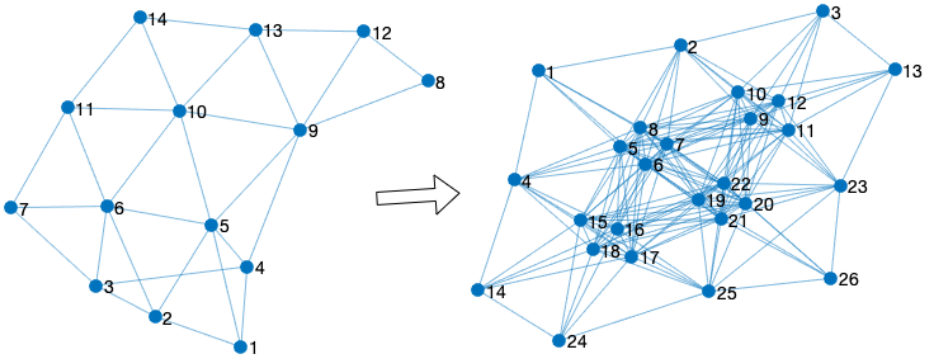

Figure 2.10: Graph representing non densified 14 beams on the left and graph representing densified 26 beams on the right

where nodes V represents the beams and edges e connect to interfering beams. The graph G is as shown in left part of Figure 2.10. However, upon densification, the number of nodes increase from 14 to 26, where 4 beams are replaced by 16 beams where the traffic demand is high. The densified graph G is as shown in right part of Figure 2.10.

However, to construct such graphs, it is important to define beam adjacency. Accordingly in this work, we define beam adjacency using Euclidean distance. We consider a satellite system with K number of beams and formulate a logical adjacency matrix, $\mathbf{A}$ which is of dimension $K \times K$. The entries of $\mathbf{A}$ define the adjacency between all K beams of the system. Accordingly each element $a_{(i,j)}$ of the $K \times K$ matrix is set to binary 1 if beam i is adjacent to beam j, and binary 0 otherwise. Furthermore, we use Euclidean distance to define adjacency between the beams such that each element $a_{(i,j)}$ is defined as,

$$a_{(i,j)} = \begin{cases} 1, & \text{if } d(i,j) <= d_{\min} \\ 0, & \text{otherwise} \end{cases} \tag{2.14}$$

where $d(i,j)$ is the distance between any two beams i and j. Hence, if the distance between two beams is less or equal to $d_{\min}$, the beams are said to be adjacent to each other. The minimum distance $d_{\min}$ is chosen wisely with reference to traditional spot beam beam footprint with a hexagonal grid layout.

We define $G = \{V, E\}$ as undirected graph that represents the satellite network, where, $V = \{v_1, v_2..., v_k\}$, is set of all nodes in G. Any edge $e(k, k')$ between two nodes v_k and $v_{k'}$ exist, when beams k and k' are adjacent to each other and can cause potential inter-beam interference.

The set of all such edges in G is denoted as E. $G = \{V, E\}$ can easily be constructed using logical adjacency matrix, $\mathbf{A}$. The entries $a_{(i,j)}$ in $\mathbf{A}$ specify the network of connections (edges) between the nodes of the graph. The location of each nonzero entry in $\mathbf{A}$ specifies an edge between two nodes.

For example, logical adjacency matrix, $\mathbf{A}$ for the beams mentioned in Figure 2.2.B is as below,

$$\begin{array}{c} \begin{array}{ccccccc} N1 & N2 & N3 & N4 & N5 & N6 & N7 \end{array} \\ \left(\begin{array}{ccccccc} 0 & 1 & 1 & 1 & 1 & 1 & 1 \\ 1 & 0 & 1 & 0 & 0 & 0 & 1 \\ 1 & 1 & 0 & 1 & 0 & 0 & 0 \\ 1 & 0 & 1 & 0 & 1 & 0 & 0 \\ 1 & 0 & 0 & 1 & 0 & 1 & 0 \\ 1 & 0 & 0 & 0 & 1 & 0 & 1 \\ 1 & 1 & 0 & 0 & 0 & 1 & 0 \end{array} \right) \begin{array}{c} N1 \\ N2 \\ N3 \\ N4 \\ N5 \\ N6 \\ N7 \end{array} \end{array}$$

and the graph that represents the logical adjacency matrix, $\mathbf{A}$ is shown in Figure 2.11 where the nodes represent the beams and the edges represent the adjacency between the beams.

2.5.2 Optimized color coding

In order to avoid inter-beam interference, we need to color the nodes of the graph G, such that no two adjacent nodes have the same color. Also, to reuse frequencies, we need to find the minimum chromatic number $\chi(G)$, which is smallest number of colors needed to color G. Accordingly, we formulate an optimization problem as,

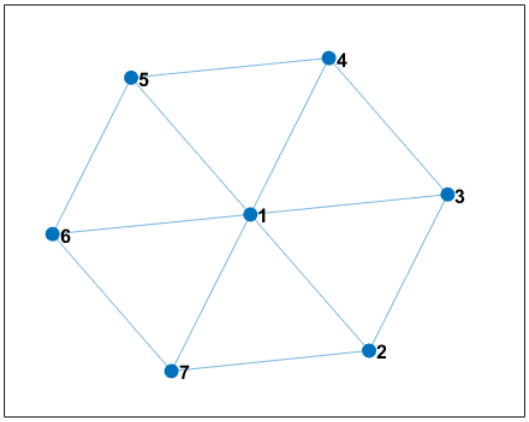

Figure 2.11: Graph obtained from the adjacency matrix to the beams in Figure 1.

$$\min_{\{V_1, V_2 \ldots V_{\chi(G)}\}} \chi(G); \tag{2.15a}$$

$$s.t. \quad V_c = \{v_k : e(k, k') = 0 \quad \forall k, k'\} \tag{2.15b}$$

$$V_{c1} \cap V_{c2} = \emptyset \quad \forall c1 \neq c2 \tag{2.15c}$$

$$\bigcup_{c=1}^{\chi(G)} V_c = V \tag{2.15d}$$

$$1 \leq \chi(G) \leq \chi(G)_{max} \tag{2.15e}$$

where the objective function is to minimize the chromatic number (number of colors) and V_C is the set of all nodes of same color. The first constraint ensures that no two adjacent nodes of graph G will have same color. The second constraint is to ensure that no vertex is assigned with two different colors. The third constraint is to ensure the union of subsets is the full set of vertices and hence all the vertices are coloured. The last constraint sets an upper bound for the number of colors required.

In order to solve the problem 2.15a, we define binary variables $x_{v_i c}$ such that when a vertex v_i is assigned a color c, $x_{v_i c}$ takes the value 1; otherwise, $x_{v_i c}$ takes the value 0. Besides, binary variable y_c=1 indicates that color c has been used, i.e., set V_c contains at least one vertex; otherwise, V_c is empty and V_c, indicating that color k was not required. We hence can reformulate the 2.15a as,

$$\min \sum_{c=1}^{\chi(G)_{max}} y_c \tag{2.16a}$$

$$s.t. \quad y_c \in \{0,1\}; \quad c = 1, ..., \chi(G)_{max} \tag{2.16b}$$

$$\sum_{c=1}^{\chi(G)_{max}} x_{v_i c} = 1; \quad \forall v_i \in V \tag{2.16c}$$

$$x_{v_i c} \in \{0,1\} \quad \forall v_i \in V \tag{2.16d}$$

$$x_{v_i c} + x_{v_j c} \leq y_c \quad \forall \{v_i, v_j\} \in E \tag{2.16e}$$

The first and the third constraint in this formulation indicates that y_c and $x_{v_i c}$ are binary variables. The second constraint ensures that exactly one color is assigned to each vertex. The last constraint connects variables x and y, allowing coloring with color c only if $y_c = 1$, and forbids the endpoints of any edge $\{i, j\}$, vertices i and j, from having the same color simultaneously.

The problem was solved by branch-and-bound method using PySCIPOpt 4.2.0 [95], a Python interface for Solving Constraint Integer Programs (SCIP) [96].

2.6 Simulation parameters and results

The considered antenna pattern (kindly provided by the European Space Agency, ESA) corresponds to a GEO 13°E satellite operating at the Ka exclusive band 19.7 to 20.2 GHz. A summary of simulation parameters are shown in Table 5.2. For simulation, we consider unicast scheduling with K users scheduled in K beams where each of the user position is randomly selected. Accordingly, before densification, we schedule 4 users in the high demand region using 4 beams. After densification with regularly densified beams, we use 16 beams to schedule 16 users in the same high demand region. Similarly, when we densify with demand based densification, we use 13 beams to schedule 13 users in the same high demand region. Also, for reliable result evaluation, we perform Monte Carlo simulations for 100 iterations and consider mean values for our result analysis.

The result analysis is organised as follows: Firstly, we assess the beam patterns in 2.6.1, then evaluate the impact of densification with 4 color frequency reuse in section 2.6.2, then in 2.6.3 we study the impact of densification with full frequency reuse and precoding. Later,

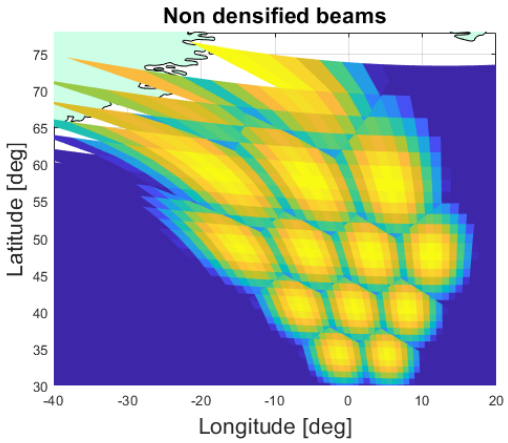

Figure 2.12: Antenna Gain of non densified beams

we study the impact of densification with dynamic frequency reuse in 2.6.4 and Finally, in 2.6.5 we analyse the impact of densification on neighbouring beam.

Table 2.1: Simulation Parameters

Satellite longitude	13 degree East (GEO)
Beam radiation pattern	Provided by ESA in CGD [97] project
User link bandwidth, B	500 MHz
Roll-off factor	20%
Terminal antenna diameter	0.6 m
Terminal antenna efficiency	60%
DL wavelength	0.01538 m

2.6.1 Beam pattern analysis

The beam pattern for 4 non-densified beams along with 10 neighbouring beams are shown in Figure 2.12. Furthermore, the gain values in dBi are shown using the color bar in Figure 2.14 for all the beam pattern plots. Evidently, there are more regions with lower values of beam pattern gain (near the beam borders). Any possible high demand users in this region are expected to experience poor SINR. Similarly, beam pattern for 16 regularly-densified beams and 13 demand driven densified beams along with the neighbouring beams are shown in Figure 2.13 and Figure 2.14 respectively. Evidently, in both the densified beam patterns, most of the regions show higher values of beam pattern gain. Hence, densification improves the beam pattern gain values.

Furthermore, Figure 2.15 provides the CDF plot of the beam pattern gain. Evidently, the

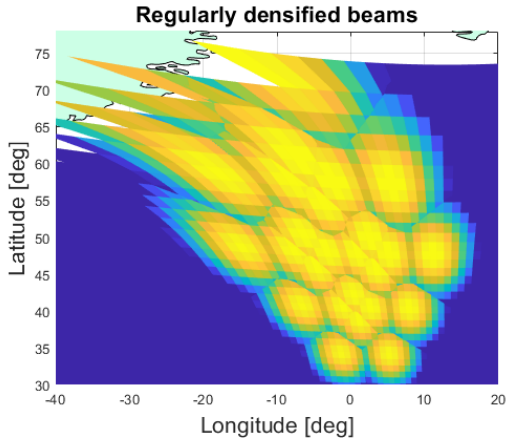

Figure 2.13: Improved antenna gain by regularly densified 16 beams

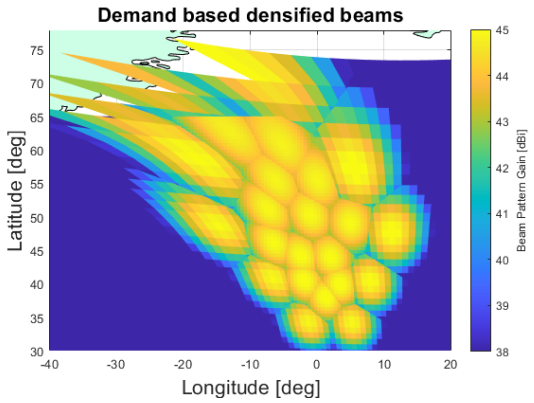

Figure 2.14: Improved antenna gain by demand driven densified 13 beams

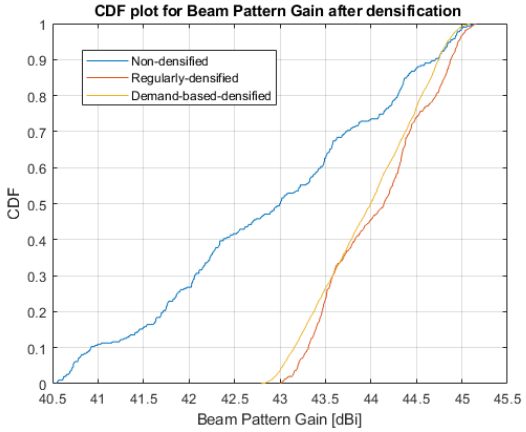

Figure 2.15: Beam Pattern gain after densification

beam pattern gain values have improved considerably (worst case gain of approximately 2.5 dB) after densification. Furthermore, regularly densified beam pattern shows slightly better performance against the demand based densification.

2.6.2 Impact of densification with 4 color frequency reuse

The table 2.2 provides the bandwidth and power allocation for 4CR frequency analysis. For fair comparison, we consider equal power and bandwidth distribution before and after densification. At target hot-spot area, the satellite total radiated power is considered as 166.67 W. This power is shared between 4 beams in the case of non-densified scenario and furthermore, it is shared between 16 beams in the regularly densified case and between 13 beams in the case of demand-driven densified case. Also, for 4CR frequency reuse, the total bandwidth of 500 MHz is divided into two, considering that the additional two colors could be obtained from polarization.

Table 2.2: Power and Bandwidth allocation for 4CR frequency reuse

Beam Pattern	**Power per beam**	**Bandwidth per beam**
Non-densified beam	41.67 W	250 MHz
Regularly densified beam	10.4175 W	250 MHz
Demand-driven densified beam	12.8215 W	250 MHz

The Figure 2.16 shows the CDF plots of the per-beam average SINR and Figure 2.17 shows the Average user SINR for 4CR frequency reuse. The SINR performance degrades from non-densified case to demand-driven densified case and further decreases when the densification is carried with 16 regular beams. Evidently, SINR decrease with the increase in the number of beams. This is majorly because higher number of beams will increase the interference signal.

Figure 2.18 shows the per beam average capacity and Figure 2.19 shows the mean capacity for 4CR frequency reuse. As the bandwidth per beam do not change upon densification with 4CR frequency reuse, the DVB-S2X defined capacity results are inline with the previously discussed SINR performance.

Due to reduced SINR with the increase in the number of beams, the densification perform poorly in terms of offered per beam average capacity by using same 4CR frequency reuse. Hence, in the following sections, we evaluate the performance of densification with other frequency reuse factors. However, from the Figure 2.20, the system capacity has increased

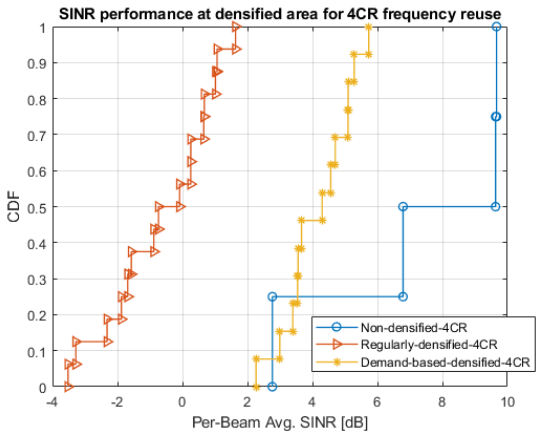

Figure 2.16: SINR performance at densified area for 4CR frequency reuse

considerably after densification, especially for demand driven densification.

Furthermore, we defined demand of beam k as $D_k = \sum_{n \in k} d_n$, where d_n is the demand of a user n served by beam k. The offered capacity per beam is denoted by $C_k = \sum_{n \in k} c_n$, where c_n is the offered capacity to a user n served by beam k. Then, we define mean demand satisfaction of beam k in percentage as $DS_k = \frac{C_k}{D_k} \times 100$, such that if $DS_k > 100$, then $DS_k = 100, \forall k$. Furthermore, we define the system demand satisfaction as $DS_{sys} = \sum_{k=1}^{K} DS_k$. Figure 2.21 shows the demand satisfaction before and after densification while using 4CR frequency reuse scheme. Evidently, it can seen that the mean beam demand satisfaction has increased upon regular densification and further increased by demand driven densification.

2.6.3 Impact of densification with full frequency reuse and precoding

In this section, we evaluate the benefits of precoding (Minimum Mean Square Error (MMSE) precoder [89]) with beam densification. The major advantage of precoding is that the total available system bandwidth (500 MHz) is now available for all beams. Furthermore, as we had exploited the benefits of polarisation in other cases, for fair comparison, the available bandwidth per beam while using FFR is 1000 MHz. The power allocation remains same as described in Table 2.2.

The Figure 2.22 shows the CDF plots of the per-beam average SINR and Figure 2.23 shows the Average user SINR for full frequency reuse. Both regular and demand based densification using FFR without precoding perform very poor. Furthermore, demand driven densification using FFR with precoding has performed slightly better than regular densification using FFR

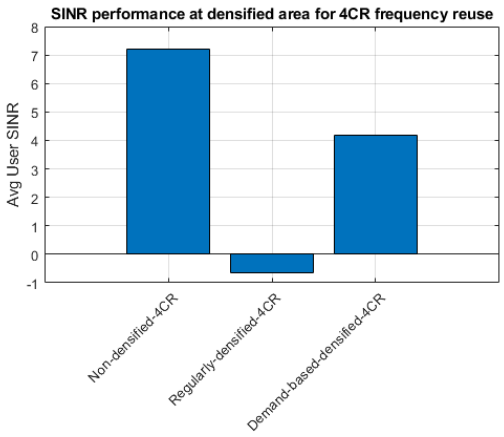

Figure 2.17: SINR performance at densified area for 4CR frequency reuse

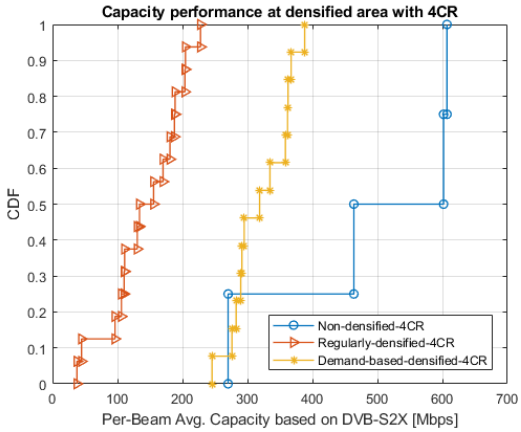

Figure 2.18: Capacity performance based on DVB-S2X at densified area for 4CR frequency reuse

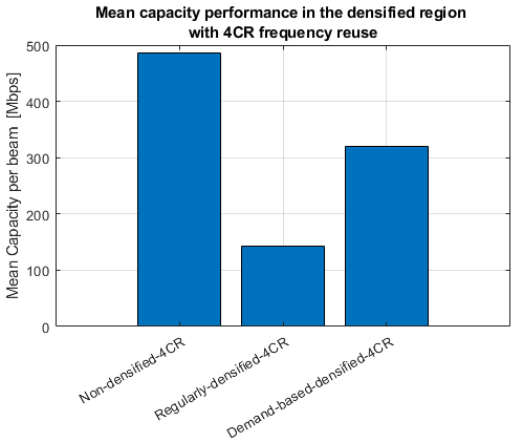

Figure 2.19: Mean capacity performance based on DVB-S2X at densified area for 4CR frequency reuse

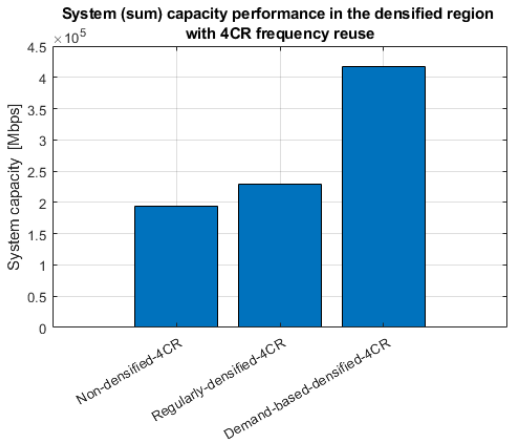

Figure 2.20: System (sum) capacity performance based on DVB-S2X at densified area for 4CR frequency reuse

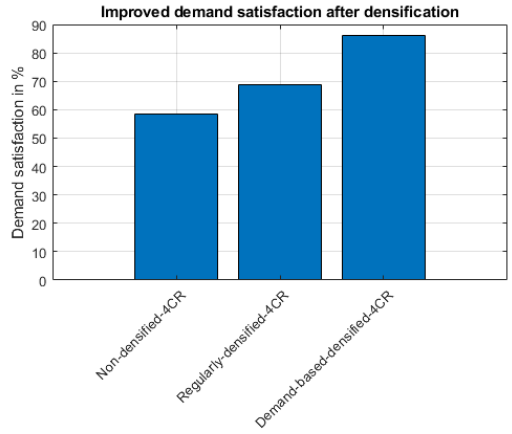

Figure 2.21: Demand satisfaction with 4CR frequency reuse

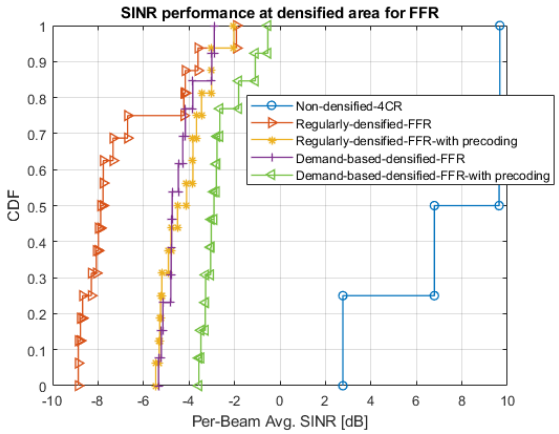

Figure 2.22: SINR performance of Precoding with FFR

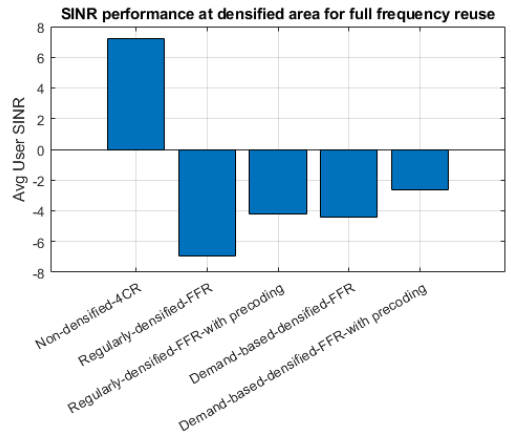

Figure 2.23: SINR performance at densified area for full frequency reuse

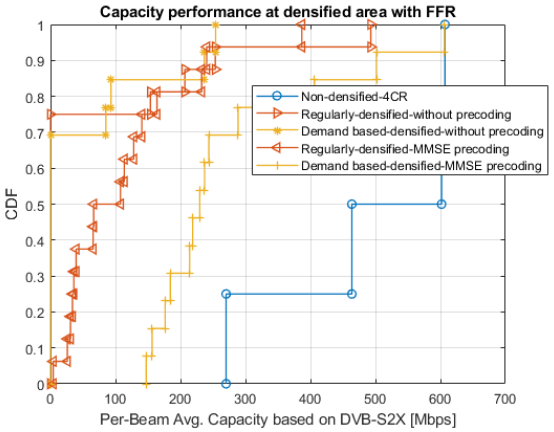

Figure 2.24: Capacity performance based on DVB-S2X at densified area for full frequency reuse

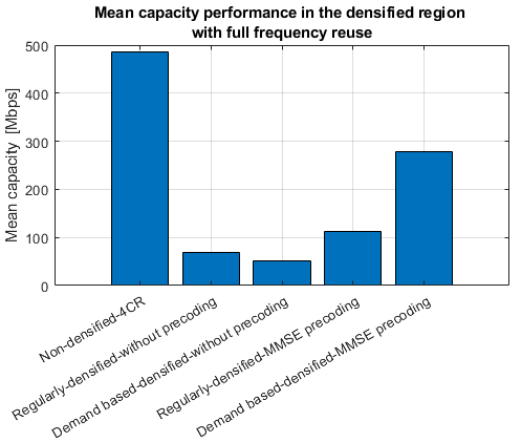

Figure 2.25: Mean capacity performance based on DVB-S2X at densified area for full frequency reuse

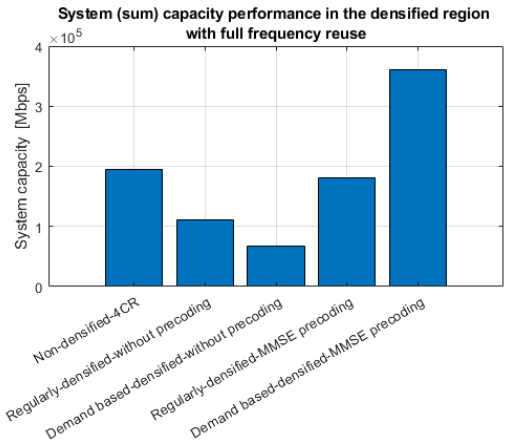

Figure 2.26: System (sum) capacity performance based on DVB-S2X at densified area for full frequency reuse

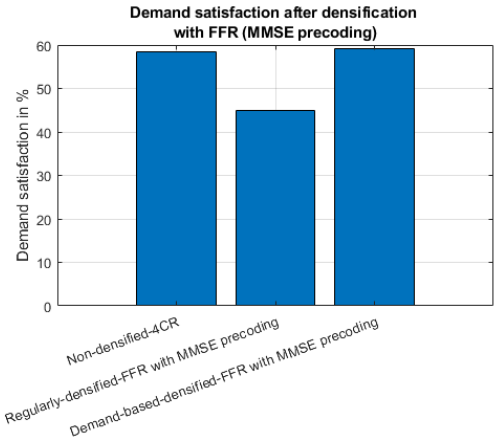

Figure 2.27: Demand satisfaction with full frequency reuse

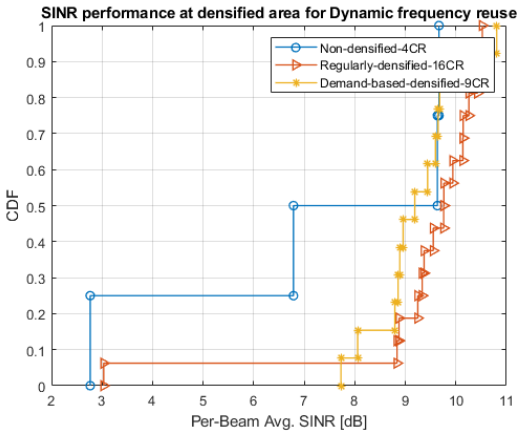

Figure 2.28: SINR performance at densified area for DFR frequency reuse

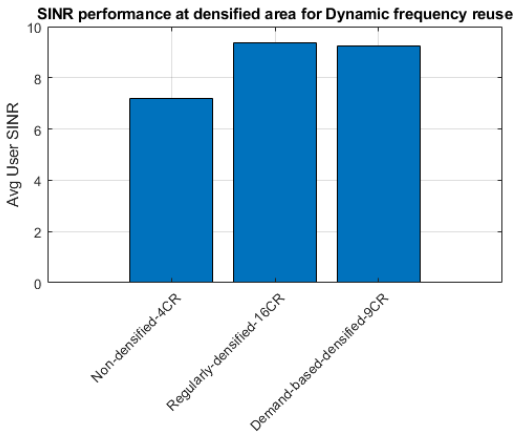

Figure 2.29: SINR performance at densified area for DFR frequency reuse

with precoding. Conclusively, it can be inferred that using full frequency reuse schemes, the SINR can degrade considerably after densification. Such poor performance in SINR is due to strong levels of interference created by increased number of beams after densification.

Figure 2.24 shows the per beam average capacity and Figure 2.25 shows the mean capacity for full frequency reuse. When precoding is not considered, in both regular and demand driven densification, we notice that the performance is very poor due to poor SINR performance and the system fails to satisfy the minimum link budget requirements. On the other hand, when precoding is considered with densification, the DVB-S2X defined capacity is relatively good even with poor SINR performance, as the bandwidth per beam availability is very high for FFR. Furthermore, from Figure 2.26, system capacity increases after densification, especially for demand based densification.

Figure 2.27 shows the demand satisfaction before and after densification while using FFR scheme. We consider only the results with precoding as the system performs poor without precoding. Evidently, it can seen that the mean beam demand satisfaction does not gain much with densification.

2.6.4 Impact of densification with Dynamic frequency reuse

In this section we evaluate the performance of other dynamic color frequency reuse schemes. For regular beam densification we use 16CR color frequency reuse scheme as we expect its interference levels to be similar to 4CR non densified beams. Furthermore, for demand driven beam densification, we use optimized color coding proposed in section V. The power allocation and bandwidth available for dynamic frequency reuse is shown in the table 2.3.

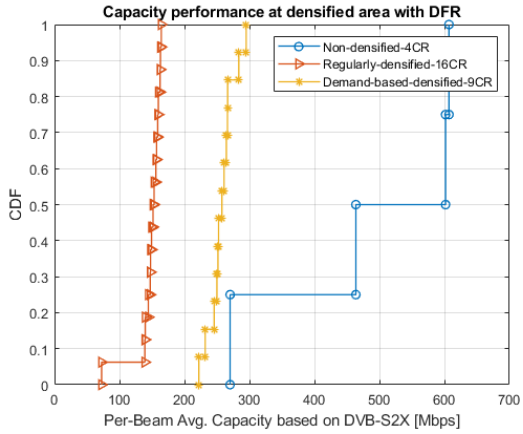

Figure 2.30: Capacity performance based on DVB-S2X at densified area for Dynamic frequency reuse

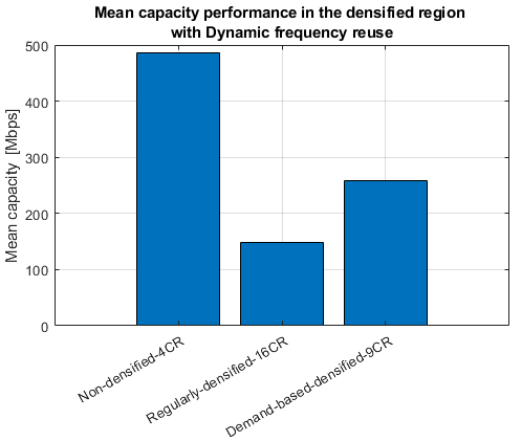

Figure 2.31: Mean capacity performance based on DVB-S2X at densified area for dynamic frequency reuse

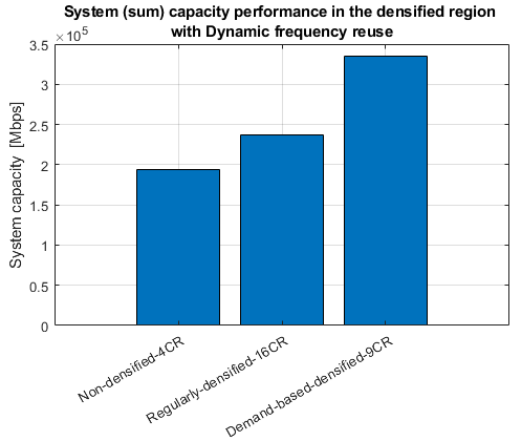

Figure 2.32: System (sum) capacity performance based on DVB-S2X at densified area for dynamic frequency reuse

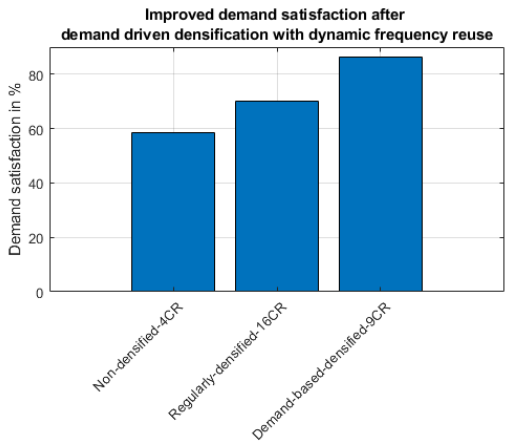

Figure 2.33: Demand satisfaction with dynamic frequency reuse

Table 2.3: Power and Bandwidth allocation for dynamic frequency reuse

Beam Pattern	**Power per beam**	**Bandwidth per beam**
Non-densified beam	41.67 W	250 MHz
Regularly densified beam	10.4175 W	62.5 MHz
Demand-driven densified beam	12.8215 W	111.11 MHz

The Figure 2.28 shows the CDF plots of the per-beam average SINR and Figure 2.29 shows the Average user SINR for dynamic frequency reuse. Regular densification with 16 CR has resulted to gain high in SINR. Furthermore, demand driven densification with dynamic color coding (9CR frequency reuse) has performed slightly poor than demand driven densification with 16CR frequency reuse. However, the worst case SINR of demand driven densification is better in comparison to Regular densification with 16 CR frequency reuse. Conclusively, it can be inferred that using higher order frequency reuse schemes, the SINR can improve considerably after densification.

Figure 2.30 shows the per beam average capacity and Figure 2.31 shows the mean capacity for dynamic frequency reuse. With the increase in colors, the available bandwidth decreases and hence DVB-S2X defined capacity reduces for 9CR frequency reuse and further reduces for 16CR frequency reuse. However, from the Figure 2.32, the system capacity is still better after densification, especially for demand based densification with 9CR frequency reuse.

The demand satisfaction for dynamic frequency reuse is shown in Figure 2.33. Evidently, the demand satisfaction has increased considerably after densification, especially for demand driven densification with 9CR reuse.

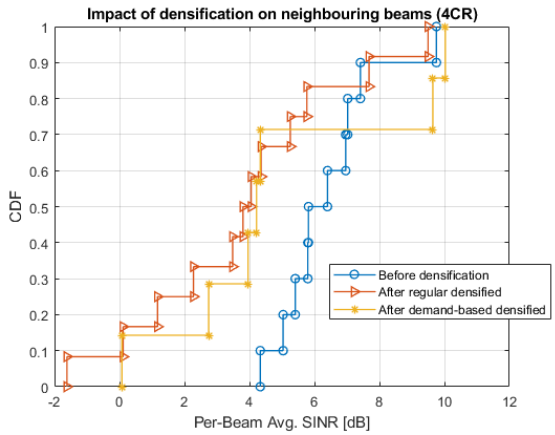

Figure 2.34: CDF plots of per beam avg SNIR on neighbouring beams

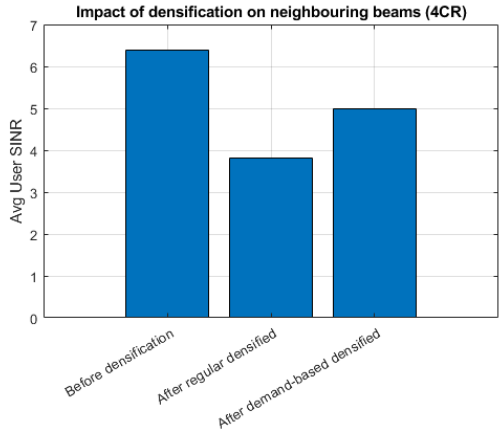

Figure 2.35: Average user SINR on neighbouring beams

2.6.5 Performance evaluation neighbouring beams of densification

In this section, we assess the impact of densification on the neighbouring beams of the densified region. Again, we consider unicast scheduling with $K = 10$ users scheduled in $K = 10$ neighbouring beams where each of the user position in the neighbouring beams are randomly selected.

Figure 2.34 and Figure 2.35 show the impact of densification on the neighbouring beams of the densified region. From CDF plot of Figure 2.34, we can infer that values of per beam average SINR of the neighbouring beams reduce considerably due to regular densification. However, after the proposed demand based densification, even though per beam average SINR of the neighbouring beams is still lower than the non densified case, it has relatively improved in comparison to regular densification. Furthermore from Figure 2.35, the average user SINR of the neighbouring beams drops after regular densification. However, it improves

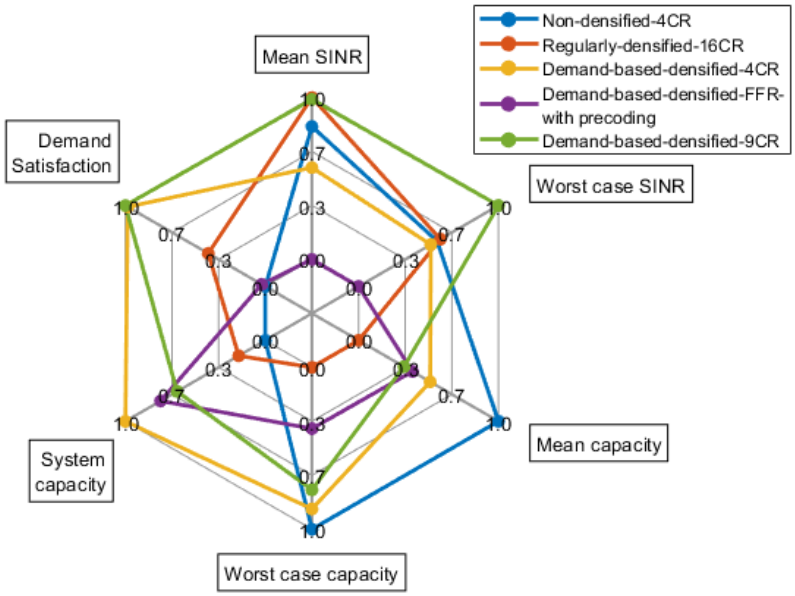

Figure 2.36: Average user SINR on neighbouring beams

considerably when we consider the proposed demand based densification. This is majorly because, regular densification increases the beam overlap on the neighbouring beams. However, when we consider the demand based densification, such overlap on the neighbouring beams is considerably reduced.

2.7 Conclusion

In this work, we first discuss the conventional multi-beam GEO satellite system and its failure to provide demand satisfaction in high demand hot spot regions. Accordingly, we then propose a regular beam densification as the first step in achieving demand satisfaction. Furthermore, considering the uneven demand distribution in the high demand region, we propose a novel dynamic beam densification procedure which leverages to choose ideal number of beams and their positions. Lastly, using graph theory, we propose a dynamic frequency allocation strategy to reduce the increased inter-beam interference upon beam densification.

To summarize the result of this work, we use a two-dimensional radar chart in Figure 2.36, displaying multivariate data in the form of a chart of six quantitative variables (normalized) such as mean SINR, worst case SINR, mean capacity, worst case capacity, system capacity and demand satisfaction. Evidently, the non-densified 4CR frequency reuse scheme fail to provide demand satisfaction with the least demand satisfaction score. Regularly densified

16CR frequency reuse scheme, slightly increases the demand satisfaction with good SINR performance but provides poor capacity results due to scarcity of the bandwidth. Furthermore, demand based densified 4CR frequency reuse provides good demand satisfaction and capacity performance but performs poor at the user SINR level. Notwithstanding, when same demand based scheme is considered with precoding, the user SINR levels are very poor. Furthermore, when the proposed demand based densified 9CR (dynamic frequency) is considered, it maximizes most of the metrics of the radar chart. Lastly, when we studied the impact of densification on the neighbouring beams, it was evident that after regular densification, the SINR performance of the neighbouring beams is affected. However, when we employ the proposed demand based densification, such adverse effects are considerably reduced. Conclusively, the proposed demand-based densification with dynamic frequency reuse is the best choice regarding most of the quantitative variables.

2.8 Acknowledgement

The authors would like to thank Dr. Nicolo Mazzali and Dr. Alberto Mengali from European Space Agency(ESA) for kindly providing the beam patterns for this study, and for their support, and constructive comments on the results.

Chapter 3

Clustering based beam footprint design

3.1 Introduction

Internet broadband services have gained immense attention not only for business competitiveness but also for helping social inclusion. While most of the broadband demand in the urban regions are satisfied using terrestrial technologies, the broadband demand in the remote locations strongly relies on satellite broadband services [98]. Lately, the increase in the demand has made satellite providers switch from legacy single beam architecture to High Throughput Satellite (HTS) systems with multiple spot beams which reuse carrier bandwidth across several beams to satisfy the rising demand [16]. Since the launch of the first high-speed, all-digital communications satellite named Advanced Communications Technology Satellite (ACTS) by NASA, technologies such as Onboard Digital Processing (ODP) and Switching has been widely popular. More recently, the shape and position of satellite beams can be adjusted using Dynamic Beamforming Networks (DBN) to enhance frequency utilization efficiency through space-division multiplexing [99]. The radiation pattern of antenna arrays can be controlled using the beamforming technique, without physical movement of the antennas [100] and hence is key enabler for the adaptive beam pattern and footprint plan.

3.1.1 Literature Review

There exist a dearth of efficient beam footprint plans in literature. The authors of [15] have made an early contribution in planing the beam layout of a reflector multi-beam antenna

Table 3.1: Table Of Acronyms

HTS	High Throughput Satellites
FMPF	Fixed Multi-beam Pattern and Footprint
AMPF	Adaptive Multi-beam Pattern and Footprint
DBN	Dynamic Beamforming Networks
ACTS	Advanced Communications Technology Satellite
ODP	Onboard Digital Processing
FSS	Fixed Satellite Sevices
QoS	Quality of service
AFR	Array-Fed Reflector
PFD	Flux Density
ESA	European Space Agency
WED	Weighted Euclidean Distance
DM	Distance Metric
PAM	Partitioning Around Medoids
CLARA	ClusteringLARge Applications
SEDAC	SocioEconomic Data and Applications Center
CDF	Cumulative Distribution Function
NCD	Normalized Capacity Deviation

with overlapping beams. The authors of [17] compare the conventional contoured beam antennas with multi-beam antenna and propose fixed beam diameters for a specified number of beams to ensure global coverage using overlapping spot beams with a hexagonal grid layout. Furthermore, the authors of [72, 101, 102] discuss the antenna requirements to plan a good beam pattern for fixed beam footprint plans. Hence, all the early works consider only the geometric feasibility of the spot beams in the beam pattern and footprint plan, and focus on having hexagonal beams of equal size and ensure global coverage. Therefore, the coverage region and the offered throughput remains same for all of the multiple spot beams irrespective of the traffic demand.

However, much recent works have focused on adaptive plans to accommodate fluctuations in traffic demand. The authors of [103] discuss the global resource management for dynamic beam steering due to changes in QoS requirements and channel conditions of users. The authors of [104] optimize beam-directivity and transmit-power according to traffic demand to improve the overall system throughput. The authors of [105] adapt satellite's transmitting antenna boresight to maximize signal to noise power ratio (SNR) of satellite ground station and minimize interference to terrestrial networks. The authors of [106] propose an optimization tool to jointly optimize the number of beams, beam width, power and bandwidth allocation

in order to match the provided data rate to the predicted traffic demand but do not optimize the beam positions and beam shape. The authors of [107] propose a mathematical model to derive multi-spot beam arrangements and discuss the relationship between the placement of a multi-spot beam and user throughput. They study only the effect of geographic distances between spot beams in the same frequency band and the geographic distances between adjacent spot beams in different frequency bands on the overall system throughput but do not implement adaptability in terms of flexible beam size and beam position in beam plan. To the best of our knowledge, none of the authors have considered the mobility aspects of the non-uniformly distributed users and dynamically changing beam demand during the beam pattern and footprint planning. Also, unlike the recent works, the proposed network planning is not a static process but a dynamic one that has to be repeated multiple times during a day. Furthermore, in all the previous works some beams are under-used while others are too crowded and hence is only a sub optimal solution.

3.1.2 Contribution

The contribution of the paper is as follows:

1. We propose a novel Adaptive Multi-beam Pattern and Footprint (AMPF) plan that achieve even traffic load distribution across all the beams in the HTS system that simplifies the radio resource management, payload allocation and frequency allocation. To achieve such plan, in this work, we not only consider spatiotemporally varying traffic demand but also the distributed and non-uniform mobile geographic locations of the users.

2. We propose a novel method for the planning of the multi-beam pattern based on geographical clustering (weighted K-means clustering) of the users, which is optimally matched to the heterogeneous demand distribution within the field of view of the satellite. Using the proposed method it is possible to reduce the variations of the traffic load among the beams, which leads to better traffic matching.

3. To ensure a required coverage region, we use Voronoi Tessellation to plan irregular non-hexagonal convex Voronoi polygons as beam regions. Such an approach is relatively new in beam pattern and footprint plan.

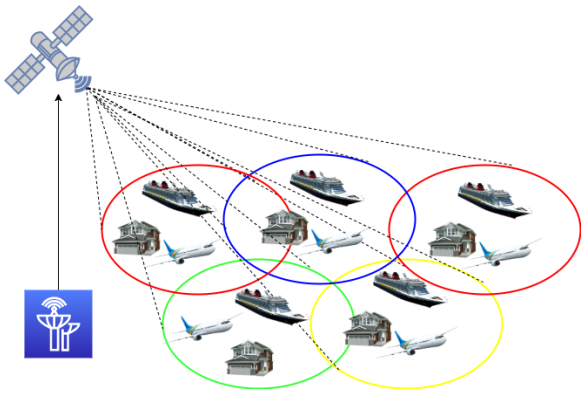

Figure 3.1: High throughput Multi-beam Satellite System architecture using four colour scheme.

4. Contrary to the related works, in AMPF plan, we propose elliptical beams which add in one more degree of freedom for beam footprint plan.

5. Lastly, unlike the previous works, to plan practical and meaningful antenna patterns, we consider the design parameters of the beam pattern and footprint parameters in the angular domain as seen from the satellite. This is because the satellite beam is defined with parameters that are in fact angles centred at the satellite. Hence, the gain pattern of the antenna which is on-board the satellite is naturally described in the satellite angular domain as ellipses. However, when these elliptical gain patterns are projected on the surface of the Earth, they undergo distortion in both beam shape (ellipses taking the shape of convex polygons) and power flux density. Hence, performing user clustering and beam planning on the satellite angular domain prevents the errors introduced by such distortions.

Notation: We use upper-case and lower-case bold-faced letters to denote matrices and vectors, respectively. $\circ$ denotes the element-wise Hadamard operations, $(\cdot)^T$ denotes the transpose of $(\cdot)$. $\|.\|$ depicts the Euclidean norm, $\subseteq$ denotes subset and $P(.)$ denotes power set. If $\mathfrak{S}$ is a set, then $|\ \mathfrak{S}\ |$ denotes cardinality of set $\mathfrak{S}$ and if $\mathfrak{M}$ is a matrix, then $|\ \mathfrak{M}\ |$ denotes determinant of matrix $\mathfrak{M}$.

3.2 System Model

3.2.1 Multi-beam Satellite System

We consider a Multi-beam Satellite system as shown in Figure 3.1 that employs multiple spot beams to provide the required coverage. Non-uniform and distributed broadband users including Fixed Satellite Services (FSS) users, aeronautical users and maritime users are considered. Furthermore, to reduce the interference at the beam edges, the four colours frequency reuse scheme scheme [108] is employed such that every beam is allocated a different carrier frequency or a different polarization to that of its neighbour.

The space-segment consist of a programmable payload GEO satellite with Array-Fed Reflector (AFR) antennas with beamforming capabilities that can alter the beam size and beam positions by digital signal processing.

The Gateway is a ground station and is connected to the internet backbone network. We assume that the optimization is done in the ground station. Also, we assume that the traffic demand does not change very aggressively over time due to the user multiplexing effect.

3.2.2 Beam Footprint and Beam Pattern

The beam footprint of a Multi-beam satellite system shows the dispersion of multiple beams with defined beam widths across the ground area of its coverage. In this work, we consider elliptical beams generated in the satellite angular domain. This adds in one more degree of freedom to optimize the beam footprints. Nevertheless, the projection of these ellipses on the surface of the Earth will result in non-elliptical polygonal beams whose geodetic shape on the surface of the Earth expressed using Earth's latitude and Earth's longitude is dependent on the curvature of the Earth [109].

A beam pattern represents the magnitude of the electric or magnetic field, as a function of the angular space. The beam centre which defines the beam position is where the antenna gain of the beam is maximum. The beam widths that define the beam shape are the locations corresponding to the 3dB reduction of the antenna gain compared to the beam centre. A beam pattern plan involves prudently choosing multiple metrics such as number of beams, beam centre and beam widths of all the beams in a Multi-beam satellite system.

The authors of [108] and [110] approximate the beam contour using Bessel function for beam gain computation. However, as we consider the beam shape to be elliptical in the

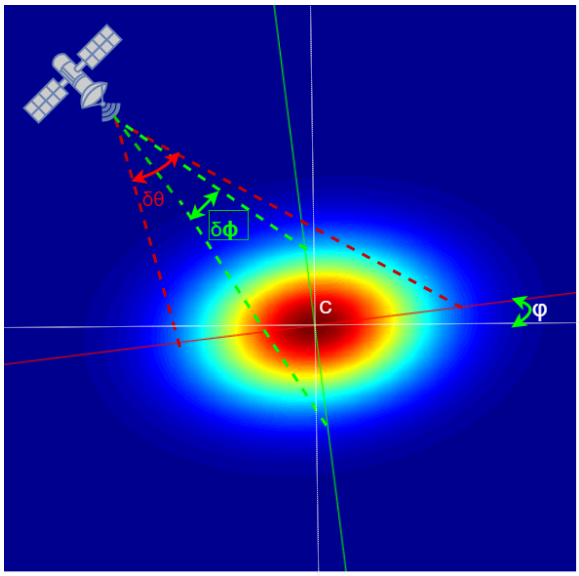

Figure 3.2: Two-dimensional Gaussian function approximation to define the beam pattern

angular domain of the satellite, we approximate the beam contour to be a two-dimensional Gaussian function. Figure 3.2 shows the heat map corresponding to the Power Flux Density (PFD) for a single beam. Every elliptical beam corresponds to a specific value of beam widths $\delta\theta$ and $\delta\phi$ (defined by semi-major axis and semi-minor axis of the elliptical beam), beam centre, C (The point of intersection of semi-minor and semi-major axis) and the beam orientation or the tilt angle, φ.

The system capacity can be increased by increasing the number of beams in the forward link of the multi-beam satellite system. However, increasing the number of beams will increase the number of amplifiers in the space segment and this will increase both the manufacturing cost and the launch cost for the satellite operators. In our design, we consider 71 transmission beams in the forward link and do not optimize over the number of beams. The 71 beams constraint is applied to have a fair comparison with the benchmark FMPF reference beam pattern provided by European Space Agency (ESA) [52, 111]. Furthermore, the number of beams corresponds to the number of information streams that can be processed in parallel by the satellite payload. Switching off beams and thus info streams would require additional configuration changes on the payload.

3.2.3 Multi-beam Satellite Channel

We consider an HTS Multi-beam Satellite system with N broadband users and K beams. The received signal y_n at the user u_n in the k^{th} beam is as expressed as,

$$y_n = \mathbf{h}_n^T \mathbf{s} + \mathfrak{N}_n, \tag{3.1}$$

where $\mathbf{h}_n \in \mathbb{C}^{K\times 1}$ is the CSI vector corresponding to this particular user. $\mathbf{s} \in \mathbb{C}^{K\times 1}$ represents the transmitted signal vector. $\mathfrak{N}_n$ is a random variable distributed as $\mathcal{CN}(0, \sigma^2)$, modelling the zero-mean Additive White Gaussian Noise (AWGN) measured at the u_n's receiving antenna.

By rearranging all the users' received signals in a vector $\mathbf{y} = [y_1 \dots y_N]^T \in \mathbb{C}^{K\times 1}$, we can rewrite the above model as,

$$\mathbf{y} = \mathbf{H}\ \mathbf{s} + \mathfrak{N}, \tag{3.2}$$

where $\mathbf{H} = [\mathbf{h}_1 \dots \mathbf{h}_N]^T$ represents the system channel matrix, which is determined by the satellite antenna gain, the path loss, the received antenna gain and the noise power. More precisely, the (n, k)th component of $\mathbf{H}$ is given by,

$$[\mathbf{h}]_{n,k} = \frac{\sqrt{G_{Rn} G_{kn}}}{(4\pi \frac{\mathfrak{D}_{nk}}{\lambda})}, \tag{3.3}$$

where G_{Rn} is the receiver antenna gain (that mainly depends on the receiving antenna aperture) and G_{kn} are the gains defined by the multibeam satellite radiation pattern and user locations. $\mathfrak{D}_{nk}$ is the distance between the satellite transmit antenna k and the nth user's receiving antenna. Usually, due to the long propagation distance, $\mathfrak{D}_{nk} \approx \mathfrak{D}_n$. Finally, λ is the wavelength of transmission.

3.3 Problem Statement

The benchmark FMPF plan system comprises of a fixed number of beams with predetermined beam shape obtained by 71-beam GEO 0E satellite operating at the Ka exclusive band 19.7 to 20.2 GHz [112–114] is as shown in Figure 3.3. The fixed plan provides coverage to the Europe region using 71 beams. However, broadband users across Europe are not uniformly distributed and the broadband traffic demand for an FSS user defers from a maritime user. Also, aeronautical and maritime users are mobile users and their positions vary with time. In

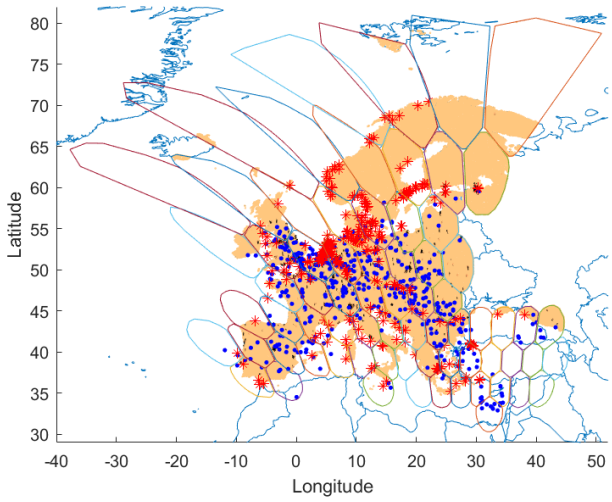

Figure 3.3: Benchmark FMPF plan beam footprint over Europe using 71 Fixed Beams showing flight user locations in blue, ship user locations in red and FSS user locations in beige.

benchmark FMPF plan, as the position and size of the beams are fixed, the offered throughput remains relatively similar across all the beams irrespective of change in the number of users in the beam and beam demand. Therefore, such rigid plans will fail to distribute broadband traffic demand across all the beams evenly and result in either under-use the offered throughput (beam capacity is unused) or overload the beam (beam demand is unmet).

Therefore, to plan adaptive beams for mobile users with variable demand, we first need to find the best partition of all the users into sets of adjacent users in an euclidean sense such that total system demand is evenly distributed among all the sets and then, plan a beam which is suitable to serve each user set.

Similar set partitioning problems but for a different application is discussed in [115] and is an optimization form of exact cover. To solve set partitioning problems, we find the best disjoint cover within some collection $\mathcal{S} = \{\mathcal{S}^1, \mathcal{S}^2 ... \mathcal{S}^K\} \subseteq \mathcal{P}(\mathcal{N})$, where $\mathcal{N}$ is the universal set containing all the broadband users in the system and $\mathcal{P}(\mathcal{N})$ is the power set of $\mathcal{N}$. We define the convex hull of any set $\mathcal{S}^k$ as,

$$\mathcal{H}^k = \sum_{n \in \mathcal{S}^k} \lambda_n \mathbf{x}_n : \lambda_n \geq 0 \quad \forall n, \quad \sum_{n \in \mathcal{S}^k} \lambda_n = 1 \tag{3.4}$$

where $\mathbf{x}_n$ as the 2D coordinate vector of a broadband user n.

We define d_n as the traffic demand and $D_k = \sum_{n \in \mathcal{S}^k} d_n$ as the beam demand that corresponds to the sum of the demand of all the users belonging to the beam k.

The objective function is fair distribution of the system demand across all the beams and is defined as,

$$\max_{\mathcal{S}} \quad \frac{\left(\sum_{k=1}^{K} D_k\right)^2}{K \sum_{k=1}^{K} D_k^2}; \tag{3.5a}$$

$$\text{Subject to} \bigcup_{k=1}^{K} \mathcal{S}^k = \mathcal{N}, \tag{3.5b}$$

$$\mathcal{S}^i \cap \mathcal{S}^j = \emptyset, \forall i \neq j \tag{3.5c}$$

$$\mathcal{S}^i \neq \emptyset, \forall i, \tag{3.5d}$$

$$\mathcal{H}^i \cap \mathcal{H}^j = \emptyset, \forall i \neq j, \tag{3.5e}$$

where the first constraint in (3.5b) ensures that all the users are under the coverage region. The second constraint in (3.5c) assures that any user will be served by only one beam. The third constraint mentioned in (3.5d) ensures that the beams have at least one user and to avoid planning beams with zero demand. The last constraint in (3.5e) guarantees that each partitioned set is a convex set and assures that the convex hulls' of partitioned sets do not overlap within the 2D Euclidean space. In this approach, the feasible solutions cover the universal set $\mathcal{N}$ rather than any of its subsets and hence is a restricted setting of set partitioning.

However, set partitioning problems are non-deterministic polynomial acceptable problems that are NP-hard and are at least as hard as the hardest problems in NP [116]. Therefore, solving the set partition problem by optimizing for best disjoint cover using classical optimization techniques is either cumbersome [117] or does not guarantee a global minimum [118].

Alternatively, partitioning problems can also be solved using clustering methods [119]. But, the optimizing problem in clustering methods is also NP-hard. However, clustering methods are iterative and offer probabilistic guarantees [120]. To define the problem using clustering approach, we consider metric spaces where we endow universe $\mathcal{N}$ with a metric space $(\mathcal{X}, r)$ such that $\mathcal{N} \subseteq \mathcal{X}$, where $\mathcal{X}$ is a set of all points in a 2D Euclidean space and r is a distance metric on $\mathcal{X}$. Then to obtain the cluster sets $\{\mathcal{T}^1, \mathcal{T}^2 ... \mathcal{T}^K\}$ that are optimized for even demand distribution, we can define the partitioning problem using clustering by,

$$\min_{\{\mathcal{T}^1,\mathcal{T}^2...\mathcal{T}^K\}} \quad \sum_{k=1}^{K}\sum_{n\in\mathcal{T}^k} r(\mathbf{x}_n, \boldsymbol{c}_{\mathcal{T}^k}) \left(\frac{\sum\limits_{n\in\mathcal{T}^k}(d_n)}{\sum\limits_{n=1}^{N}(d_n)} \right); \tag{3.6a}$$

$$\text{Subject to} \quad \bigcup_{k=1}^{K} \mathcal{T}^k = \mathcal{N}, \tag{3.6b}$$

$$\mathcal{T}^i \cap \mathcal{T}^j = \emptyset, \forall i \neq j, \tag{3.6c}$$

$$\mathcal{T}^i \neq \emptyset, \forall i, \tag{3.6d}$$

$$\boldsymbol{c}_{\mathcal{T}^k} = \frac{1}{\sum\limits_{n\in\mathcal{T}^k} d_n} \sum_{n\in\mathcal{T}^k} d_n \mathbf{x}_n. \tag{3.6e}$$

The objective function is the weighted distance of each cluster member from the cluster center, where $r(\mathbf{x}_n, \boldsymbol{c}_{\mathcal{T}^k}) = ((\mathbf{x}_n - \boldsymbol{c}_{\mathcal{T}^k})(\mathbf{x}_n - \boldsymbol{c}_{\mathcal{T}^k})')$ is the euclidean distance between any user n and the cluster center $\boldsymbol{c}_{\mathcal{T}^k}$. Weights are added to distribute the demand evenly among all the beams and are defined as the ratio of beam demand $\left(\sum_{n\in\mathcal{T}^k} d_n\right)$ to the system demand $\left(\sum_{n=1}^{N} d_n\right)$.

In the constraint (3.6e), $\boldsymbol{c}_{\mathcal{T}^k}$ is two element vector in the 2D Euclidean space representing the weighted cluster centroid of the cluster k. The clustered sets $\{\mathcal{T}^1, \mathcal{T}^2...\mathcal{T}^K\}$ are by default convex sets and satisfies the constraint in (3.5e) and hence is not included in the clustering problem. It should be noted that even though the two problems are not equivalent, the clustering approach follows a similar rationale and provides easier structure.

Furthermore, the convex hulls $\{\mathcal{H}^1, \mathcal{H}^1...\mathcal{H}^K\}$ encompassing the clusters $\{\mathcal{T}^1, \mathcal{T}^2...\mathcal{T}^K\}$ are convex polygons in the 2D Euclidean space. Therefore, we have an additional problem on how to translate the vertex vectors of the convex polygon into simple beam shape that can be used as a template by the antenna and beamforming network designers. Henceforth, we propose to approximate convex polygons into ellipses. Early works [121] [122] in literature addresses the mathematical problem of approximating a convex polygon into an ellipse. However, in this work, we use an approach similar to [123] for its simplicity. Accordingly, if (x, y) represents vertex variables of the convex hull $\mathcal{H}^k$ in 2D Euclidean space, then any general bivariate quadratic curve which can be expressed as,

$$ax^2 + 2bxy + cy^2 + 2dx + 2fy + g = 0, \tag{3.7}$$

should satisfy the Equations,

$$\Delta = \begin{vmatrix} a & b & d \\ b & c & f \\ d & f & g \end{vmatrix} \neq 0, \tag{3.8a}$$

$$J = \begin{vmatrix} a & b \\ b & c \end{vmatrix} > 0, \tag{3.8b}$$

$$\frac{\Delta}{a+c} < 0, \tag{3.8c}$$

to be represented as an ellipse ($\mathcal{E}^k$) for which we need to find the best parameters for a, b, c, d, f, g in the Least Square sense [123].

The ellipses $\{\mathcal{E}^1, \mathcal{E}^1 ... \mathcal{E}^K\}$ represents K proposed beam footprints. The center ($\boldsymbol{c}_k$) of the ellipse ($\mathcal{E}^k$) represents the position of beam k in 2D Euclidean space. The semi-major and semi-minor axis ($\delta\theta_k$, $\delta\phi_k$) along with the rotation angle φ_k of the ellipse ($\mathcal{E}^k$) represents the shape of the beam k.

3.4 Proposed Solution

In the proposed AMPF plan, we first obtain cluster sets that evenly distributes the traffic throughput demand across all the beams. Later we approximate the convex hull of the cluster sets to ellipse by choosing beam positions ($\boldsymbol{c}_k$), beam size ($\delta\theta_k$, $\delta\phi_k$) and beam shape (φ_k) of all the K beams. In this section, we discuss the steps involved in achieving such a plan.

1. Firstly, to generate physically meaningful antenna patterns and to avoid the distortions introduced due to the curvature of the Earth, we transform the geographical coordinates of the user locations to the coordinates of the satellite angular domain.

2. Then, based on the location and broadband traffic demand of the users in the satellite angular domain, the broadband users are grouped into K clusters using weighted k-means clustering. The users in the same cluster will represent all the users under a beam.

3. Later, to ensure full coverage, we use Voronoi Tessellation and define the beam borders.

4. However, the beam shapes generated using Voronoi Tessellation are irregular polygons.

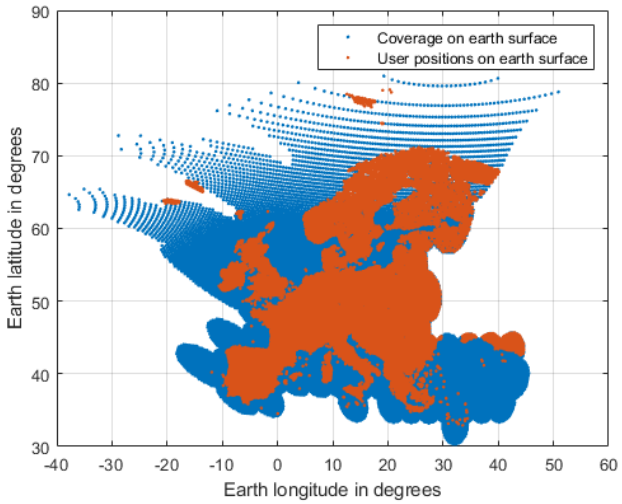

Figure 3.4: Sampled coverage area of the benchmark FMPF beams (shown in blue) and the user positions (shown in red) on the surface of the Earth.

Hence, considering the mathematical tractability and for topological packing, we approximate the Voronoi Polygons by ellipses. Now, the centre of the ellipses ($\boldsymbol{c}_k$) will define the K beam positions, the semi-major and semi-minor axis of the ellipses ($\delta\theta_k$, $\delta\phi_k$) will define the boundary of the beams and angle of rotation of ellipses (φ_k) will define the shape of the proposed beams.

5. The proposed beams in satellite angular domain are now projected back on the surface of the Earth for visualization.

6. Furthermore, to measure the performance of the proposed plan with the benchmark FMPF plan, we fit a 2D Gaussian elliptical function on the approximated ellipse and perform link budget calculations.

3.4.1 Domain Transformation

The sampled coverage area of the benchmark FMPF beams and the user positions on the surface of the Earth obtained using [124] are expressed as geodetic positions using latitude and longitude, as shown in Figure 3.4. Figure 3.5 shows the relation between the latitude/longitude on the Earth's surface and azimuth/elevation on the satellite angular domain. In the spherical coordinate system, considering the centre of the Earth as origin, we use a spherical-ordered-triple (R_e radius-of-the-Earth (6,871,000 meters), Latitude (angle in degrees), Longitude (angle in degrees)) to describe the geodetic position of any user on the

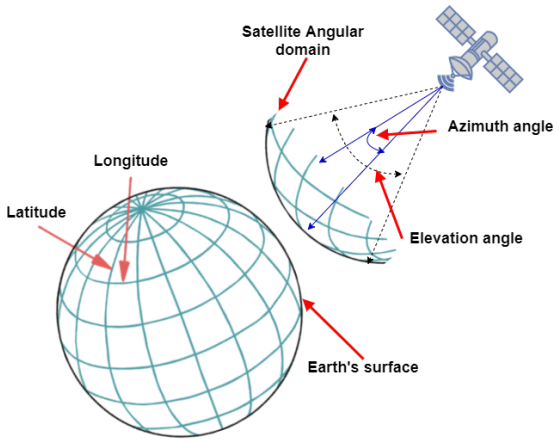

Figure 3.5: Difference between Earth's latitude-longitude domain and satellite angular domain. Latitude, longitude, elevation and azimuth angles are in degrees.

surface of the Earth. In the Cartesian coordinate system, the location of the user on the surface of the Earth is described using a Cartesian-ordered-triple in which each coordinate represents a distance.

We first convert the user position (Lat_U/Lon_U) from the spherical coordinate system to the Cartesian coordinate system expressed as Cartesian-ordered-triples $(X_{U,E}, Y_{U,E}, Z_{U,E})$ [125] using,

$$X_{U,E} = R_e \times \cos(Lat_U) \times \cos(Lon_U), \tag{3.9a}$$

$$Y_{U,E} = R_e \times \cos(Lat_U) \times \sin(Lon_U), \tag{3.9b}$$

$$Z_{U,E} = R_e \times \sin(Lat_U). \tag{3.9c}$$

Similarly, we also convert the satellite position from the spherical coordinate system (Lat_S/Lon_S) to the Cartesian coordinate system $(X_{S,E}, Y_{S,E}, Z_{S,E})$. For such conversion, we consider a geostationary satellite with no tilt that orbits directly above the Earth's equator at the 0-degrees latitude and 0-degree longitude at an elevation of 35,786,000 meters. Then using user and satellite Cartesian-ordered-triples we estimate the position of the user considering the satellite as the origin using,

$$X_{U,S} = X_{U,E} - X_{S,E}, \tag{3.10a}$$

$$Y_{U,S} = Y_{U,E} - Y_{S,E}, \tag{3.10b}$$

$$Z_{U,S} = Z_{U,E} - Z_{S,E}. \tag{3.10c}$$

Finally, we convert the user position from the Cartesian coordinate system to the spherical coordinate system [125] to get the user position in satellite angular domain using,

$$azimuth_U = \tan^{-1} \frac{Y_{U,S}}{X_{U,S}}, \tag{3.11a}$$

$$elevation_U = \tan^{-1} \frac{Z_{U,S}}{\sqrt{(X_{U,S})^2 + (Y_{U,S})^2}}. \tag{3.11b}$$

The geodetic positions are converted into the angular domain of the satellite and expressed in azimuth and elevation angles as shown in Figure 3.6.

3.4.2 Clustering of distributed users

Distributing the total broadband traffic demand across all the antenna beams evenly is not a straightforward solution because of the uneven geographic distribution of the broadband users and the geometric shape limitations of the antenna beam footprint. Hence, we use Cluster Analysis or Clustering to group traffic users into clusters and serve them under a beam [90]. There exist a plethora of literature [91] on clustering methods with application in computer vision and pattern recognition. The use of such clustering methods based on partition for beam pattern and footprint plan in Multi-beam satellite systems, which we propose in this paper, is a novel approach.

In Data Mining [126], Clustering is used to categorize the sample data into groups or clusters such that the objects in the same cluster are more related to each other than to the objects in different clusters. Using a similar approach, we considered the geographical locations and traffic demand of N broadband users as the sample data and assigned them to K clusters with each cluster to be converted to a beam in a later stage. We use the same number K for the number of clusters and beams, since each beam will serve one cluster. We have analysed various clustering algorithms such as k-means, k-medoids, Partitioning Around

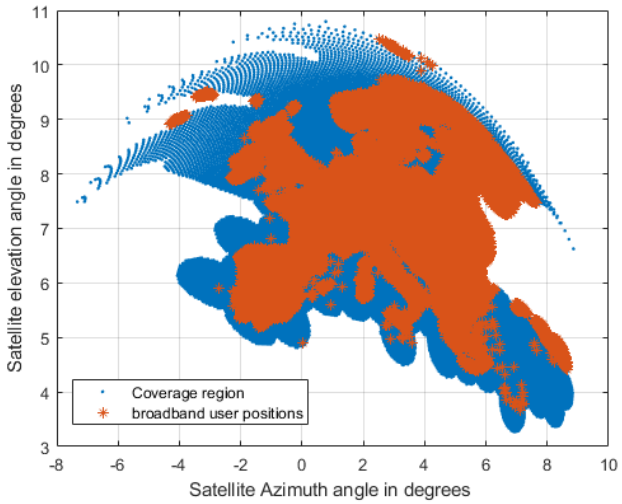

Figure 3.6: Sampled coverage area of the benchmark FMPF beams (shown in blue) and the user positions (shown in red) in satellite angular domain

Medoids (PAM) and Clustering LARge Applications (CLARA) [127].

As all the above mentioned clustering methods assign each observation from the observation set to different cluster sets by minimizing the squared Euclidean distance from the data point to the mean or median location of its assigned cluster, they could be used to partition the N broadband users into K number of clusters $\{\mathcal{T}^1, \mathcal{T}^2 ... \mathcal{T}^K\}$ with $\{\boldsymbol{c}_{\mathcal{T}^1}, \boldsymbol{c}_{\mathcal{T}^2} ... \boldsymbol{c}_{\mathcal{T}^K}\}$ as cluster centres. However, among the various known clustering methods, we decided to employ weighted k-means clustering using iterative Lloyd's algorithm [128] approach. Lloyd's algorithm is known as a centroid tessellation, which is beneficial for the beam design, since the beam center is likely to point in the direction of the dominant group of users. Hence, the demand can be better satisfied. The steps of Lloyd's Iteration Partition Clustering is shown in Algorithm 2.

The initial K cluster centres in Step-1 of the Algorithm 6 are chosen as cluster seeds using the k-means++ algorithm [129] for faster computation which converges better than random seeding. In Step-2, the distance matrix ($\mathfrak{R}_{K\times N}$) is computed using the Distance Metric (DM) between all the users and the cluster centres. Then using the distance matrix $\mathfrak{R}_{K\times N}$, the users are grouped into clusters to their nearest cluster centre. The Distance Metric used to compute the distances in the distance matrix $\mathfrak{R}_{K\times N}$ are a Weighted Euclidean Distances (WED) and is expressed as,

$$\mathrm{WED}_{(\mathbf{x}_\mathrm{n},\boldsymbol{c}_{\mathcal{T}^\mathrm{k}})} = ((\mathbf{x}_\mathrm{n} - \boldsymbol{c}_{\mathcal{T}^\mathrm{k}})(\mathbf{x}_\mathrm{n} - \boldsymbol{c}_{\mathcal{T}^\mathrm{k}})') \left(\frac{\sum\limits_{\mathrm{n}\in\mathcal{T}^\mathrm{k}} (\mathrm{d_n})}{\sum\limits_{\mathrm{n=1}}^{\mathrm{N}} (\mathrm{d_n})} \right), \tag{3.12}$$

where d_n is the broadband traffic demand of any user n. The WED will ensure that the clustering is based not only on their geographical location but also on their broadband traffic demand. In Step 4, a weighted version of the mean user position is computed as a cluster centre $\boldsymbol{c}_{\mathcal{T}^k}$ using,

$$\boldsymbol{c}_{\mathcal{T}^k} = \frac{1}{\sum\limits_{n\in\mathcal{T}^k} d_n} \sum_{n\in\mathcal{T}^k} d_n \mathbf{x}_n. \tag{3.13}$$

The Step-2 to Step-4 are repeated in Lloyd's iteration fashion for better clustering. The algorithm stops either when the cluster assignments do not change or when the maximum number of iterations are reached. We assume the maximum number of iterations to be 500 is usually sufficient for a good convergence. Upon the termination of the algorithm, all the broadband users will be grouped into K clusters $\{\mathcal{T}^1, \mathcal{T}^2 ... \mathcal{T}^K\}$.

Algorithm 2: Loyd's Iteration Partition Clustering Algorithm

Input : $K, X, d, D_{K\times N}, C_s, DM, M$
Output : $\{\mathcal{T}^1, \mathcal{T}^2 ... \mathcal{T}^K\}$

K= Total number of beams,
$X = \{\boldsymbol{x}_1, \boldsymbol{x}_2 ... \boldsymbol{x}_N\}$ = Broadband user set,
$d = \{d_1, d_2 ... d_N\}$ = User demand in Mbps,
$C_s = \{\boldsymbol{c}_{\mathcal{T}^1}, \boldsymbol{c}_{\mathcal{T}^2} ... \boldsymbol{c}_{\mathcal{T}^k}\}$ = Initial seeds for cluster centres,
DM = Distance Metric,
$\mathfrak{R}_{K\times N}$ = distance matrix,
M = Maximum number of iterations
[Step 1] Choose cluster centres $\{\boldsymbol{c}_{\mathcal{T}^1}, \boldsymbol{c}_{\mathcal{T}^2} ... c_{\mathcal{T}^k}\}$ defined by C_s selected as per $k-means++$ Algorithm.
while *(Cluster assignments do not change) OR (M is not reached)* **do**
  [Step 2] Compute distance $\mathfrak{R}_{K\times N}$ between each of $\{\boldsymbol{c}_{\mathcal{T}^1}, \boldsymbol{c}_{\mathcal{T}^2} ... \boldsymbol{c}_{\mathcal{T}^k}\}$ and all of $\{\boldsymbol{x}_1, \boldsymbol{x}_2 ... \boldsymbol{x}_N\}$ using DM shown in (3.12).
  [Step 3] Assign $\{\boldsymbol{x}_1, \boldsymbol{x}_2 ... \boldsymbol{x}_N\}$ users to K clusters $\{\mathcal{T}^1, \mathcal{T}^2 ... \mathcal{T}^K\}$ based on the minimum distance between the users and cluster centre using $\mathfrak{R}_{K\times N}$.
  [Step 4] Compute new cluster centres $\{\boldsymbol{c}_{\mathcal{T}^1}, \boldsymbol{c}_{\mathcal{T}^2} ... \boldsymbol{c}_{\mathcal{T}^k}\}$ by using (3.13).
end

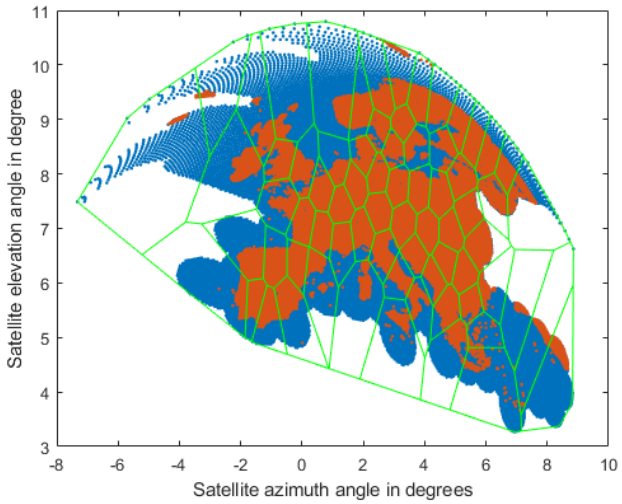

Figure 3.7: Beam boundaries (shown using green convex polygons) defined by Voronoi Tessellations in satellite angular domain. Sampled coverage area is shown in blue and the user positions are shown in red

3.4.3 Voronoi Tessellation

As clustering is based on current broadband user positions, all broadband users in the cluster will be covered by the cluster contour. So, we can define the boundary of the beam around the clustered users in the satellite angular domain. But, by defining the cluster boundary as beam boundary, we may create uncovered regions between beams where there is no coverage. Also, as the geographical locations of the maritime and the aeronautical broadband users change, it is necessary to plan beam boundaries such that no area remains uncovered. Also, for a fair comparison with the benchmark FMPF plan, we would like to guarantee the coverage in all areas, where the coverage is provided by the benchmark design method. For this we employ Voronoi Tessellation [130] in order to define the beam boundaries.

The definition of the Voronoi Tessellation [131] can be expressed as,

$$\begin{aligned} \mathrm{dom}(\mathcal{M},\mathcal{N}) &= \{x \in \mathcal{X} :\ r(x,\mathcal{M}) \leq r(x,\mathcal{N})\} \\ \text{where}, r(x,\mathcal{N}) &= \inf\{r(x,n) : n \in \mathcal{N}\} \end{aligned} \tag{3.14}$$

where if $(\mathcal{X}, r)$ is a metric space where $\mathcal{X}$ is a set of all points in a 2D Euclidean space and r is a distance metric on $\mathcal{X}$, then given two nonempty sets $\mathcal{M}, \mathcal{N} \subseteq \mathcal{X}$, the dominance region $dom(\mathcal{M},\mathcal{N})$ of $\mathcal{M}$ with respect to $\mathcal{N}$ is the set of all $x \in \mathcal{X}$ which are closer to $\mathcal{M}$ than to

$\mathcal{N}$. In other words, for any point in a set of co-planar points, a boundary could be derived encompassing it such that the region inside the boundary includes all points nearer to it than to any other point in the set. Furthermore, such boundary defines one Voronoi polygon. The collection of all Voronoi polygons for every point in the set is called a Voronoi Tessellation.

We consider the cluster centres $\{\boldsymbol{c}_{\mathcal{T}^1}, \boldsymbol{c}_{\mathcal{T}^2} ... \boldsymbol{c}_{\mathcal{T}^K}\}$ obtained by weighted k-means user clustering in Euclidean plane. Any centre $\boldsymbol{c}_{\mathcal{T}^k}$ is simply a point in the Euclidean plane, and its corresponding Voronoi cell V_u consists of every point in the Euclidean plane whose Euclidean distance to $\boldsymbol{c}_{\mathcal{T}^u}$ is less than or equal to its Euclidean distance to any other centre $\boldsymbol{c}_{\mathcal{T}^{v \neq u}}$. Each such Voronoi cell is obtained from the intersection of geometric half-spaces, and hence it is a convex polygon. The collection of such convex Voronoi polygons distributed in the satellite coverage region of Europe in the angular domain is shown in Figure 3.7. We approximate the boundary of Voronoi polygons as beam contour and the geographic centres $\{\boldsymbol{c}'_1, \boldsymbol{c}'_2 ... \boldsymbol{c}'_K\}$ of Voronoi polygons as beam centres. However, from the antenna pattern perspective, the irregular Voronoi polygons cannot be approximated as beams. Hence, we have to use the vertices of the Voronoi polygons to compute the beam border by approximating the Voronoi polygons to ellipses.

3.4.4 Elliptic approximation

Considering the mathematical tractability and topological packing, we can approximate the beam footprint to either a circle or an ellipse. However, a circular approximation of the Voronoi polygons will overlap beams and will cause inter-beam interferences. Hence, to reduce overlapping of beams and to have full coverage, we approximate the Cartesian coordinates of the boundaries of the Voronoi polygon vertices into ellipses to represent them as beam footprint.

Accordingly, we divide (3.7) on both sides by a and move x^2 to the right-hand side as,

$$2bxy + cy^2 + 2dx + 2fy + g = -x^2, \tag{3.15}$$

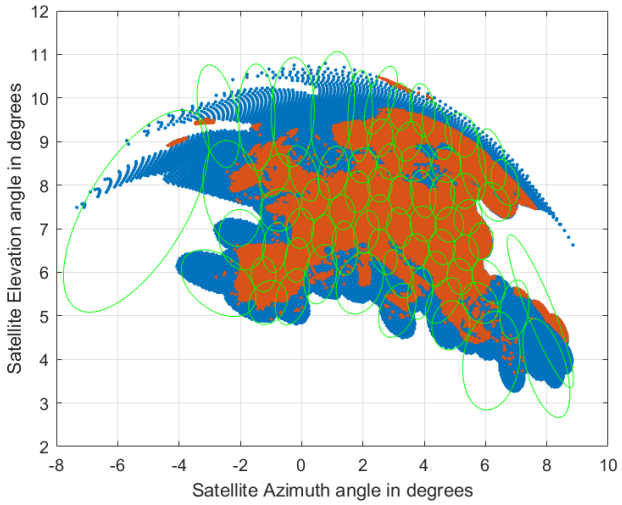

Figure 3.8: Beam Footprint as ellipses (shown using green) over Europe using 71 Adaptive Beams in satellite angular domain. Sampled coverage area is shown in blue and the user positions are shown in red

and then define M and p as,

$$M = \begin{bmatrix} 2x_1y_1 & y_1^2 & 2x_1 & 2y_1 & 1 \\ 2x_2y_2 & y_2^2 & 2x_2 & 2y_2 & 1 \\ \vdots & \vdots & \vdots & \vdots & \vdots \\ 2x_sy_s & y_s^2 & 2x_s & 2y_s & 1 \end{bmatrix}, \tag{3.16a}$$

$$p = \begin{bmatrix} b & c & d & f & g \end{bmatrix}^T, \tag{3.16b}$$

such that we can represent (3.15) as $M \times p = b'$. To solve for p, we use an estimation technique in (3.15) and represent it as $M \times p = b'$. As we know the elements in M which are the vertices of the covex Voronoi polygon, we find the pseudo inverse (M^+) matrix of M. Then we assume $b' = -x^2$ and solve for p as $p = M^+ \times b'$. Hence, by solving for p, we will have best parameters for a, b, c, d, f, g in the Least Square sense.

The parameters a, b, c, d, f, g are now used to obtain center, semi-major axis, semi-minor axis and the phase angle of the ellipse [132]. The centre of the ellipse is obtained using,

$$x_0 = \frac{cd - bf}{b^2 - ac}, \tag{3.17a}$$

$$y_0 = \frac{af - bd}{b^2 - ac}. \tag{3.17b}$$

The semi-major axis and the semi-minor axis are derived using,

$$axis_1 = \sqrt{\frac{2(af^2 + cd^2 + gb^2 - 2bdf - acg)}{(b^2 - ac)(\sqrt{(a-c)^2 + 4b^2}) - (a+c)}}, \tag{3.18a}$$

$$axis_2 = \sqrt{\frac{2(af^2 + cd^2 + gb^2 - 2bdf - acg)}{(b^2 - ac)(-\sqrt{(a-c)^2 + 4b^2}) - (a+c)}}, \tag{3.18b}$$

where the bigger axis among $axis_1$ and $axis_2$ is the semi-major axis and smaller axis among $axis_1$ and $axis_2$ is the semi-minor axis.

The angle of rotation of the ellipse that best fits the Voronoi convex polygon is derived using,

$$\varphi = \begin{cases} 0 & \text{for } b = 0; a < c \\ \frac{1}{2} & \text{for } b = 0; a > c \\ \frac{1}{2}\cot^{-1}\frac{a-c}{2b} & \text{for } b \neq 0; a < c \\ \frac{\pi}{2} + \frac{1}{2}\cot^{-1}\frac{a-c}{2b} & \text{for } b \neq 0; a > c. \end{cases} \tag{3.19}$$

The approximated ellipses from the Voronoi polygon in the satellite angular domain is shown in Figure 3.8. The centres of the ellipses ($\boldsymbol{c}_k$) will represent the proposed adaptive beams centres/positions. The semi-major and semi-minor axis of the approximated ellipses ($\delta\theta_k$, $\delta\phi_k$) defines the boundary of the proposed adaptive beams. The angle of rotation of approximated ellipses (φ_k) represents the orientation of the proposed adaptive beams.

The approximated ellipses on the satellite antenna domain projected on the surface of the Earth are shown in Figure 3.9. The domain conversion of the ellipses from the satellite antenna domain to the surface of the Earth is the reverse operation of what is discussed in 3.4.1. It can be noticed that, on the surface of the Earth, the ellipse are distorted due to the curvature of the Earth.

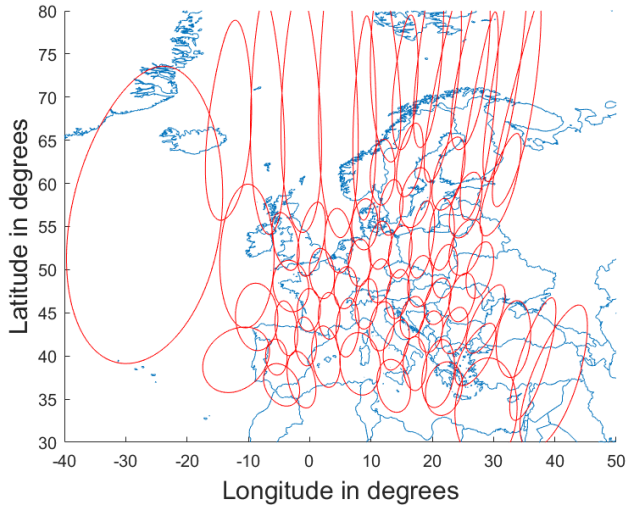

Figure 3.9: Projection of 71 ellipses (shown in red) on the surface of the Earth over Europe

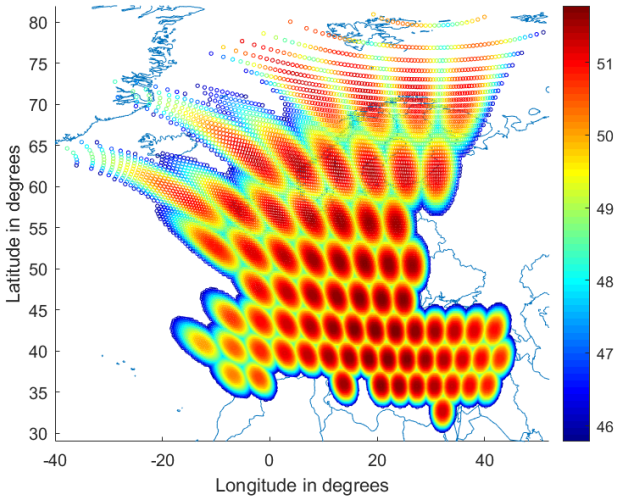

Figure 3.10: Antenna pattern of FMPF plan where the colour bar represents Antenna gain values on the surface of the Earth.

3.4.5 Antenna gain calculation

In real satellite antenna pattern of FMPF benchmark [112–114] shown in Figure 3.10, the antenna gain values distributed across the coverage region is sampled at coverage points on the surface of the Earth. In the satellite angular domain, the coverage points and their corresponding antenna gain values are shown in Figure 3.11. The proposed AMPF beams are elliptical in the angular domain of the satellite and hence, we approximate the antenna gains of the AMPF antenna pattern using two-dimensional Gaussian elliptical function. The

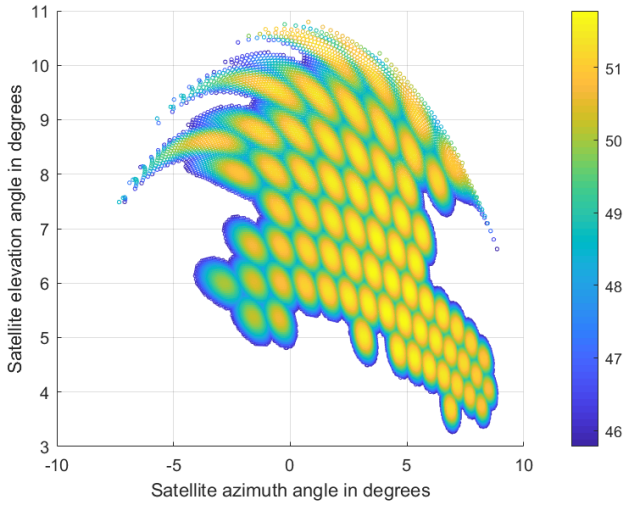

Figure 3.11: Antenna pattern of FMPF plan where the colour bar represents Antenna gain values on the satellite angular domain.

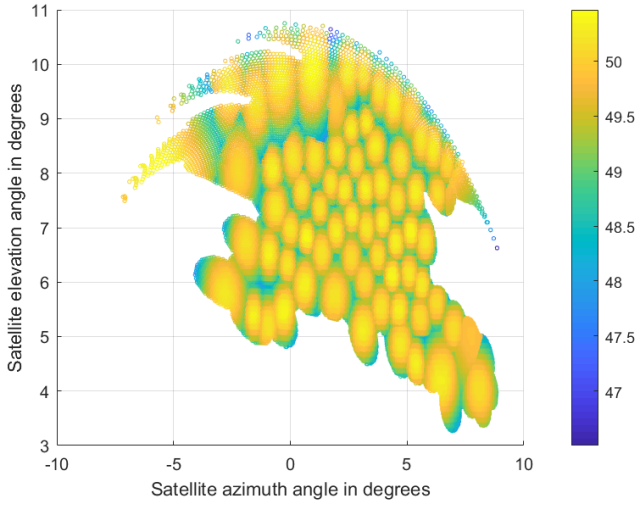

Figure 3.12: Antenna pattern of proposed AMPF plan where the colour bar represents Antenna gain values on the satellite angular domain.

antenna gain at any point of the AMPF elliptical beam could be modelled using,

$$f(x,y) = A\exp(-(m_1(x-x_o)^2 + 2m_2(x-x_o)(y-y_o) + m_3(y-y_o)^2)), \quad (3.20)$$

where the matrix $\begin{bmatrix} m_1 & m_2 \\ m_2 & m_3 \end{bmatrix}$ is positive-definite matrix [133].

As the proposed elliptical AMPF beams are fitted with the two-dimensional Gaussian elliptical function, the semi-major axis of the ellipse ($\delta\theta$) is fitted with σ_X of the Gaussian

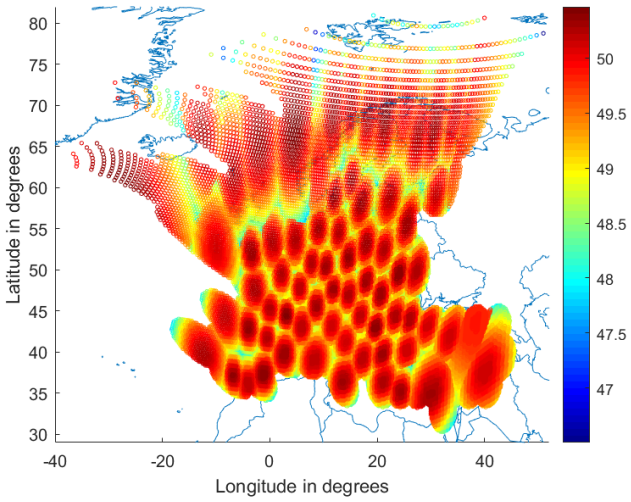

Figure 3.13: Antenna pattern of proposed AMPF plan where the colour bar represents Antenna gain values on the surface of the Earth.

function and semi-minor axis of the ellipse ($\delta\phi$) of the ellipse is fitted with σ_Y of the Gaussian function. The coefficient A is the amplitude of boresight point or maximum antenna gain. The centre of the Gaussian function (intersection point of σ_x and σ_y) is the centre (x_0, y_0) of the ellipse. The values of $m1, m2$ and $m3$ are defined using,

$$m_1 = \frac{\cos^2\varphi}{2\sigma_X^2} + \frac{\sin^2\varphi}{2\sigma_Y^2}, \tag{3.21a}$$

$$m_2 = -\frac{\sin 2\varphi}{4\sigma_X^2} + \frac{\sin 2\varphi}{4\sigma_Y^2}, \tag{3.21b}$$

$$m_3 = \frac{\sin^2\varphi}{2\sigma_X^2} + \frac{\cos^2\varphi}{2\sigma_Y^2}. \tag{3.21c}$$

For a fair comparison between the proposed AMPF pattern and the benchmark FMPF pattern, Power Flux Density (PFD) measured in Watts per square meters W/m^2 of the proposed FMPF beams should be similar to the PFD of benchmark FMPF beams. Also, the total transmission power of the proposed AMPF scheme should be approximately equal to the FMPF benchmark plan. We achieve this by optimising antenna gains of the AMPF beams at the sampled coverage points on the surface of the Earth. Accordingly, we first integrate the power at sampled coverage points of every beam in the FMPF benchmark pattern and then normalise the power of every beam in the AMPF beams, such that the power of every proposed AMFP beam is equal to the average power of the FMPF benchmark beams.

Table 3.2: Simulation Parameters

Satellite longitude	0 degree East (GEO)
Total Number of Beams, N_B	71
Uplink C/N	18.4 dB
Power per beam	13 W
Number of beams per TWTA	1
Number of carriers per TWTA	1
Number of carriers per beam	1
Carrier Frequency	19.96 GHz
Carrier Bandwidth	216 MHz
Useful Bandwidth	216 MHz
Roll off	0.05
Symbol Rate	205 Msps
OBO	3.8 dB
NPR	20 dB
Payload degradations	2 dB
Free space distance	37000 km
Wavelength	0.015182186
Free space path loss	209.7215455 dB
Rain Fade (99.5%)	2 dB
Other losses	2 dB

After fitting the two-dimensional Gaussian function upon the proposed elliptical AMPD beams and optimising its PFD to the average PFD of the FMPD beams, we can obtain the antenna gain value at any sampled coverage points on the surface of the Earth. In the satellite angular domain, the sampled coverage points and their corresponding antenna gain values of the proposed AMPF antenna pattern are shown in Figure 3.12. Also, Figure 3.13 shows the antenna gain values of the proposed AMPF antenna pattern at sampled coverage points on the surface of the Earth. Furthermore, using this antenna gain values, we can determine SNR and the offered throughput for any user at sampled coverage points on the surface of the Earth.

3.5 Simulation and Results

3.5.1 Data Set Model and link budget

The data sets that are employed for simulations are collected from authentic sources to present an accurate traffic model. The simulation parameters and the link budget information

considered for the proposed AMPF plan is summarized in the Table 3.2.

Also, we consider a total number of $N = 60617$ users distributed across the coverage area of $K = 71$ beams whose location and demand is extracted using the SnT traffic simulator [124]. We denote the traffic demand of the generic user n, in *bps*, as d_n using [124]. The SnT traffic emulator [124] models the broadband traffic demand distribution over Europe including users from Population distribution for broadband Fixed Satellite Services (FSS), aeronautical satellite communications, and vessel distribution for maritime services. The number of flights corresponding to their coverage area is considered, where the aeronautical data is deduced from anonymized and unfiltered flight-tracking source [2]. The container ship distribution for maritime is included and evaluated by dataset obtained from vessel tracking web site (VesselFinder) which includes ship positions and marine traffic detected by global AIS network [3]. The Population data is used to generate the traffic distribution for broadband Fixed satellite services (FSS) terminals and has been extracted from the NASA Socioeconomic Data and Applications Center (SEDAC) population database [4]. These large-scale and fine-grained datasets guarantee the reliability and the consistency of our traffic pattern analysis and modelling.

3.5.2 Numerical Results

Demand Distribution

The beam demand D_k (in bps) of a beam k is the summation of traffic demand of all the users belonging to the beam k and is expressed as,

$$D_k = \sum_{n \in \mathcal{T}^k} d_n, \tag{3.22}$$

and the total system demand (in bps) is the summation of all the beam demands in the Multi-beam HTS system and is expressed using,

$$D_{sys} = \sum_{k=1}^{K} D_k, \tag{3.23}$$

where $n = 1, 2...N$ are the number of users, $k = 1, 2...K$ are the number of beams, d_n (in bps) is traffic demand of the user n. $\mathcal{T}^k$ is the set containing all the users that belong to beam k.

The main objective of this work is to distribute D_{sys} evenly among the K beams. To verify

this, we computed beam demands $D_k \forall k$ for both benchmark FMPF plan and proposed AMPF plan and plotted Empirical Cumulative Distribution Function (CDF) as shown in Figure 3.14. In AMPF plan, probability of having any beams with zero demand is zero whereas in FMPF plan, probability of having any beams with zero demand is around 0.1. Also, the probability of having beams with lower demand (< 8 Gbps) is higher in FMPF plan than AMPF plan and the probability of having beams with higher demand (> 26 Gbps) is higher in FMPF plan than AMPF plan.

Hence, the proposed AMPF plan has clearly reduced beam demand for beams with high demands and distributed it to the beams with relatively lower demand. Furthermore, it ensures that no beam is planned with zero demand. Whereas, in the benchmark FMPF plan, the total system demand is more unequally distributed. Also, some beams are having zero beam demand that has to be met. This is majorly because in rigid fixed plan, the geographical broadband user locations and their traffic demand is ignored and hence some beams are pointed to geographic locations on the Earth where no broadband users are present. Alternatively, the proposed AMPF plan distributes system demand more evenly and ensures that beams are always assigned with an adequate beam demand that have to be met.

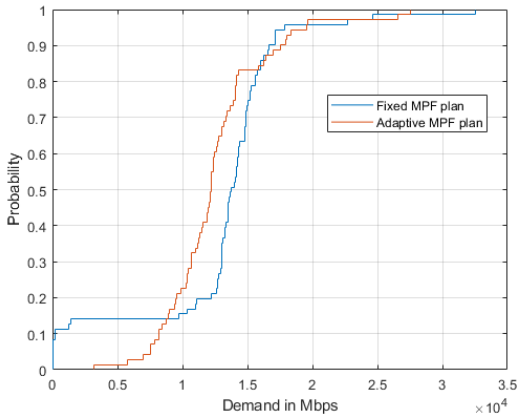

Figure 3.14: Empirical Cumulative Distribution Function (CDF) showing the system demand distribution across all the beams

The Jain's Fairness Index ($\mathfrak{J}$) [134] is a well-known fairness metric, which in this context measures how evenly the demand is distributed across all the beams. Specifically, if D_k is the summation of demand of all the users in beam k, the Jain's fairness index is defined as,

$$\mathfrak{J} = \frac{(\sum_{k=1}^{K} D_k)^2}{K \sum_{k=1}^{K} D_k^2}, \tag{3.24}$$

and ranges between $\frac{1}{K}$ and 1, where $\frac{1}{K}$ signifies that the system is least fair and 1 signifies that the system is most fair. The Jain's fairness index is computed for both benchmark FMPF plan and proposed AMPF plan at different time stamps of a day and is shown in Figure 3.15. It is evident that the proposed AMPF plan performs better with value much closer to 1 in comparison to the benchmark FMPF plan.

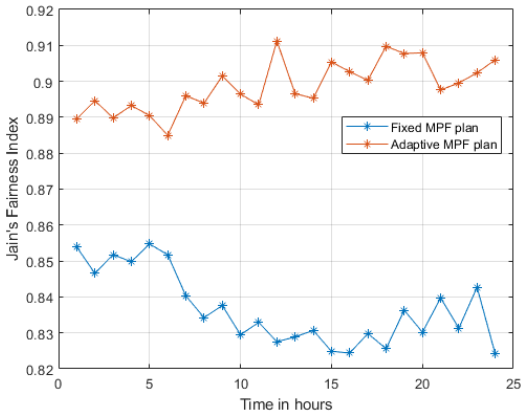

Figure 3.15: Jain's Fairness Index ($\mathfrak{J}$) at different time stamps of a day.

Demand requested and Offered Throughput

The throughput demand $d_{\forall n,k}$ requested by any user n in beam k is defined using,

$$d_{\forall n,k} = \frac{1}{|\mathcal{T}^k|} \sum_{n \in \mathcal{T}^k} d_n, \tag{3.25}$$

where $\mathcal{T}^k$ is the set containing all the users that belong to beam k and d_n (in bps) is traffic demand of the user n. The cardinality of a set $\mathcal{T}^k$ is denoted $|\mathcal{T}^k|$.

In FMPF benchmark antenna pattern, the antenna gain values distributed across the coverage region is sampled at coverage points on the surface of the Earth. We define such sampled coverage points as $p = 1, 2...P$, where P is the total number of sampled coverage points under the entire coverage region of the satellite in FMPF plan. We define Signal-to-Noise ratio (SNR) as SNR_p^F at any sampled coverage point p in the FMPF plan. Also, as the granularity of the sampled coverage point is fine, we approximate the SNR experienced by any user n to the SNR of the closest sampled coverage point p.

The offered throughput ($R^F_{\forall n,k}$) to any user in a beam k can be defined using,

$$R^F_{(\forall n,k)} = \frac{1}{|P^F_k|}\left(\sum_{p\in P^F_k} B\log_2(1+SNR^F_p)\right), \tag{3.26}$$

where B is the system bandwidth and the set P^F_k is the set containing all the sampled coverage points that belong to beam k. The cardinality of a set P^F_k is denoted $|P^F_k|$. For the benchmark FMPF plan, the SNR at a sampled coverage point (p) is computed using the FMPF benchmark antenna pattern from the dataset provided by [124]. Also, we use four colour frequency reuse scheme which makes inter-beam interference negligible.

To ensure a fair comparison between the FMPF plan and the proposed AMPF plan, we consider computing the offered throughput of proposed AMPF plan at previously defined sampled coverage points $(p = 1, 2...P)$ of FMPF plan. Accordingly, in the proposed AMPF plan, we define SNR at any sampled coverage point p as SNR^A_p. The offered throughput $(R^A_{(\forall n,k)})$ to any user n in a beam k can be defined using,

$$R^A_{(\forall n,k)} = \frac{1}{|P^A_k|}\left(\sum_{p\in P^A_k} B\log_2(1+SNR^A_p)\right), \tag{3.27}$$

where SNR at sampled coverage points (p) are computed using antenna gain values at sampled coverage points obtained by fitting the two-dimentional Gauusian function as discussed in 3.4.5. The set P^A_k is the set containing all the sampled coverage points that belong to beam k.The cardinality of a set P^A_k is denoted $|P^A_k|$.

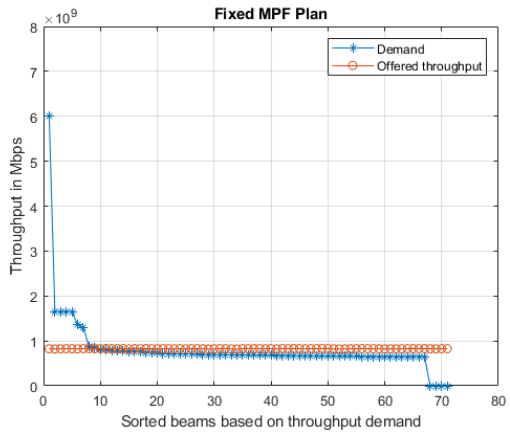

Figure 3.16: Throughput demand requested and offered throughput to any user in the benchmark FMPF plan beams.

Figure 3.16 shows the throughput demand requested by any user in the benchmark FMPF

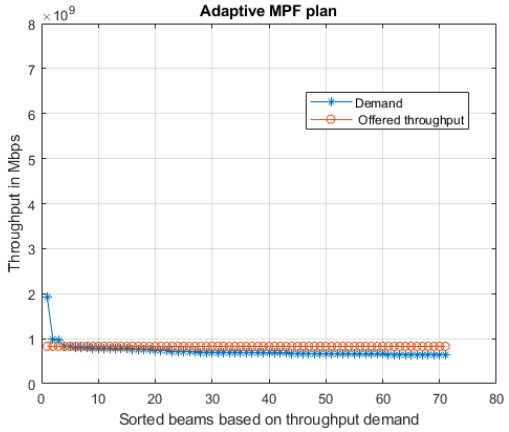

Figure 3.17: Throughput demand requested and offered throughput to any user in the proposed AMPF plan beams.

plan beams. For better visualization the beams are sorted based on the throughput demand before plotting. From Figure 3.16 it is evident that throughput demand requested by any user in beams 1 to 6 are very high. Also, as there are no users from beam 63 to 71, the throughput demand requested by any user is zero. However, the offered throughput to any user in the FMPF beams remains same. Hence, the demand requested by any user in beams 1-6 are not met. Also, the offered throughput to beams 63-71 is unused due to the absence of users.

Figure 3.17 shows the throughput demand requested by any user in the proposed AMPF plan beams. For better visualization the beams are sorted based on the throughput demand before plotting. From the Figure 3.17, it is evident that throughput demand requested by any user in all the beams is almost identical. Hence, the offered throughput to any user in the AMPF beams is met in almost all the beams.

Capacity unused/unmet

Considering $R_{\forall n,k}$ as the offered throughput and $d_{\forall n,k}$ as throughput demand for any user in beam k, We define a set U_1 that contains all the values of k that satisfies $R_{\forall n,k} > d_{\forall n,k}$ and set U_2 that contains all the values of k that satisfies $d_{\forall n,k} > R_{\forall n,k}$. Then unused capacity

and unmet capacity for the whole system can be computed using,

$$C_{unused} = \sum_{k \in U_1} (R_{\forall n,k} - d_{\forall n,k}), U_1 = \{\forall k | R_{\forall n,k} > d_{\forall n,k}\}, \tag{3.28a}$$

$$C_{unmet} = \sum_{k \in U_2} (d_{\forall n,k} - R_{\forall n,k}), U_2 = \{\forall k | d_{\forall n,k} > R_{\forall n,k}\}. \tag{3.28b}$$

The Normalized Capacity Deviation (NCD) in percentage for the benchmark FMPF plan and the proposed AMPF plan system can be computed using,

$$NCD = \frac{(C_{unused} + C_{unmet})}{\sum_{k=1}^{K} d_{\forall n,k}}. \tag{3.29}$$

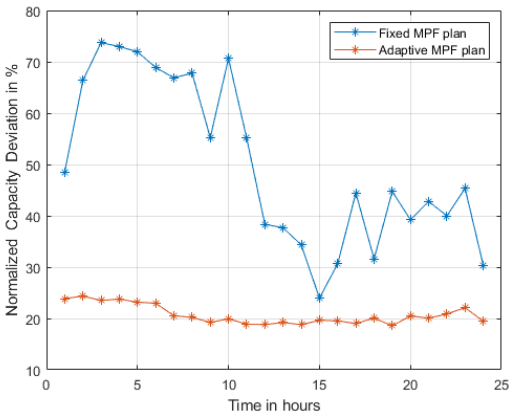

Figure 3.18: Normalized Capacity Deviation (NCD) in percentage at different time stamps of a day.

The geographic locations of the broadband users and their requested throughput demand changes with time. Hence, Using (3.28a), (3.28b) and (3.29), the NCD for the benchmark FMPF plan and proposed AMPF plan is computed at different time instances of a day. From Figure 3.18, it is evident that the proposed AMPF plan performs better than the benchmark FMPF plan throughout the day. Furthermore, the Normalized Capacity Deviation of benchmark FMPF plan changes drastically with time. While at 03:00 time stamp, 73% of the capacity is unused/unmet, at 15:00 time stamp, 23% of the capacity is unused/unmet. This clearly shows that the benchmark FMPF plan performs poorly when the geographic locations of the users and their traffic demand is variable. Meanwhile, the Normalized Capacity Deviation of proposed AMPF plan remains relatively same throughout the day and hence will be more suitable for mobile non-uniformly distributed broadband traffic users with variable

traffic demand.

The dynamics of the load changes play a vital role in the success of the proposed scheme. Nevertheless, based on the data obtained from [135–137], the traffic demand varies slowly compared to the time needed for beam adaptation. Accordingly, in our simulations, we introduced adaptability based on the load changes once every hour. However, this adaptation could be made more often or even less often depending upon the changes in the traffic demand. Another approach is to trigger the proposed AMPF planning whenever a threshold change is noticed. Nevertheless, the complexity of the proposed AMPF scheme concerning demand dynamics strongly depends on the frequency of adapting the plan. Hence, such decisions are purely based on satellite operators operational decisions on how often they would want to adopt and hence was beyond the scope of this study.

3.6 Conclusion

In this work, we present a comprehensive overview of the beam pattern and footprint planning in a High Throughput Multi-beam Satellite communication systems. Also, we include a detailed analysis of the benchmark Fixed Multi-beam Pattern and Footprint (FMPF) plan and its drawbacks, especially for non-uniform and mobile broadband user distribution with heterogeneous traffic demand. As the FMPF plan fails to distribute the total system demand across all the beams evenly, we propose an Adaptive Multi-beam Pattern and Footprint (AMPF) plan as a relatively better solution. A step by step procedure involved in AMPF plan such as satellite angular domain transformation, weighted k-means clustering of users, Voronoi Tessellation for full coverage region, Ellipse approximation of Voronoi polygon has been discussed in detail.

The simulations conducted using reliable data-sets clearly show a better performance of the proposed AMPF plan in comparison to the benchmark FMPF plan. The proposed AMPF plan distributes the total system demand more evenly and also guarantees coverage region similar to FMPF plan. Also by choosing proposed AMPF plan over the fixed rigid plan, the unused/unmet system capacity reduces.

Chapter 4

Demand Driven Adaptive User Scheduling

4.1 Weighted Semi-orthogonal Scheduling

4.1.1 Introduction

The trend of user demand shifting from broadcast services to broadband services has made satellite industries investigate High Throughput Satellite (HTS) systems, moving from single-beam to multibeam coverage pattern. Precoding for Multibeam HTS systems has been proposed as an effective co-channel interference mitigation technique able to boost the spectral efficiency and, as a consequence, to improve the overall system throughput performance [32, 52].

However, the performance of precoded Multibeam HTS systems is profoundly affected by the scheduling decisions [8, 138, 139]. In particular, the achievable throughput decreases whenever the user channel vectors within the adjacent beams are collinear. Therefore, the optimal performance is achieved when proper user scheduling selects users with orthogonal channel vectors to be served simultaneously [112, 140].

The joint user scheduling and precoding problem is non-convex and NP-hard. This means that multiple locally optimal points exists and theoretical guarantees are weak or non-existent. Hence, obtaining the optimal solution requires an exhaustive search-based user grouping and scheduling, which quickly become impractical due to exponential complexity. This was the approach followed in ESA PreDem project [111]. Some recent works have addressed the joint problem by proposing sub-obtimal solutions that reach stationary points of the

original problem [141, 142]. Still, the complexity is not negligible and most of the literature have opted to split the design into two steps. As a consequence, channel orthogonality as defined in [143], has been widely used in the satellite community to deal with the scheduling problem. Furthermore, in [144], the authors use the cosine similarity metric to sequentially select the users with most orthogonal channel vectors. In [145], the authors make use of the spectral clustering technique, whose primary goal is to generate clusters of users with orthogonal channel characteristics. As an alternative approach, the authors in [146] propose geographic user clustering approach and use Euclidean distance to relate channel vectors and impose channel orthogonality. In a comparable inclination, the authors in [147] propose a geographical scheduling algorithm and schedule together users belonging to similar locations in their respective beams. Similarly, the authors in [148] propose a user grouping scheme using random pre-processing and the before mentioned Euclidean norm.

On the other hand, the capability to flexibly allocate on–board resources over the service coverage is becoming a must for future broadband multibeam satellites [112, 149]. The primary goal is to assign the system capacity where it is actually needed. In contrast to the majority of recent scheduling studies, in this paper we target the scheduling design not only from the maximum throughput perspective but also considering the aforementioned demand matching problem. In particular, we proposed the so-called Weighted Semi-Orthogonal Scheduling (WSOS) algorithm, which is a sub-optimal low-complexity sequential scheduling that weights the orthogonality coefficient given by the cosine similarity metric with a coefficient computed according to the user demand requirements. The proposed WSOS algorithm can be seen as a method to dynamically allocate bandwidth to users based on user traffic demand and instantaneous queue status. Furthermore, the proposed scheduling mechanism prevents high usage users from starving other users via fairness guarantees. The latter can be seen as a minimum resource assignment that ensures the availability of a basic amount of satellite resources no matter how busy the network is.

Notation: We use upper-case and lower-case bold-faced letters to denote matrices and vectors, respectively. $\circ$ denotes the element-wise Hadamard operations. $(\cdot)^T$ denotes the transpose of $(\cdot)$. $|\,.\,|$ and $\|.\|$ depict the amplitude and Euclidean norm, respectively.

4.1.2 System Model

Unicast Multibeam Satellite System

Traditional HTS systems consider the use of multiple spot beams to cover a desired service area, with fractional frequency reuse across beams. In particular, several beams can reuse the same frequency band and polarization, as far as they have significant spatial separation to avoid interference. Figure 4.1 provides the typical 4-color frequency reuse (4CR), where beams with the same color are sharing resources.

In this work, we will consider unicast scheduling, where the DVB-S2X [11] defined XFECFRAME includes data that belongs to a single user. In other words, one user is scheduled per frame. At each time instance, a single XFECFRAME is transmitted per beam, and hence, only one user (denoted in yellow in the Figure 4.1) is served by a specific beam.

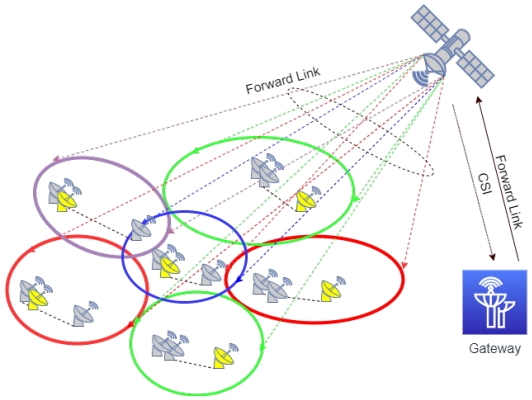

Figure 4.1: System Architecture: Multibeam High Throughput-Satellite System with four colour scheme

To further boost the spectral efficiency of the system, full frequency reuse (FFR) combined with spatial interference mitigation techniques has been recently considered [144]. Serving all beams with the same satellite spectral resource facilitate a beam-free scheduling approach, where resources from low demand beams can be exploited by neighboring high-demand beams.

In this paper, we focus on Multibeam HTS architectures operating under FFR and implementing linear precoding as inter-beam interference mitigation technique as shown in Figure 4.2. Geographically fixed users assuming Fixed Satellite Services (FSS) are considered for simplicity. However, the data requested by the users are independent and mutually exclusive.

We assume that the precoding computation and implementation takes place in a single gateway, which uploads the precoded signals to the satellite through an ideal noise-free feeder

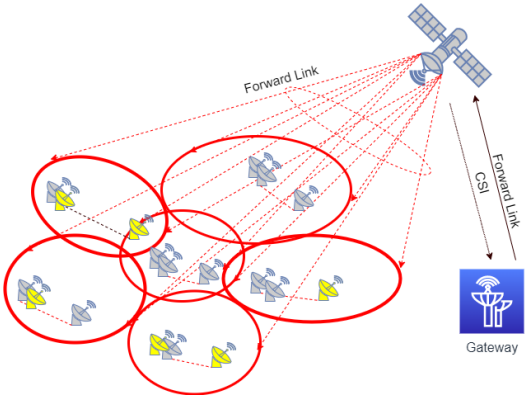

Figure 4.2: System Architecture: Precoded Multibeam High Throughput-Satellite System

link. Precoding techniques require full channel state information (CSI) at the gateway side. To this end, DVB-S2X [11] defines SF pilot symbols that are transmitted at specific locations in the downlink frame. In general, users know the value of these pilot symbols a priori. Consequently, the correlation properties of expected values and the received values of these pilot symbols defines the measurements of the channel quality. These measurements will be reported by the UE to the network using the satellite return link. For the sake of simplicity, in this paper, we assume perfect CSI knowledge at the gateway side. The impact of imperfect CSI is kept for future works.

Multibeam Satellite Channel

A single feed per beam (SFPB) payload antenna architecture is assumed, where the number of transmitting antennas is equal to the total number of beams denoted by K. The received signal y_k at the user u_k in the k^{th} beam is as expressed in (4.1), where $\mathbf{h}_k \in \mathbb{C}^{1\times K}$ is the channel vector between the transmitting satellite antennas and the user u_k. $\mathbf{x}_k \in \mathbb{C}^{K\times 1}$ represents the transmitted precoded signal vector from the K satellite antennas, and n_k is a random variable distributed as $\mathcal{CN}(0,\sigma^2)$, modelling the zero-mean Additive White Gaussian Noise (AWGN) measured at the u_k's receiving antenna.

$$y_k = \mathbf{h}_k\mathbf{x}_k + n_k, \quad k = 1, 2, ..., K \tag{4.1}$$

By rearranging all the users' received signals in a vector $\mathbf{y} \in \mathbb{C}^{K\times 1}$, we can rewrite the above model as,

$$\mathbf{y} = \mathbf{H}\ \mathbf{x} + \mathbf{n}, \tag{4.2}$$

where $\mathbf{H} = [h_1 \dots h_K]^T \in \mathbb{C}^{K \times K}$ represents the system channel matrix, and $\mathbf{n} \in \mathbb{C}^{K \times 1}$ is the AWGN components for all the users.

Since full frequency reuse is considered, the transmitted symbols $\mathbf{x}$ are precoded to mitigate the co-channel interference. In particular, we define $\mathbf{W}$ as the precoding matrix and the precoded signal is given by,

$$\mathbf{x} = \mathbf{W}\ \mathbf{s}. \tag{4.3}$$

In (4.3), the information vector $\mathbf{s}$ contains the raw symbols coming from the DVB-S2x modulator and satisfies $[\mathbf{s}\mathbf{s}^H] = \mathbf{I}$. The precoding matrix $\mathbf{W}$ is assumed to be obtained with the well-known MMSE design [144, 150], which is can be expressed as,

$$\mathbf{W}_{RZF} = \eta' \boldsymbol{H}^{\boldsymbol{H}} (\boldsymbol{H}\boldsymbol{H}^{\boldsymbol{H}} + \boldsymbol{\alpha I})^{-\mathbf{1}}, \tag{4.4}$$

where α is a predefined regularisation factor [150] and η is the power allocation factor defined in (4.5) with P_{tot} being the total available power.

$$\eta = \sqrt{\frac{P_{tot}}{\text{Trace}(\mathbf{W}\mathbf{W}^{\dagger})}} \tag{4.5}$$

The complex channel matrix $\mathbf{H}$ stated in (4.2) is defined as,

$$\boldsymbol{H} = \boldsymbol{\Phi B} \tag{4.6}$$

where $\mathbf{B} \in \mathbb{R}^{K \times K}$ models the path loss, the satellite antenna radiation pattern, the received antenna gain and the noise power. In particular, the i^{th} and j^{th} components of $\mathbf{B}$ are given as,

$$b_{ij} = \frac{\sqrt{G_{Rm} G_{km}}}{(4\pi \frac{\mathfrak{D}_{mk}}{\lambda})} \tag{4.7}$$

where G_{Rm} is the receiver antenna gain (that mainly depends on the receiving antenna aperture) and G_{km} are the gains defined by the multibeam satellite radiation pattern and user locations. $\mathfrak{D}_{mk}$ is the distance between the satellite transmit antenna k and the m^{th} user's receiving antenna. Usually, due to the long propagation distance, $\mathfrak{D}_{mk} \approx \mathfrak{D}_m$. Finally, λ is the wavelength of transmission.

The diagonal phase matrix $\Phi \in \mathbb{R}^{K \times K}$ is the signal phase rotations induced by the different propagation paths and is generated as shown in (4.8) where Φ_x is a uniform random

variable in $[2\pi, 0]$ and $[\phi]_{xy} = 0, \forall x \neq y$.

$$[\Phi]_{xx} = e^{i\phi_x}, \forall x = 1...K \tag{4.8}$$

4.1.3 Proposed Demand-based Scheduling

Problem Statement

In multibeam HTS using Time Division Multiple Access (TDMA), the resource sharing among different beams and receivers should be designed effectively. Consequently, the goal of the forward link satellite scheduler is to optimise bandwidth utilisation by jointly considering the channel conditions and the different broadband user demands. Such an approach is relatively new and unexplored in the related works.

Furthermore, satellite operators and service providers are compelled to provide any agreed throughput to broadband users. Such agreed throughput will be defined in a legal contract termed as the Service-Level Agreement (SLA). Consequently, the satellite operators are obliged to provide every broadband user with the agreed levels of the metrics defined in the SLA. This further pushes the need for improved scheduling algorithms which jointly intends to achieve the SLA defined user demand.

Proposed WSOS Solution

While most of the literature focused on scheduling designs that maximize the achievable capacity of the system, very few research has been done in demand-based scheduling. Herein, we propose an iterative sub-optimal scheduling method, which on the one hand intends to orthogonalize as much as possible the users' channels, while on the other hand prioritizes the users demanding higher traffic. The orthogonality-based user selection was initially proposed in [143], which highlighted the importance of selecting users with orthogonal channels in order to not compromise the channel matrix inversion procedure in (5.6).

Given a cluster of K beams, the goal is to select K users from the user pool of M users at each scheduling time, $t = 1, ..., T$. We assume the users' demand to be denoted as $(d_1, \ldots, d_M)$.

The proposed method is summarized in Algorithm 3. In order to take into account the traffic demand d_m in the scheduling, we associate to the generic user m, a coefficient

$\alpha_m \in [0,1]$ as defined in (4.9), which shall be seen as the priority that a given user m has in the initial scheduling time $t = 1$. Such coefficient is simply a normalised version of the demand d_m and is expressed in (4.9), for each m = *1,2,3 ...,* M. Thus, $\alpha_m = 1$ is associated with the highest traffic demand and $\alpha_m = 0$ with the lowest.

$$\alpha_m = \frac{d_m}{\max_m(d_m)} \tag{4.9}$$

In the following, we explain the procedure in Algorithm 3. The first scheduled user U_1 is the one maximizing the metric defined in (4.10).

$$U_1 = \max(\alpha_m.\|\mathbf{h}_m\|) \tag{4.10}$$

After the first user has been scheduled, in order to schedule the remaining *K-1* users, the metric w_m in (4.11) is sequentially calculated for each user $m = 1, \ldots,$ M, with Λ denoting the set of indexes of the previously scheduled users.

$$w_m = \max(\alpha_m.(1 - \sum_{j\in\Lambda} \frac{|\ \mathbf{h}_j\mathbf{h}_m^H\ |}{\|\mathbf{h}_j\|\|\mathbf{h}_m\|})) \tag{4.11}$$

At each step the scheduled user U_k is the one maximizing the metric w_m, which jointly accounts for the priority and for the orthogonality to the previously scheduled users. The WSOS scheduling is followed by precoding to mitigate the interference of the semi orthogonal scheduled channels.

At some point, it is important to update the priority coefficients α_m, and specifically to rescale it to account for those users which have low demand and have not been yet scheduled. In this paper, we propose the priority update based on the average offered rate, where the priorities in a given instant are updated considering the average rate provided to the users until that particular time instant. This approach, which requires the storage of the offered rates for a specific temporal window, can dynamically account for the average demand satisfaction at each user. More specifically, the coefficient of a served user m at the scheduling instance t is updated as per (4.12), with d_m denoting the demand and $E_m(R_m)$ the average rate until instant t.

$$\alpha_m^{new}(t) = \frac{d_m(t)}{E_m(R_m(t))} \tag{4.12}$$

Algorithm 3: Proposed WSOS algorithm

Input : M, d_m, K, T
Output : U_k

Calculate $\alpha_m(t=1) = \frac{d_m(t=1)}{max_m(d_m(t=1))} \leftarrow \forall m$ where $\alpha_m \in [0,1]$
Set $\Lambda = \emptyset$
for $t = 1$ **to** T **do**
  for $m = 1$ **to** M **do**
    $U_1 = \max(\alpha_m(t).\|\mathbf{h}_m\|)$
  end
  Update set: $\Lambda = \Lambda \in U_1$
  for $k = 2$ **to** K **do**
    for $m = 1$ **to** M **do**
      $w_m = \max(\alpha_m(t).(1 - \sum_{j\in\Lambda} \frac{|\mathbf{h}_j \mathbf{h}_m^H|}{\|\mathbf{h}_j\|\|\mathbf{h}_m\|}))$
    end
    U_k is the user m of w_m.
    Update set: $\Lambda = \Lambda \in U_k$
  end
  Update α_m such that $\alpha_m(t) = \frac{d_m(t)}{E_m[R_m(t)]}$
end

The temporal window T is heuristically chosen based on the reduction rate of the priority coefficients. In the numerical simulations, T is fixed to 100. Further, the performance of the scheduling procedure is enhanced by promoting the underserved users when restoring the priorities (every T scheduling instances), in order to improve fairness.

4.1.4 Simulation and result analysis

Performance Metrics definition

Jain's Fairness Index [134] is a well-known fairness metric, which in this context measures how the provided rate matches the demand at a user level. Specifically, defining the satisfaction u_m of the generic user m as the ratio between the offered rate s_m and the demanded rate d_m, the Jain's fairness index is defined as per the (4.13) and ranges between $\frac{1}{M}$ and 1 where M defines the total number of users.

$$J = \frac{(\sum_{m=1}^{M} u_m)^2}{M \sum_{m=1}^{M} u_m^2} \tag{4.13}$$

Sum Rate (C) as defined in (4.14) is the average sum throughput delivered by the multibeam system in a particular window of time, where C_k represents the average beam

throughput.

$$C = \sum_{k=1}^{K} C_k \tag{4.14}$$

Simulation results

In this section, we present numerical results of the Monte Carlo simulations to validate the proposed Weighted Semi-Orthogonal Scheduling (WSOS) scheme.

The considered benchmark is Semi-Orthogonal Scheduling (SOS) as defined in [143, 144] which is not designed to account for user demand. Another benchmark is the Demand-Based Scheduling (DBS) which is purely designed to satisfy the demand without considering the channel orthogonality. The Geographical scheduling is intentionally not included, as its performance is expected to be worse than SOS, since the phase of the channel components are ignored.

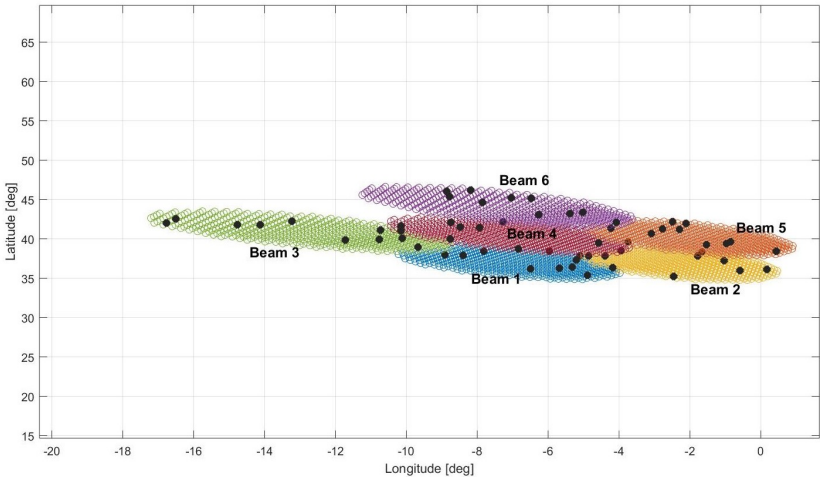

Figure 4.3: Considered beam cluster, with users' positions considered for scheduling.

The antenna pattern corresponds to a 71-beam GEO 13E satellite operating at the Ka exclusive band 19.7 to 20.2 GHz in accordance to [112–114] and the simulation parameters are as shown in Table 4.1. Also, we consider a total number of $M = 60$ users distributed across $K = 6$ beams as shown in Figure 4.3. Users locations and demands have been extracted from the SnT traffic simulator [124]. Furthermore, we consider a sum power-constrained system with a per-beam power of 20 dBW and a bandwidth of 500 MHz.

The scheduling performance is assessed both at beam and user level, by evaluating the average per-beam user rate as well as the rate for each user, and by comparing them with

Table 4.1: Simulation Parameters

Satellite longitude	13 degree East (GEO)
Satellite total radiated power, P_T	6000 W
Total Number of Beams, N_B	71 (Only 6 beams are considered)
Number of HPA, N_{HPA}	36 (2 beams per HPA)
Beam Radiation Pattern	Provided by ESA
Downlink carrier Frequency	19.5 GHz
User link bandwidth, B_W	500 MHz
Roll-off Factor	20%
Duration of time slot. T_{slot}	1.3 ms
Number of time slots	100
Antenna Diameter	0.6
Terminal antenna efficiency	60%
DL wavelength	0.01538 m

the demand.

The per-beam average user rate is shown in Figure 4.4 and compared with the average per-beam demand. It can be observed from Figure 4.4 that the proposed scheme satisfies the requested beam demand for all beams. On the other hand, the benchmarks achieve an offered rate either completely mismatched from the demand as in the case of SOS scheme or not meeting the demand in all the beams as in the case of the DBS. Furthermore, even though the DBS attains a rate that follows quite well the average demand, at many instances the demand is not satisfied (Beam 3, 4 and 5). This is because the cluster demand is too high to be met without proper precoding-tailored user scheduling.

Figure 4.5 provides the results at user level. In particular, Figure 4.5 compares the average offered user capacity versus the user requested demand for the proposed WSOS scheme as well as the two considered benchmarks, i.e. DBS and SOS. Clearly, the conventional SOS is not matching the user demands, resulting on some users receiving capacity that is not requested and some others where the offered capacity falls short is satisfying the users' demands. The DBS scheme provides a quite accurate demand matching but it faces some issues in satisfying the high demand requests. Finally, the proposed WSOS is shown to provide a good trade-off between demand satisfaction and the offered capacity.

Additional insights are given in Table 5.1, where the sum rate and the Jain's fairness index of users' satisfaction are provided for the considered scheduling schemes. The obtained Jain's indexes clearly show that the proposed scheme provides greater fairness in comparison

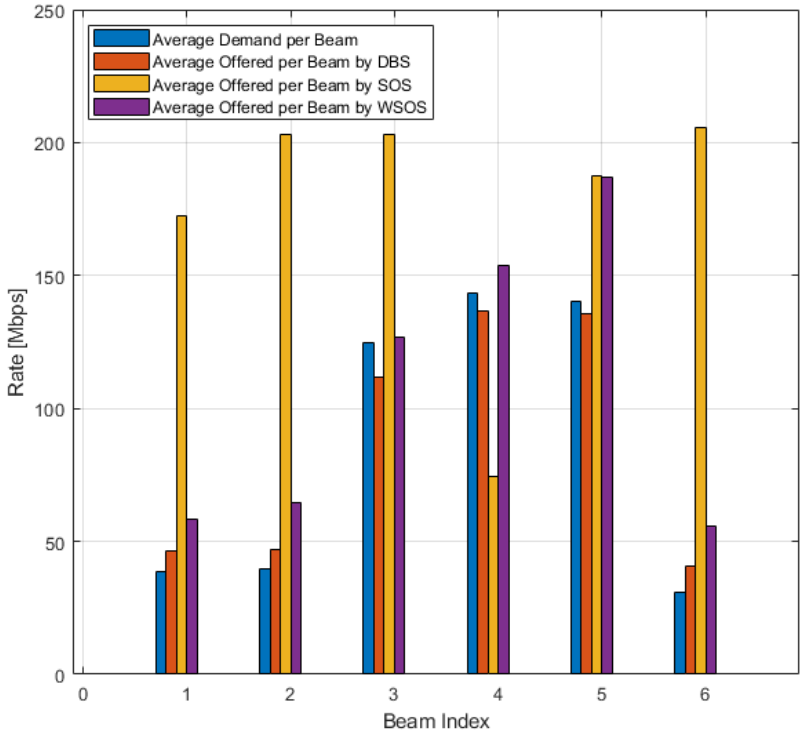

Figure 4.4: Per-beam Average User Rate vs. Average Demand

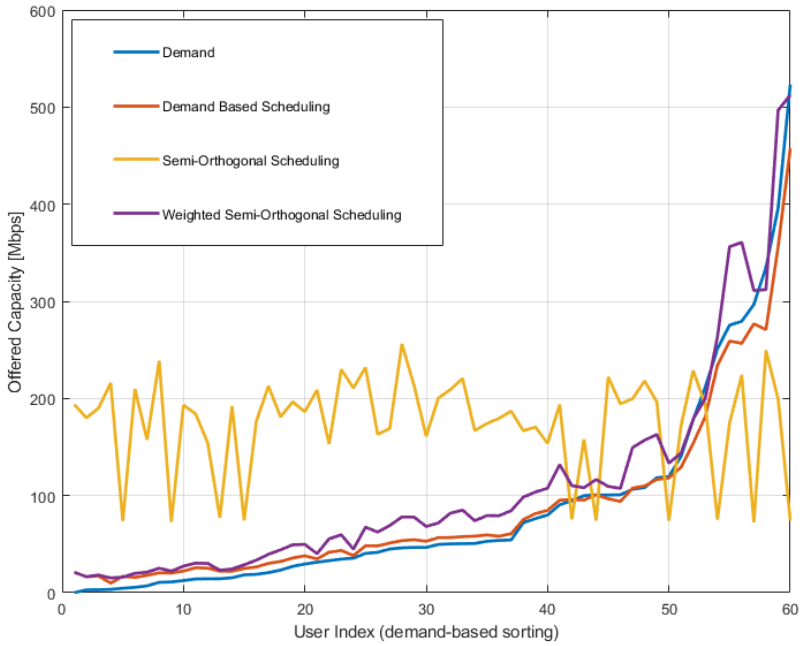

Figure 4.5: Per-user Rate vs. Demand

to the benchmarks (i.e. index is always close to 1). Also, the achieved sum rate is higher than the DBS scheme. As expected, SOS has a better sum rate in comparison to the proposed WSOS. Nonetheless, the proposed scheme offers better trade-off in terms of fairness, which is considerably more crucial and demand dependent.

Table 4.2: Sum rate and Jain's fairness index of users' satisfaction for the considered scheduling schemes, with Priority update based on average offered rate.

	WSOS	**SOS**	**DBS**
Sum Rate (Gbps)	6.2749	10.8339	5.6286
Jains's Fairness Index	0.9102	0.0169	0.8317

4.1.5 Conclusions and Future Work

This paper proposed a novel user scheduling algorithm for precoded-based multibeam GEO satellite communications systems, including the design perspective of allocating resources according to the users' demands. The proposed Weighted Semi-Orthogonal Scheme (WSOS) provides a trade-off between the channel orthogonality needed for effective precoding performance and the user demand requirements. Numerical simulations conducted in MATLAB have evidenced better performance of the WSOS algorithm with respect to benchmark schemes in terms of balancing the demand satisfaction, user fairness and offered throughput.

A possible extension of this work would be the adaptation to multicast systems, where more than one user is scheduled at the physical frame defined by the standard DVB-S2X [11]. For sharing the frame, multiple users are usually grouped based on similar SNIR, and the modulation and coding scheme is selected based on the SNIR of the weakest user. Such grouping is necessary in order to guarantee that all the users, sharing the XFECFRAME, can decode the frame correctly. Hence, the proposed WSOS algorithm can be enhanced to face such challenges.

4.2 Interference-aware Demand-based User Scheduling

4.2.1 Introduction

The current broadband services are provided by the satellite operators using state of the art multi-beam satellite systems where the resulting inter-beam interference is mitigated using four colour frequency reuse scheme [52, 53]. However, the demand for broadband services is evolving and in recent years, due to mobile nature of the users, broadband demand is more dynamic than ever [5]. On the other hand, the ever-growing data demand together with the inherent satellite spectrum scarcity necessitates spectral efficient transmission. To meet such growing demand and to optimally exploit spectral resources across the satellite network, operators are looking forward to implement full frequency reuse in combination with co-channel interference mitigation techniques [88, 151, 152].

Linear precoding techniques have been recognized as an effective processing tool to mitigate the inter-beam interference resulting from aggressive spectrum reuse schemes [153]. The most popular low-complexity precoding design in satellite communications is the so-called Minimum Mean Square Error (MMSE) precoding [8, 88, 148, 154], which exploits the Channel State Information (CSI) at the satellite gateway side by operating on the signal before transmission. The MMSE precoding is sometimes known in the literature as zero-forcing precoding, since its closed-form solution involves the channel matrix inversion. To overcome stability issues, a regularization factor is typically applied to the channel matrix to facilitate the inverse calculation. Precoding for satellite communications has reached a high Technology Readiness Level (TRL) with its recent demonstration over a real satellite system using DVB-S2X specifications [89], confirming its feasibility for practical systems.

User scheduling plays a key role in precoded communication systems [155, 156]. Typical systems involve a large number of users, particularly for satellite communications, claiming for an efficient time-multiplexing approach led by the user scheduler block. For MMSE-based precoded-systems, their performance is largely degraded when serving spatially correlated users [21]. This is because the scheduling determines the actual channel matrix to be inverted. As highlighted in [8], precoding and user scheduling should be ideally jointly optimized to achieve the optimal performance due to their coupled nature [142, 157, 158].

On the other hand, satellite operators and service providers are obliged to provide pre-agreed levels of throughput to broadband users. Such agreed throughput is typically defined

in a legal contract termed as the Service-Level Agreement (SLA) [159]. Furthermore, satellite resources are scarce and expensive, and have to be efficiently used [46,64]. It is expected that users within the coverage area will have different traffic demand needs [112,160]. Therefore, demand-aware strategies are preferred to avoid situations where users' demand is low compared to the supplied capacity. While the demand-aware radio resource allocation has been extensively studied in the literature (see Section I.A), herein we focus on the user scheduling, which is a low-complexity degree of freedom that allow the non-uniform distribution of capacity across users.

Related Works

Interference avoidance and interference mitigation has been extensively discussed in both satellite and terrestrial communications systems. Early works include Dirty Paper Coding (DPC) as an effective interference mitigation coding scheme [161]. However, due to the high complexity of DPC, many heuristic precoding techniques such as Zero Forcing (ZF) and Regularized ZF/MMSE have been explored [162–168]. Given its maturity [89], in this work we selected MMSE precoder for precoding and focus on the effective user scheduling algorithm to mitigate the inter beam interference and offer user demand satisfaction.

Considering the user scheduling in precoded-satellite systems, the authors of [8,157] discuss the failure of precoding to mitigate the inter-beam co-channel interference during the scheduling of users with co-linear channels and hence, express the need for scheduling orthogonal users across beams.

Even though precoding is performed after user scheduling in the physical layer transmission chain, there exists a strong coupling between both. So, considering the joint nature of precoding and user scheduling, the works in [142,157,158] suggest a joint solution where they propose sub-optimal solutions that reach stationary points of the original problem. However, the joint user scheduling and precoding problem is non-convex and NP-hard. This means that multiple locally optimal points exist, and theoretical guarantees are weak or non-existent. Furthermore, obtaining the optimal solution requires an exhaustive search-based user grouping and scheduling, which quickly become impractical due to exponential complexity. This was the approach followed in ESA PreDem project [169], confirming the unsustainable complexity. As a consequence, most of the literature have opted to precode and schedule separately, but considering their coupling as intuitions for their design. Hence, to

improve the performance of precoding and the consequent system offered capacity, multiple authors in literature, including [170–172], have scheduled orthogonal users to multiple beams at the same time.

As a simplistic approach, some of the authors achieve such orthogonality between scheduled users based on geographical location. The authors in [173] propose geographic user clustering approach and use Euclidean distance to relate channel vectors and impose channel orthogonality. In a comparable approach, the authors in [146] propose a geographical scheduling algorithm and schedule together users belonging to similar locations in their respective beams. Similarly, the authors in [148] propose a user grouping scheme using random pre-processing and the before mentioned Euclidean norm. Another similar approach to interference avoidance is as by the authors of [174], where using graph theory in cellular networks, they propose a Least Beam Collision (LBC) algorithm to reduce inter-cell interferences (ICI) which works by avoiding the scheduling of any two adjacent cells simultaneously to the beam which may interfere with each other. In [145], the authors propose cross-layer scheduling algorithm that make use of the spectral clustering technique, whose primary goal is to generate clusters of users with orthogonal channel characteristics. Also, the authors of [175] propose interference aware scheduling using partial channel state information (CSI) and minimise scheduling users in the interfering beams together. The authors of [176] investigate user scheduling for multicast transmission with full frequency reuse and multicast precoding. However, as an enhancement, other authors have considered the channel characteristics using Euclidean norm and cosine similarity. Accordingly, channel orthogonality and the semi-orthogonal scheduling as defined in [177], has been widely used in the satellite community to deal with the scheduling problem. Furthermore, in [144], the authors use the cosine similarity metric to sequentially select the users with most orthogonal channel vectors.

While these aforementioned works effectively improve the overall system throughput, they have not considered the actual user traffic demands. The latter can translate into systems that are pushing the satellite limits to achieve high capacity, while this is not actually requested by the users.

Regarding the satellite-based demand matching problem, there has been few works addressing this from different perspectives. To support the dynamic growth of satellite technology and operational requirements, recent developments have focused on generic flexible payload technology [178, 179]. Considering time-domain flexibility, authors have proposed

beam-hopping designs considering users' quality of service [180]. The user demand satisfaction was part of the formulation in [44, 63], which focused on frequency and/or power allocation. More recently, some works have focused on re-configurable beam sizes and positions to match the traffic demand with four color frequency coding with a simplified resource allocation [68, 84]. However, demand matching can be further enhanced by proper user scheduling where the primary goal is to assign the system capacity where it is actually needed. Hence, in this paper, we emphasise scheduling algorithms that majorly consider demand matching problem and do not just intend to maximize the offered throughput.

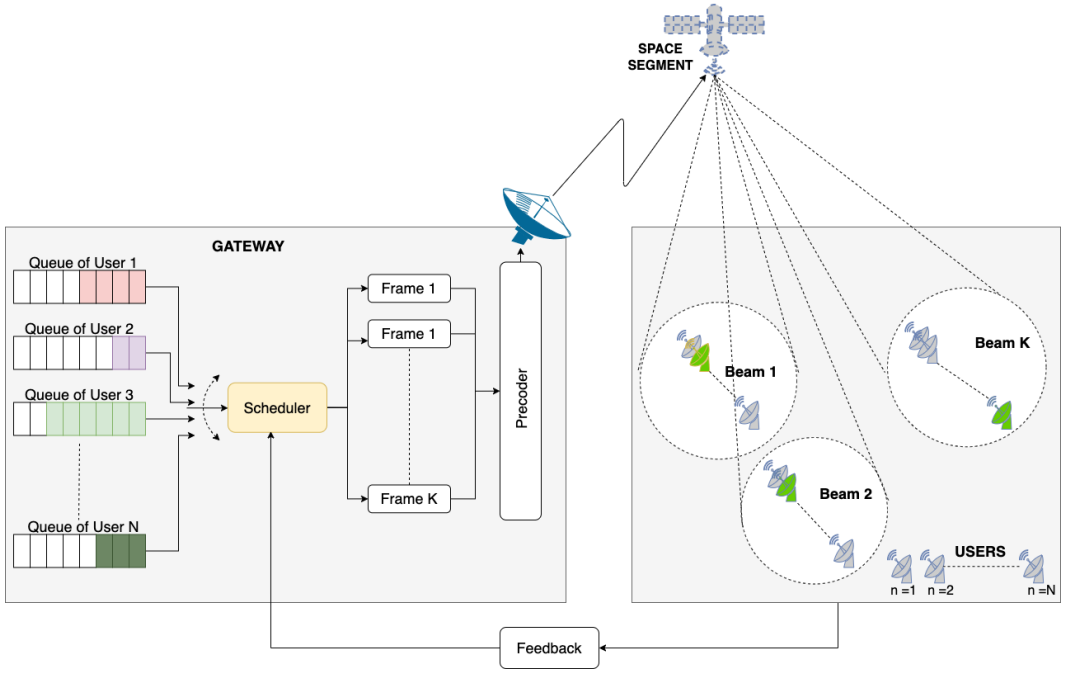

Figure 4.6: High throughput multi-beam satellite high-level system architecture.

Contribution

The major contribution and novelty of this paper aims on including demand-driven adaptability at user scheduling while using MMSE design for precoding. To the best of the authors' knowledge, all related works have so far focused on maximizing the offered throughput by mitigating inter-beam interference using precoding and scheduling. However, as capability to flexibly allocate on–board resources over the service coverage is becoming a must for future broadband multi-beam satellites, in this work, we consider demand matching as our prime objective. In other words, this work aims to assign the system capacity where it is actu-

ally needed and hence the proposed scheduling design is based not only from the maximum throughput perspective but also considering the aforementioned demand matching problem. The detailed contribution of the paper can be listed as follows:

1. The user scheduling problem is typically based upon a predefined user-beam assignment. In most works of literature, a "beam-free" approach [181] is followed where the users are orthogonally assigned to beams based on the beam gain that is observed by the users. Such an approach fails to exploit the unused resources of neighbouring beams in hot-spot scenarios. Hence, we propose a novel semi-beam-free user-beam assignment, where users are assigned to beams only when they are in close vicinity of the main beam. Accordingly, such assignments not only allow the use of resources of low-demand beams to serve users in neighboring hot-spot regions but also avoids high dimension scheduling problem that translates in long computational times.

2. Next, as most of the related works fail to express a distinct relation between any user, beam and time, we define a novel scheduling model and, furthermore, unlike the related works that do not address demand driven systems, we formulate demand satisfaction using an appropriate queue model.

3. While all the related works consider co-channel interference and perform user scheduling to maximize the offered capacity or improve fairness, we consider both co-channel interference and user demand requests and formulate a generalized problem statement for the interference-aware demand-based user scheduling. In particular, we make use of the queue model and assume an initial queue status proportional to the user demand, and our objective is to minimize the remaining data in the users' queues after a particular time interval.

4. Lastly, we analyse the problem statement which turns out to be of non-convex nature and propose a novel heuristic interference-aware demand-based user scheduling algorithm which follows a 5-step approach. First, we group the users into sectors based on their geographical locations. Then we categorize sectors as interfering and non-interfering classes. We use graph theory to perform edge pruning to simplify the future steps. Later, we perform class scheduling to minimize the inter-beam interference while dwelling just enough to satisfy the sectors' demand. Finally, we perform a user schedul-

ing within each sector of the beam with the goal to accurately satisfy the particular users' demand.

Notation: We use upper-case and lower-case bold-faced letters to denote matrices and vectors, respectively. $\circ$ denotes the element-wise Hadamard operations. $(\cdot)^T$ denotes the transpose of $(\cdot)$. $|\,.\,|$ and $\|.\|$ depict the amplitude and Euclidean norm, respectively.

4.2.2 System Model

Multi-beam Satellite System

We consider a multi-beam satellite system that includes a ground segment (single gateway with ideal feeder link is assumed) and a space segment (single non-regenerative GEO HTS) as shown in Figure 4.6. In the forward link, the multi-beam satellite system provides service to N number of single-antenna users using K spot beams where $N >> K$, which are distributed across the coverage area of the satellite. The user distribution on-ground is typically non-uniform, e.g. airport surrounding areas are typically more congested than residential low-populated areas. In addition, the demand requests of users depend on the final service, e.g. satellite backhauling terminals tend to aggregate cellular requests of many users resulting in high demand, while residential broadband VSAT terminals typically requests low traffic. Figure 4.7, shows beam footprint over Europe using 71 fixed beams with flight user locations in blue, ship user locations in red and FSS user locations in beige, from which, it is evident that broadband users across Europe are not uniformly distributed. Also, different users have different throughput demand and QoS requirements.

In this paper, we focus on a bent-pipe GEO satellite system where all the signal processing blocks are implemented on ground at the gateway side. Therefore, the computation and implementation of the precoding matrix is performed at the gateway. After that, the precoded signals are transmitted through the feeder link to the satellite and the satellite performs a frequency shift, amplifies and forwards the precoded signals to the final users on ground.

Low-complexity linear precoding techniques are considered to alleviate the complexity burden of the gateway [87]. The forward link air interface is assumed to be based on DVB-S2(X) [11], which considers Adaptive Coding and Modulation (ACM) allowing real-time adaptation of transmission parameters according to the link conditions.

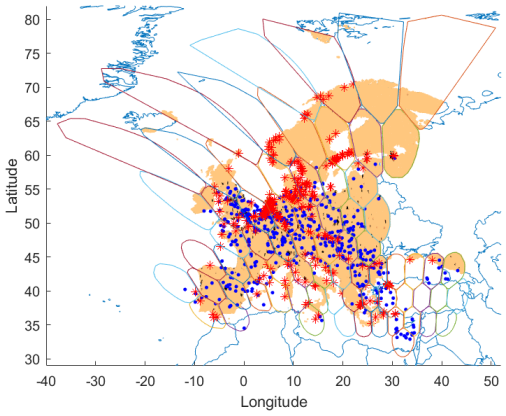

Figure 4.7: Footprint over Europe using 71 Fixed Beams showing flight user locations in blue, ship user locations in red and FSS user locations in beige.

Multi-beam Satellite Channel

The satellite antenna architecture is assumed to be able to generate a total number of K beams. For the methodology presented in this paper, it does not matter if the beams are conformed with a single-feed-per-beam (SFPB) architecture or a multiple-feed-per-beam (MFPB). The received signal of user n is y_n and is expressed as,

$$y_n = \mathbf{h}_n^T \mathbf{x} + \mathfrak{N}_n, \tag{4.15}$$

where $\mathbf{h}_n \in \mathbb{C}^{K\times 1}$ is the CSI vector corresponding to this particular user. By rearranging all the users' received signals in a vector $\mathbf{y} = [y_1 \dots y_N]^T \in \mathbb{C}^{K\times 1}$, the above model can also be expressed as,

$$\mathbf{y} = \mathbf{H}\ \mathbf{x} + \mathfrak{N}, \tag{4.16}$$

by considering $\mathbf{H} = \Phi\mathbf{B} \in \mathbb{C}^{K\times K}$, where $\mathbf{B} = [\mathbf{b}_1 \dots \mathbf{b}_N]^T \in \mathbb{R}^{K\times K}$ is the system channel matrix whose the (n, k)th component is given by,

$$[\mathbf{b}]_{n,k} = \frac{\sqrt{G_{Rn}G_{kn}}}{(4\pi\frac{\mathfrak{D}_{nk}}{\lambda})}, \tag{4.17}$$

where λ is the wavelength of transmission, G_{kn} is the gain of beam k in the direction of user n , G_{Rn} is the user's receive antenna gain and $\mathfrak{D}_{nk}$ is the distance between the satellite transmit antenna and user's receiving antenna. The phase matrix $\Phi \in \mathbb{C}^{K\times K}$ is expressed as,

$$[\Phi]_{xx} = e^{i\phi_x}, \forall x = 1...K \tag{4.18}$$

where Φ_x is a uniform random variable in $[2\pi, 0]$ and $[\phi]_{xy} = 0, \forall x \neq y$.

The precoded signal is given by,

$$\mathbf{x} = \mathbf{W}\ \mathbf{s}. \tag{4.19}$$

where $\mathbf{W}$ is the precoding matrix and $\mathbf{s}$ is vector of transmit symbols that satisfies $[\mathbf{s}\mathbf{s}^H] = \mathbf{I}$. The precoding matrix $\mathbf{W}$ is obtained with the well-known MMSE design, which can be expressed as,

$$\mathbf{W}_{RZF} = \eta' \boldsymbol{H^H(HH^H + \alpha_r I)^{-1}}, \tag{4.20}$$

where α_r is a predefined regularisation factor and η is the power allocation factor defined as,

$$\eta = \sqrt{\frac{P_{tot}}{\text{Trace}(\mathbf{W}\mathbf{W}^\dagger)}}, \tag{4.21}$$

with P_{tot} being the total available power.

Beam-User Set ($\mathfrak{G}_k$) Formulation

As a pre-scheduling step, each user needs to be associated with potential beams from where it can receive service. The latter is known as user-beam association. Typically, users are associated to a single beam, from whom best beam-pattern gain is observed. However, it is beneficial to consider multiple beams associated to each user, particularly for those user located far from the beam center. The latter is particularly interesting when dealing with uneven user distributions, which may result in congested and uncongested beams. In such cases, the resources of uncongested beams can be exploited to alleviate the congestion of neighboring beams.

The objective of this section is to come up with an adequate user-beam association, which will be considered as baseline for the proposed interference-aware demand-based scheduling. Accordingly, for every beam k, we need to formulate a unique user pool called Beam-User Set ($\mathfrak{G}_k$). This set $\mathfrak{G}_k$ contains all the users that beam k can schedule. By employing a time division multiplexing access (TDMA) scheme, each beam will schedule only one user from the set $\mathfrak{G}_k$ at each scheduling interval t.

We make use of a binary relation matrix $\mathbf{G} \in \mathbb{B}^{N \times K}$, where each element, $g_{(n,k)} =$

$\{0,1\}, \forall(n,k)$ is a binary variable that denotes the user assignment to the beam. A simple approach to formulate $\mathbf{G}_k$ is to consider all the N users associated to all beams. This is sometimes referred as "beam-free" approach in the literature. In such case, $\mathbf{G}_k = \mathcal{N}, \forall k.$ where $\mathcal{N}$ is the set of all N users. Accordingly, the previously proposed binary relation matrix $\mathbf{G} \in \mathbb{B}^{N \times K}$, is all-ones matrix, and hence every element, $g_{(n,k)} = \{1\}, \forall(n,k)$. Even though such an approach is beneficial for its holistic approach, assigning specific users to beams with poor antenna gain is an inefficient design. This is because users with poor channel gain in any beam will never be scheduled in that beam if the link budget cannot be closed. Furthermore, the beam-free approach result in high dimensional combinatorial problems when formulating scheduling techniques, resulting in computationally complex designs.

Hence, the potential number of beams from which a particular user is able to receive enough beam-pattern gain is limited to only few beams. Accordingly, we propose to reformulate the user-beam association problem as follows,

$$g_{(n,k)} = \begin{cases} 1, & \text{if } d(n,k) <= d_{\min} \\ 0, & \text{otherwise} \end{cases} \tag{4.22}$$

where $d(n,k)$ is the Euclidean distance between the geographical location of the user (x_n) and the beam center (c_k) and is defined as,

$$d(n,k) = ((\mathbf{x}_n - \boldsymbol{c}_k)^T(\mathbf{x}_n - \boldsymbol{c}_k)), \tag{4.23}$$

and $d_{\min}$ is the beam boundary measured from the beam center that decides user association to a beam and is used to penalize the inefficient user-beam associations.

Figure 4.8 shows a simplified model with 3 beams and different beam-overlapping based on the value of $d_{\min}$ in problem (4.22). Accordingly, Users in region R4 can be shared between 3 beams and users in regions R1, R2, and R3 can be shared between 2 beams.

Figure 4.9 shows the benefits of sharing users between two beams. In such cases, when a user of high demand (denoted in red) belongs to beam-user set of two adjacent beams, the high-demand user can be scheduled more often by either of the two beams, which can lead to better demand satisfaction.

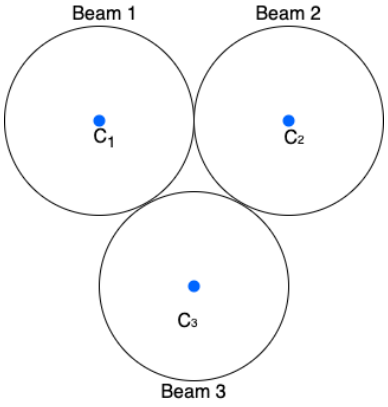

(a) No user sharing

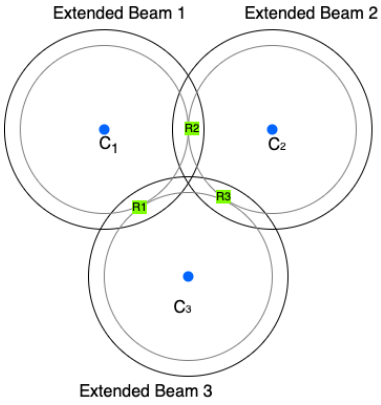

(b) Users in regions R1, R2, and R3 can be shared between 2 beams

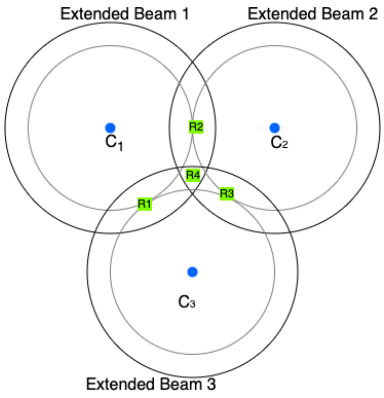

(c) Users in region R4 can be shared between 3 beams. Users in regions R1, R2, and R3 can be shared between 2 beams

Figure 4.8: Different user-beam association scenarios

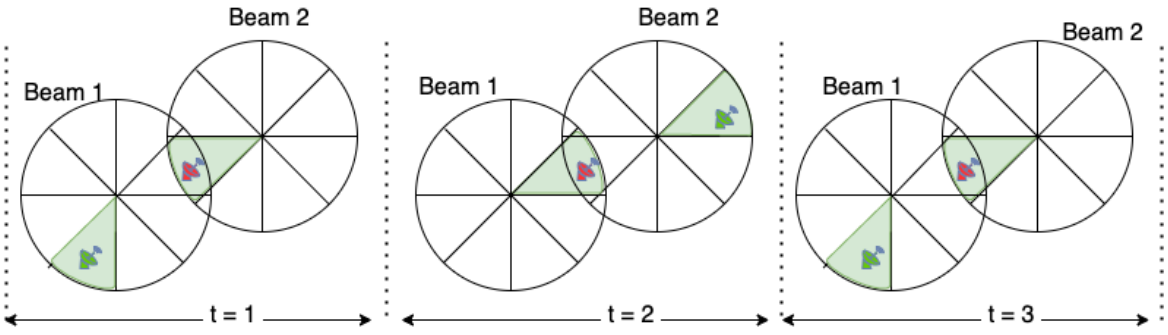

Figure 4.9: Shared user at overlapping region of two beams can be scheduled more often by either of the two beams

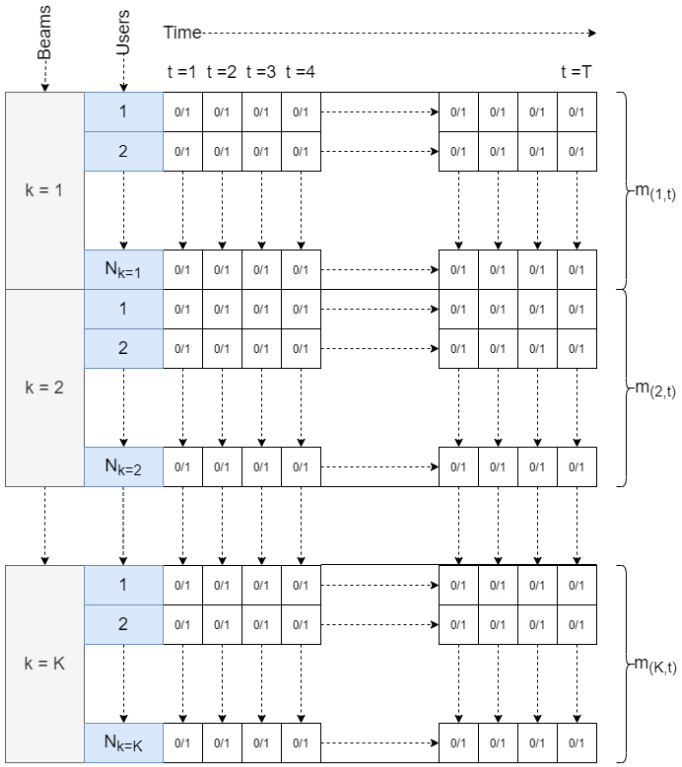

Figure 4.10: Scheduling model

Scheduling Model

The scheduling model as illustrated in Figure 4.10 is used to express the relation between the scheduled user n to beam k at any time instance t. In this work, to develop a relation between users, beams and time slots, we formulate a binary relation matrix $\mathbf{M}$ of size $K \times T$, where every row element of M is defined as $m_{(k,t)} = [u^k_{(1,t)}, u^k_{(2,t)} ... u^k_{(N_k,t)}]^T$. The value of N_k varies for different values of k and is the cardinality of Beam-User Set ($N_k = |\mathfrak{G}_k|$). Also, $u^k_{(n,t)} = \{0, 1\}, \forall(n, k, t)$ is a binary variable that denotes whether a user n is scheduled to a beam k at time t or not.

In this work, we formulate the relation matrix $\mathbf{M}$ using block-wise scheduling methodology, i.e. we consider a time window composed of T successive scheduling time-slots. More precisely, the scheduling optimization is solved only once every T, and provides the scheduling solution for each of the scheduling time-slots included in the considered time window. In such approach, we assume, that the user demand does not change drastically within the time window T, and also the channel characteristics remain invariant (which is typically the case for GSO systems assuming reasonable scheduling periods). The CSI is assumed to be

perfectly estimated following the Super-Frame (SF) pilot structure defined in DVB-S2X [11].

Queue Model

The objective of the proposed scheduling is two-fold: reduce interference and satisfy the users' demand. Focusing on the latter, herein we introduce the queue model. Essentially, the scheduling design will aim at emptying the users' queues by the end of the T scheduling time-slots. The demand requirements of the users in the satellite network are usually expressed in bits per second (bps). Accordingly, the initial queue status of any user n can be defined in bits as,

$$Q(n,0) = \mathfrak{d}_n \times T, \tag{4.24}$$

where $\mathfrak{d}_n$ is the demand of any user n and T is the total number of time-slots, for example, each time-slot duration can be $1.3ms$. Furthermore, the instantaneous queue status of any user n in bits at any time t is defined as,

$$Q(n,t) = Q(n,(t-1)) - (C_{(n,t)} \times \tau) \tag{4.25}$$

where τ is the duration of every scheduling slot in seconds and $Q(n,(t-1))$ is the queue status at any time instance $(t-1)$. $C_{(n,t)}$ is the offered capacity to a user n at the time t and is defined as,

$$C_{(n,t)} = \sum_{k=1}^{K} C^k_{(n,t)} \times u^k_{(n,t)}, \tag{4.26}$$

where $C^k_{(n,t)}$ is the offered capacity to a user n by beam k at the time t and is defined as,

$$C^k_{(n,t)} = B \log\left(1 + SINR^k_{(n,t)}\right), \tag{4.27}$$

where B is the user bandwidth and $SINR^k_{(n,t)}$ is the signal to interference plus noise ratio offered by beam k to user n at time t and is defined as,

$$SINR^k_{(n,t)} = \frac{\mathbf{h}^H_{nn}\mathbf{w(t)}_n s(t)_n}{\sum\limits_{k=1(k\neq n)}^{K} \mathbf{h}^H_{kn}\mathbf{w(t)}_k s(t)_k + \mathfrak{N}(\mathfrak{t})_n}, \tag{4.28}$$

where $s(t)_k$ is the encoded information signal transmitted from the k^{th} beam at time t. $\mathbf{w(t)}_k$ is the associated beamforming vector for $k = 1, 2, ..., K$ and $\mathfrak{N}(\mathrm{t})_n$ is a random variable distributed as $\mathcal{CN}(0, \sigma^2)$, modelling the zero-mean Additive White Gaussian Noise (AWGN) measured at the user n's receiving antenna at time t.

Assuming T scheduling windows, the desired situation would be that each queue is emptied at the end of T time slots, i.e. $Q(n, T) = 0, \forall n$.

4.2.3 Generalized Scheduling Problem Statement

In this section, we present the generalized scheduling problem formulation. As anticipated in the previous section, our goal is to ensure that all users' queues are vacated or with very few remaining bits at the end of the scheduling window interval T. Based on this intuition, we formulate the objective function using (4.25). The optimizing variable $\mathbf{M}$ is as described in Section 4.2.2 and the optimization problem is as follows,

$$\min_{\mathbf{M}} \frac{1}{N} \sum_{n=1}^{N} Q(n, T) \tag{4.29a}$$

$$s.t. \quad u^k_{(n,t)} = \{0, 1\}, \forall (n, k, t) \tag{4.29b}$$

$$\sum_{n=1}^{N_k} u^k_{(n,t)} = 1, \forall k, t \tag{4.29c}$$

$$u^i_{(n,t)} = u^j_{(n,t)} \neq 1, \forall i \neq j, n, t \tag{4.29d}$$

where the first constraint in (4.29b) ensures that $u^k_{(n,t)}$ is a binary variable; The second constraint in (4.29c) ensures that only one user is scheduled for any value of k at any time t. As explained in 4.2.2, it is possible to have same users assigned for different beams i.e $n \in \mathfrak{G}_{k1}$ and $n \in \mathfrak{G}_{k2}$. Hence, there is a possibility of same user being scheduled by different beams at the same time t. This is precluded in the third constraint in (4.29d) which ensures that no two beams schedule same user n at the the same time t.

The optimization problem in (4.29a) is non-linear and non-convex in nature. This is majorly because:

1. The objective function in (4.29a) is a function of the offered capacity, which is a function of the SINR. In the SINR expression, the inter-beam interference appears in the

denominator and it depends on the optimization variable (i.e. the actual user scheduling).

2. Optimization variable **M** is a binary matrix. Therefore, the problem (4.29a) reduces to a mixed integer optimization problem that are very hard (technically NP-hard).

Hence, problem (4.29a) is difficult to solve efficiently using classical optimization techniques. Accordingly, in this paper, we propose a heuristic interference-aware demand-based user-scheduling algorithm.

4.2.4 Interference-aware demand-based user scheduling

In this section, we describe the proposed heuristic interference-aware demand-based user scheduling where channel orthogonality is maintained by carefully selecting users that least interfere with each other, while considering the actual user demands.

The proposed approach considers the users of each beam to be grouped into sectors based on their geographical locations. The main intuition to avoid interference is to schedule sectors across beams ensuring non-adjacency between them. In other words, the channel orthogonality is maintained by not scheduling users in two adjacent sectors of different beams at the same time. Such an approach does not require the Channel State Information (CSI) at the gateway and hence unaffected from faulty or outdated CSI errors. Furthermore, the proposed interference-aware demand-based user scheduling targets the user demand matching by ensuring that the users' queue status at the end of time period T is ideally empty.

The proposed scheduling is composed of 5 main steps which are detailed in Figure 4.11. Next, we provide a high-level explanation of each step.

The step-1 i.e. sector formulation of interference-aware demand-based user scheduling is a one time procedure for all beams and does not need to be recalculated unless the beam pattern changes. In conventional systems the number of beams and the shape of the beams will remain fixed. However, recent advanced works [68,84] have proposed demand based adaptable beam designs and footprint planning, where the beam footprints adapt to change according to user demands. In any case, beam pattern adaptations are not expected to take place in short time intervals. The step-2 of class definition is also a one time procedure which strongly depends on how we formulate the sectors in the step-1. In this step sectors are grouped into interfering classes and non-interfering classes. In step-3, the graph construction and edge pruning is

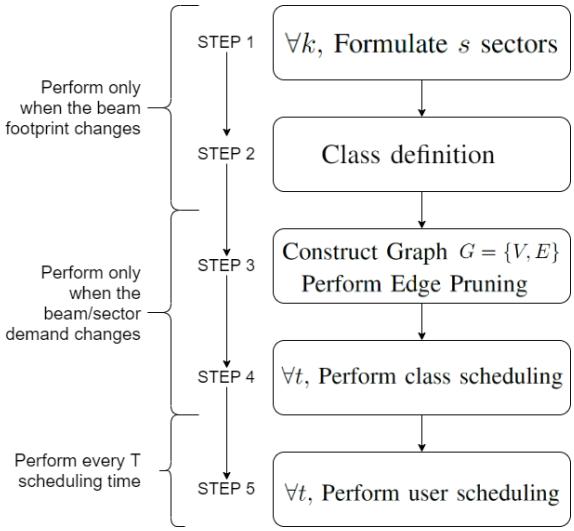

Figure 4.11: Steps involved in interference-aware demand-based user scheduling.

done to accelerate the subsequent steps. Again, Step 3 has to be performed only in case of significant demand variations across sectors. The main step of the proposed scheduling is step-4, where the class scheduling is performed. This step has to be carried out only when the demand of the classes changes. Once the coarse scheduling of classes is determined, the last step-5 addresses the demand-based user scheduling within each sector independently.

In the forthcoming sections, we provide a detailed description of each step.

Sector Formulation

We consider K beams indexed from 1 to K where each beam has s_k sectors. For simplicity, we consider s_k is fixed $\forall k$ and denote it as s. Figure 4.12 shows a scenario with six beams, each beam is divided into six sectors. The total of N users is distributed across all the beams. The sector demand is the sum of demand of all the users under a sector s and can be defined as,

$$d_s = \sum_{n \in s} \mathfrak{d}_n. \tag{4.30}$$

Class definition

The interbeam interference in the network is dominantly dependent on the geographic location of the sectors in the beam [146]. Highest interference is noticed when users in two adjacent sectors of different beams are scheduled together. Therefore, we can classify the sectors in

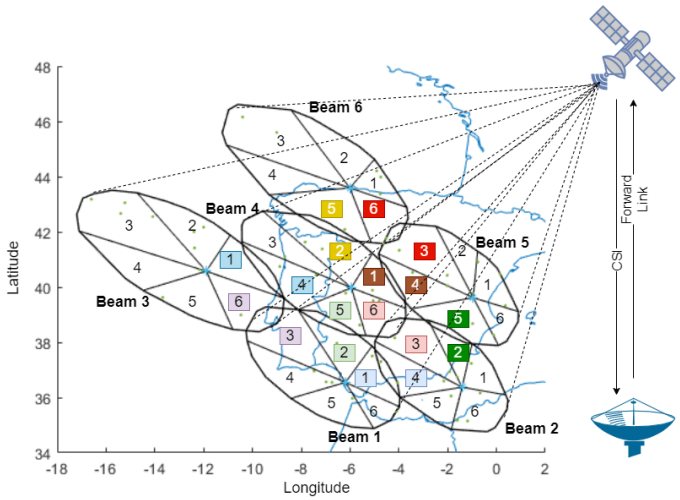

Figure 4.12: System model of 6 beams, where each beam is divided into 6 sectors.

each beam into classes according to the neighbouring beams' sectors they may interfere with. Specifically, for beam k, the sectors which may cause inter-beam interference to beam k' are classified into an interfering class denoted by the set $\mathcal{C}_{k\to k'}$, and the sectors in beam k which do not interfere with any neighboring beam are classified into an interference-free class denoted by the set $\mathcal{C}_{k\to k}$. For example, in Figure 4.12, $\mathbf{C}_1(2) = \mathcal{C}_{1\to 2} = \{1\}$, is a interfering class because sector 1 of beam 1 may cause inter-beam interference to beam 2 and $\mathbf{C}_1(1) = \mathcal{C}_{1\to 1} = \{4,5,6\}$ is a non-interfering class because the sectors 4,5 and 6 of beam 1 does not cause interference to any of the other beams under consideration. Similarly, $\mathbf{C}_2(1) = \mathcal{C}_{2\to 1} = \{4\}$ and $\mathbf{C}_2(2) = \mathcal{C}_{2\to 2} = \{1,5,6\}$. Accordingly, for the 6 beams in the Figure 4.12, we formulate 24 classes as shown in the shown in Table 4.3 and define the set $\mathbf{C} = \{\mathbf{C}_1(1), \mathbf{C}_1(2)...\mathbf{C}_6(3)\}$ as set of all the classes in the system.

Furthermore, $d_{k\to k'}$ is the class demand of an interfering class $\mathcal{C}_{k\to k'}$ and is defined as,

$$d_{k\to k'} = \sum_{s\in\mathcal{C}_{k\to k'}} d_s, \quad \forall k' - k \tag{4.31}$$

for all k' adjacent to k and $d_{k\to k}$ is the class demand of an non interfering class $\mathcal{C}_{k\to k}$ and is defined as,

$$d_{k\to k} = \sum_{s\in\mathcal{C}_{k\to k}} d_s, \tag{4.32}$$

Table 4.3: Class Definition using sectors

Name	Definition	Sectors	Name	Definition	Sectors
$\mathbf{C}_1(1)$	$\mathcal{C}_{1\to1}$	{4,5,6}	$\mathbf{C}_4(2)$	$\mathcal{C}_{4\to2}$	{6}
$\mathbf{C}_1(2)$	$\mathcal{C}_{1\to2}$	{1}	$\mathbf{C}_4(3)$	$\mathcal{C}_{4\to3}$	{4}
$\mathbf{C}_1(3)$	$\mathcal{C}_{1\to3}$	{3}	$\mathbf{C}_4(4)$	$\mathcal{C}_{4\to4}$	{3}
$\mathbf{C}_1(4)$	$\mathcal{C}_{1\to4}$	{2}	$\mathbf{C}_4(5)$	$\mathcal{C}_{4\to5}$	{1}
$\mathbf{C}_2(1)$	$\mathcal{C}_{2\to1}$	{4}	$\mathbf{C}_4(6)$	$\mathcal{C}_{4\to6}$	{2}
$\mathbf{C}_2(2)$	$\mathcal{C}_{2\to2}$	{1,5,6}	$\mathbf{C}_5(1)$	$\mathcal{C}_{5\to2}$	{5}
$\mathbf{C}_2(3)$	$\mathcal{C}_{2\to4}$	{3}	$\mathbf{C}_5(2)$	$\mathcal{C}_{5\to4}$	{4}
$\mathbf{C}_2(4)$	$\mathcal{C}_{2\to5}$	{2}	$\mathbf{C}_5(3)$	$\mathcal{C}_{5\to5}$	{1,2,6}
$\mathbf{C}_3(1)$	$\mathcal{C}_{3\to1}$	{6}	$\mathbf{C}_5(4)$	$\mathcal{C}_{5\to6}$	{3}
$\mathbf{C}_3(2)$	$\mathcal{C}_{3\to3}$	{2,3,4,5}	$\mathbf{C}_6(1)$	$\mathcal{C}_{6\to4}$	{5}
$\mathbf{C}_3(3)$	$\mathcal{C}_{3\to4}$	{1}	$\mathbf{C}_6(2)$	$\mathcal{C}_{6\to5}$	{6}
$\mathbf{C}_4(1)$	$\mathcal{C}_{4\to1}$	{5}	$\mathbf{C}_6(3)$	$\mathcal{C}_{6\to6}$	{1,2,3,4}

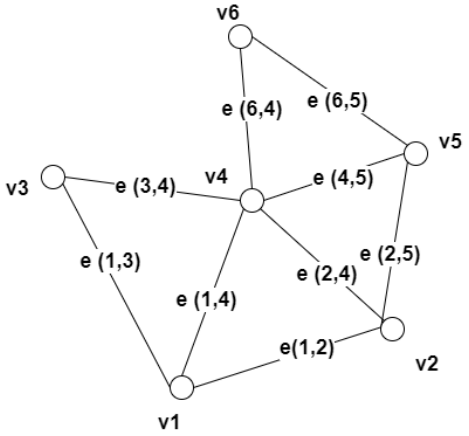

Figure 4.13: Graph Model of the system model in Figure 4.12

Graph construction and Edge Pruning based on class demand

This step is performed to simplify the class scheduling of the next step. Inspired by [174], we formulate the class-based graph model and perform edge pruning. Accordingly, as shown in Figure 4.13, we model the satellite network as graph G where the nodes represent the beams in the network and are denoted as v_k. We define the node set as a union set of all nodes i.e $V = \{v_1, ..., v_K\}$. As interference typically occur between adjacent beams, we also define $\mathcal{K}_k = \{k' : k'(adj)k\} \cup \{k\}$, where $\mathcal{K}_k$ represents a set of all the adjacent beams to beam k and itself. Furthermore, for any two adjacent beams k and k', the beams in $\mathcal{C}_{k\to k'}$ and $\mathcal{C}_{k'\to k}$ form an undirected edge $e(k, k')$ connecting the two nodes v_k and v'_k. The set of all edges in G is denoted as E, and we obtain $G = \{V, E\}$ as an undirected graph that represents the network.

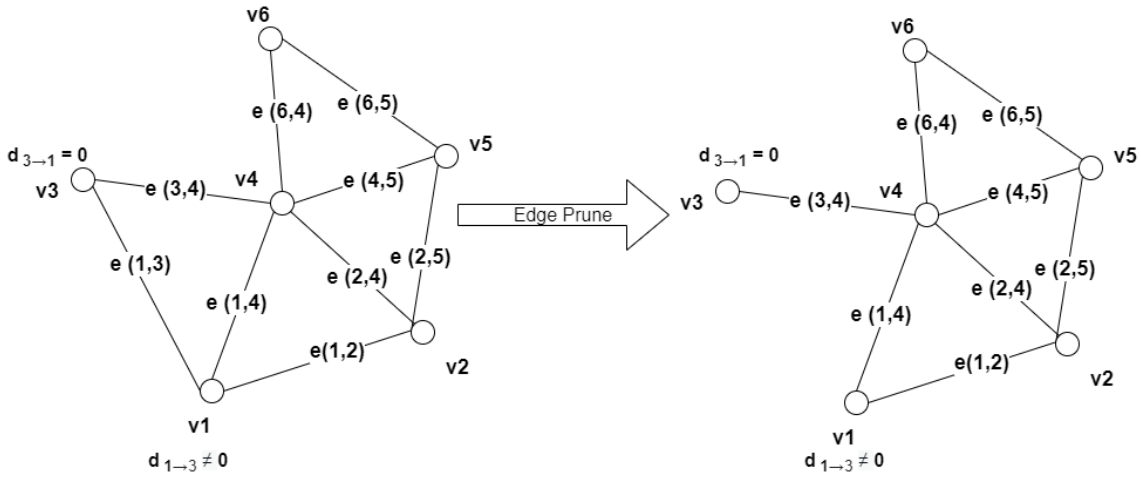

Figure 4.14: Example of edge pruning

Due to non availability of broadband users in any of the sectors of a class $\mathcal{C}_{k\to k'}$, the demand $d_{k\to k'}$ can be 0 and hence, scheduling of the class $\mathcal{C}_{k\to k'}$ should be precluded. Similarly, for any two adjacent nodes v_k and v'_k having classes $\mathcal{C}_{k\to k'}$ and $\mathcal{C}_{k'\to k}$, respectively, that form an undirected edge $e(k,k')$, the demand $d_{k\to k'}$ can be zero. Then, $\mathcal{C}_{k'\to k}$ becomes non interfering class and the edge, $e(k,k')$ can be pruned to simplify the subsequent scheduling procedure. This is achieved by adding any sectors in $\mathcal{C}_{k'\to k}$ to non interfering class $\mathcal{C}_{k'\to k'}$ as shown in Algorithm 4.

Class scheduling

The impact of scheduling in precoding performance can be alleviated by scheduling orthogonal users at any time instance t. Hence, we propose a novel class scheduling as a pre-step to user scheduling to obtain orthogonality in the scheduled users.

Interference between any user in beam k and k' is high when a sector in beam k belonging to class $\mathcal{C}_{k\to k'}$ is scheduled along with a sector in beam k' belonging to class $\mathcal{C}_{k'\to k}$. Hence, avoiding such class assignments requires careful class scheduling such that orthogonal sectors are scheduled at any time instance t. On the other hand, we need to ensure that the demand requisites of all the classes and users are met at the end of T scheduling period. Considering these points, we define a new class scheduling model as shown in Figure 4.15.

Consequently, $\forall k' \in \mathcal{K}_k$, we define a new class scheduling binary matrix $\boldsymbol{P}$ where every element of $\boldsymbol{P}$ denoted by $p^t_{k\to k'}$ is used to denote if a class $\mathcal{C}_{k\to k'}$ is scheduled at time t or not, i.e. if $p^t_{k\to k'} = 1$, we select a class $\mathcal{C}_{k\to k'}$ for scheduling at time t.

Algorithm 4: Class demand based Edge pruning to reduce the number of classes for scheduling

Input : $E, d_{k\to k'}, d_{k'\to k}$
Output : $d_{k'\to k'}, d_{k\to k}, \mathbf{C}$

$\forall e(k,k') \in E$;
if $d_{k\to k'} = 0$ *and* $d_{k'\to k} \neq 0$ **then**
  1. Delete $e(k,k')$; /* Prune edge */
  2. Compute $\mathcal{C}_{k'\to k'} = \mathcal{C}_{k'\to k'} \cup \mathcal{C}_{k'\to k}$ and update $\mathcal{C}_{k'\to k'} \in \mathbf{C}$; /* Update classes */
  3. Delete $\mathcal{C}_{k\to k'}$ and update $\mathbf{C}$; /* Delete Class with no demand */
  4. $d_{k'\to k'} = d_{k'\to k'} + d_{k'\to k}$; /* Update class demand */
else if $d_{k\to k'} \neq 0$ *and* $d_{k'\to k} = 0$ **then**
  1. Delete $e(k,k')$; /* Prune edge */
  2. Compute $\mathcal{C}_{k\to k} = \mathcal{C}_{k\to k} \cup \mathcal{C}_{k\to k'}$ and update $\mathcal{C}_{k\to k} \in \mathbf{C}$; /* Update classes */
  3. Delete $\mathcal{C}_{k'\to k}$ and update $\mathbf{C}$; /* Delete Class with no demand */
  4. $d_{k\to k} = d_{k\to k} + d_{k\to k'}$; /* Update class demand */
else if $d_{k\to k'} = 0$ *and* $d_{k\to k'} = 0$ **then**
  Delete $e(k,k')$; /* Prune edge */
else
  Retain edge;
end

The primary objective of the class scheduling problem is to avoid adjacent sectors to be simultaneously scheduled while activating sectors based on their aggregated demand requests.

Considering the aggregated sector demand d_s defined in 4.30, we estimate the total number of scheduling time-slots needed for sector s to satisfy its demand d_s as,

$$\tau_n = T \times \frac{\mathfrak{d}_n}{B \times f_{DVB-S2X}(SNR)}. \tag{4.33}$$

where T denotes the total window length in time-slots, $f_{DVB-S2X}(SNR)$ is spectral efficiency as a function of SNR defined in DVB-S2X [11], and the denominator $(B \times f_{DVB-S2X}(SNR))$ denotes the supplied capacity per scheduled time-slot assuming that the interference has been completely mitigated by the precoding technique. Clearly, 4.33 provides a best-case approximation, which will result with an underestimate of time-slots when residual interference exists. However, we will demonstrate via simulation results in Section 4.2.5 the effectiveness of the proposed approach.

Accordingly, we define the class aggregated demand as,

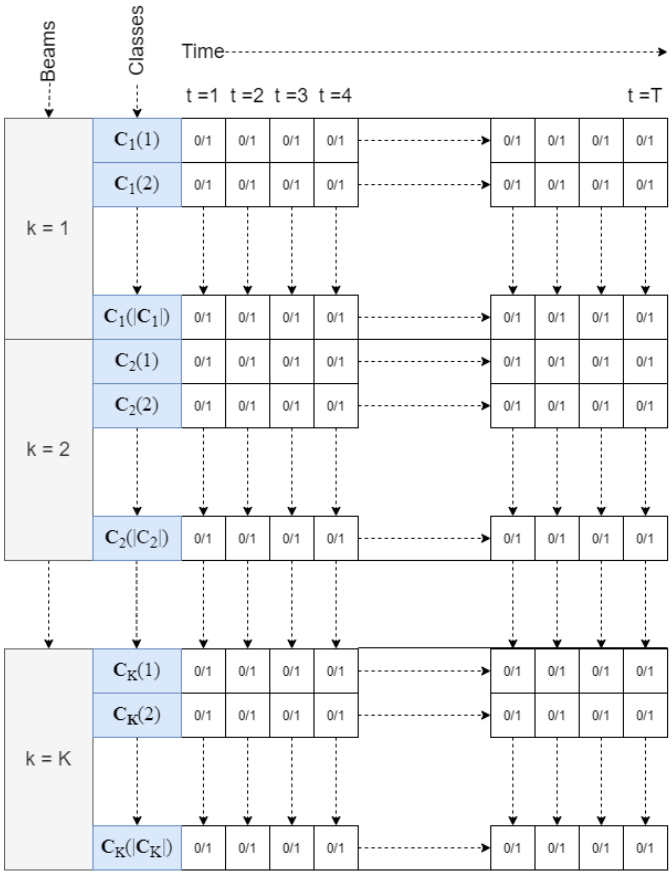

Figure 4.15: Class scheduling model

$$\tau_{k\to k'} = \sum_{s\in\mathcal{C}_{k\to k'}} \sum_{n\in s} \tau_n, \quad \forall k' \in \mathcal{K}_k. \tag{4.34}$$

where $\mathcal{K}_k$ represents a set of all the adjacent beams to beam k and itself i.e. $\mathcal{K}_k = \{k' : k'(adj)k\} \cup \{k\}$.

Considering the class scheduling matrix $\boldsymbol{P}$, we can express the demand-matching error of class k as follows,

$$CDS_k = \sum_{k'\in\mathcal{K}_k} |\tau_{k\to k'} - \sum_{t=1}^{T} p^t_{k\to k'}|, \tag{4.35}$$

where CDS_k accounts for the difference of time-slots requested by class k and the number of time-slots assigned by the proposed scheduling process.

Then, to satisfy the demand of every class $\tau_{k\to k'}$ and to reduce inter-beam interference,

we formulate following optimization problem,

$$\min_{\mathbf{P}} \quad \sum_{k=1}^{K} CDS_k \tag{4.36a}$$

$$s.t. \quad p^t_{k\to k'} \in \{0,1\}, \forall k, k', t \tag{4.36b}$$

$$\sum_{k=1}^{K} \sum_{k'\in\mathcal{K}_k} p^t_{k\to k'} = K, \forall t \tag{4.36c}$$

$$\sum_{k'\in\mathcal{K}_k} p^t_{k\to k'} = 1, \forall k, t \tag{4.36d}$$

$$p^t_{k\to k'} + p^t_{k'\to k} \leq 1, \forall k \neq k' : \forall t \tag{4.36e}$$

$$p^t_{k\to k'} = 0, \forall \mathcal{C}_{k\to k'} = \emptyset : \forall t \tag{4.36f}$$

where the objective function accounts for the error of the demand mismatch considering all system classes. In the first constraint, binary variable $p^t_{k\to k'}$ is used to select a class. The second constraint ensures that K classes are selected for K beams out of all the available classes. The third constraint ensures that only 1 class is scheduled in a beam. The fourth constraint ensures that non interfering classes are scheduled at any time t and hence orthogonality is maintained at class level. The last constraint make sure that no empty classes are scheduled and hence edge pruning discussed in section 4.2.4 need not be done at every value of t.

The class scheduling problem in (4.36a) has the optimization variable matrix, $\mathbf{P}$, which is binary in nature. Hence, the problem in (4.36a) can be identified as a mixed-integer programming problem with indicative variables ($p^t_{k\to k'} \in \{0,1\}, \forall k, k', t$) and is a combinatorial problem by nature. Some state-of-the-art solvers, e.g., MOSEK [182,183], can be used to solve problems such as (4.36a), where the solvers perform what is effectively an exhaustive search among the integer variables to determine the correct solution. However, MOSEK speeds up the search with intelligent and innovative ways as described in [184] and sub-optimal solutions can be obtained when the branching algorithm discovers at least one feasible integer solution. MOSEK considers the problem (20a) as conic type and uses mixed integer optimizer to formulate a primal feasible problem and deduce to integer optimal solution. For details on how MOSEK addresses mixed integer problems, the reader is referred to [184] for further reading.

Demand based user scheduling

By the end of class scheduling step, we will have a clear answer on which sectors are activated at each time slot. However, it remains to be determined which users within those sectors are scheduled. This problem is discussed in this section.

The proposed demand-based user scheduling follows a very simple approach [185], which is detailed in Algorithm 5. In particular, the users with larger queue size are scheduled with priority in an attempt to maintain queue stability.

Algorithm 5: Demand Based User Scheduling

Input : $T, \mathfrak{d}_n, B, f_{DVB-S2X}(SNR), \mathbf{P}, \mathbf{C}$
Output : $\mathbf{M}$

1. 1. Compute the initial users' queue status i.e. $\tau_n(t=1)\ \forall\ n$ using (4.33);
2. **for** $t = 1$ **to** T **do**
3. **for** $k = 1$ **to** K **do**
4. 2. From the set of classes C, obtain the scheduled class $\mathcal{C}_{k\to k'}$ using $p^t_{k\to k'}$ of $\mathbf{P}$ as per Section 16
5. 3. Select any user $n \in \mathcal{C}_{k\to k'}$ who has $\max(\tau_n(t))$;
6. 4. Update $u^k_{(n,t)} = 1 \in \mathbf{M}$ for the scheduled user n;
7. 5. For the scheduled user n, update the queue using $\tau_n(t+1) = \tau_n(t) - 1$;
8. 6. For all the other users, retain queue status using $\tau_n(t+1) = \tau_n(t)$;
9. **end**
10. **end**

4.2.5 Simulation and Results

The considered antenna pattern corresponds to a 71-beam GEO 13°E satellite operating at the Ka exclusive band 19.7 to 20.2 GHz. This is the same beam-pattern as considered in [112–114]. A summary of simulation parameters are shown in Table 5.2. Also, for the sake of clarity, we consider 6 out of the total 71 beams available and a total number of $M = 60$ users distributed across $K = 6$ beams. Users' locations and demands have been extracted from the SnT traffic simulator [5, 57]. Furthermore, we consider a sum power-constrained system of 120 dBm and system bandwidth of 500 MHz.

In our simulation, we consider the steps of 4.2.4, sector formulation as shown Figure 4.12 with 6 sectors in every beam. Higher number of sectors will provide better sector segregation. However, the choice of 6 sectors per beam was considered for its simplicity. Then, we formulate 24 classes in accordance with as per 4.2.4. Furthermore, in accordance

Table 4.4: Simulation Parameters

Satellite longitude	13 degree East (GEO)
Satellite total radiated power, P_T	6000 W
Total Number of Beams, N_B	71 (Only 6 beams are considered)
Number of HPA, N_{HPA}	36 (2 beams per HPA)
Beam Radiation Pattern	Provided by ESA
Downlink carrier Frequency	19.5 GHz
User link bandwidth, B_W	500 MHz
Roll-off Factor	20%
Duration of time slot. T_{slot}	1.3 ms
Number of time slots	100
Antenna Diameter	0.6
Terminal antenna efficiency	60%
DL wavelength	0.01538 m

to 4.2.4 we prune classes $\mathcal{C}_{1\to4}$, $\mathcal{C}_{5\to6}$ and $\mathcal{C}_{6\to5}$ as they have no users present in them. In accordance to 16, we perform class scheduling using MOSEK solver [182] of CVX and user scheduling was performed in accordance with demand.

We consider multiple benchmark schemes for a fair comparison with the proposed scheme such as,

1. Simplistic random scheduling where the scheduled users are randomly selected from the user-beam set.

2. Semi-orthogonal scheduling (SOS) which selects most orthogonal users with best channel conditions [112].

3. Geographical scheduling [146] which orders cells into sectors and schedules users in increasing orders of sectors.

4. Demand based heuristic weighted semi-orthogonal scheduling (WSOS) technique proposed in [186] that considers both channel orthogonality and user demand for scheduling users.

For better result analysis, we compare two different demand profiles. Firstly, we consider a profile of moderately uniform demand distribution and then, we evaluate for a profile with nonuniform demand distribution. A moderately uniform demand distribution profile is shown in Figure 4.16.a, where the user demand is relatively more evenly distributed among all the

users. In other words, high demand users are not close to each other. On the other hand, as shown in Figure 4.16.b, for nonuniform demand distribution profile, users with high demand are more close to each other. Hence, as shown in the Figure 4.16.c, at beam level, the demand is more evenly distributed for moderately uniform demand distribution profile in comparison to nonuniform demand distribution profile.

We define user demand satisfaction for any user n, as the ratio of offered capacity to the requested demand and is expressed in percentage using,

$$UDS_n = \frac{\sum_{t=1}^{T} C_{(n,t)}}{\mathfrak{d}_n} \times 100, \tag{4.37}$$

where $C_{(n,t)}$ is defined in (4.26).

Furthermore we define mean offered instantaneous throughput for all the users in a beam k as,

$$\bar{C}_t^k = \frac{\sum_{n=1}^{N} C_{(n,t)}^k \times u_{(n,t)}^k}{N} \tag{4.38}$$

where $C_{(n,t)}^k$ is defined in (4.27) and the mean requested instantaneous demand as,

$$\bar{D}_t^k = \frac{\sum_{n=1}^{N} \mathfrak{d}_n \times u_{(n,t)}^k}{N}. \tag{4.39}$$

Demand satisfaction at beam level for any beam k is defined using (4.38) and (4.39), as the ratio of mean offered throughput to mean requested demand by all the users in the beam k and is expressed in percentage using,

$$BDS_k = \sum_{t=1}^{T} \frac{\bar{C}_t^k}{\bar{D}_t^k} \times 100. \tag{4.40}$$

Numerical Results for moderately uniform demand distribution

For moderately uniform demand distribution, the demand satisfaction at beam level is as shown in the Figure 4.17.a. By performing random scheduling, demand is not satisfied for three beams and in semi-orthogonal scheduling, demand of four beams are not satisfied. This is because semi-orthogonal scheduling focuses on users with best channel conditions without paying attention to the actual demands. By performing Geographical scheduling, there is

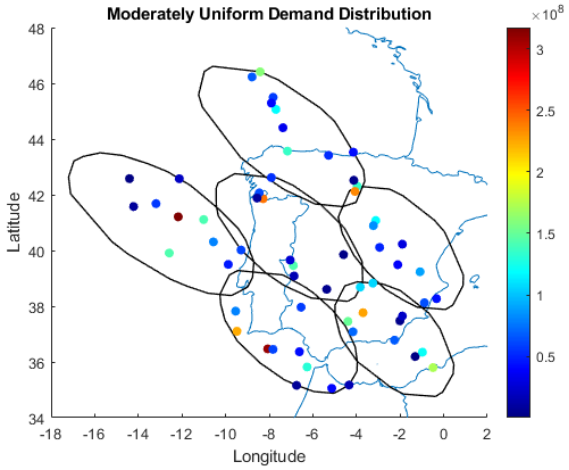

(a) Users locations whose demand distribution is moderately uniform. Colorbar denotes the demand in Mbps

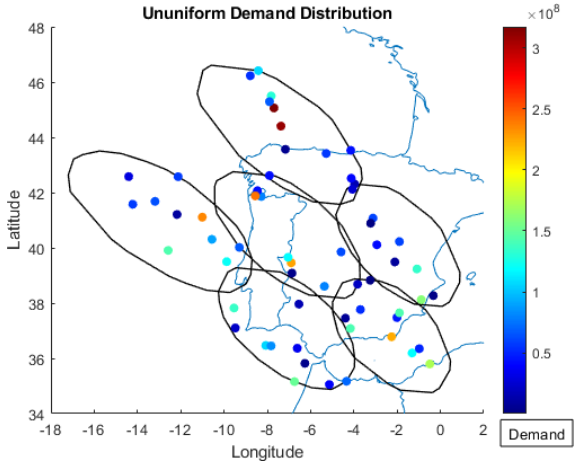

(b) Users locations whose demand distribution is nonuniform. Colorbar denotes the demand in Mbps

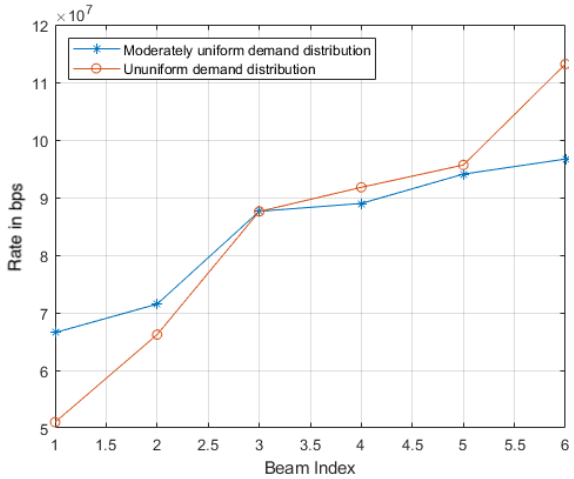

(c) Demand distribution comparison at beam level

Figure 4.16: Comparison between different demand distribution profiles

improvement in demand matching but the performance is still poor in two beams. The weighted semi-orthogonal scheduling performs better than the semi-orthogonal scheduling but also fails to match demand in three beams by a very fine margin. Furthermore, in the case of moderately uniform demand distribution, the proposed interference-aware demand-based scheduling algorithm perform similar to weighted semi-orthogonal scheduling at the beam level.

The demand satisfaction at the user level provides better demand matching insights and is as shown in the Figure 4.17.b. Even though the weighted semi-orthogonal scheduling and the proposed interference-aware demand-based user scheduling performs similarly at beam level, the proposed interference-aware demand-based user scheduling performs better at the user level. The other benchmarks such as random scheduling, semi-orthogonal scheduling and weighted-semi-orthogonal scheduling performs poor in comparison to the proposed interference-aware demand-based scheduling.

Figure 4.17.c provides insights on how well the offered throughput trend follows the demand trend. It is evident that the offered throughput of non demand based scheduling algorithms such as random, semi-orthogonal and geographical scheduling, does not follow the demand trend at all. Accordingly, some users with lower demand are served better and some users with higher demand are neglected. However, demand based scheduling algorithms such as weighted-semi-orthogonal and the proposed interference-aware demand-based scheduling perform very well in demand matching. Nevertheless, even with good demand matching, many users are under-served in the weighted-semi-orthogonal scheduling where as in the proposed interference-aware demand-based scheduling most of the users' demand has been met.

Numerical Results for nonuniform demand distribution

In moderately uniform demand distribution profile, as shown in Figure 4.17, even though the weighted semi-orthogonal scheduling (WSOS) [186] does not outperform the proposed interference-aware demand-based scheduling algorithm, WSOS performs considerably well in terms of demand matching. However, when we evaluate the proposed interference-aware demand-based scheduling and the benchmarks in nonuniform demand distribution profile, as shown in Figure 4.18.a and Figure 4.18.b, weighted semi-orthogonal scheduling fails to provide demand satisfaction both at beam and user level. This is because the heuristic

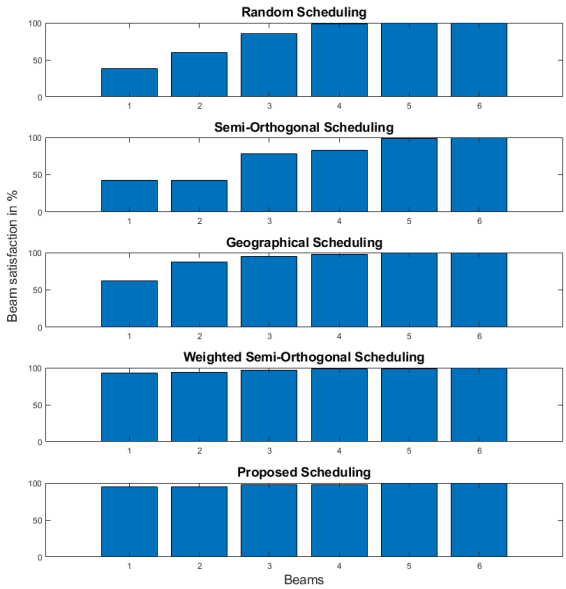

(a) Demand Satisfaction at Beam Level

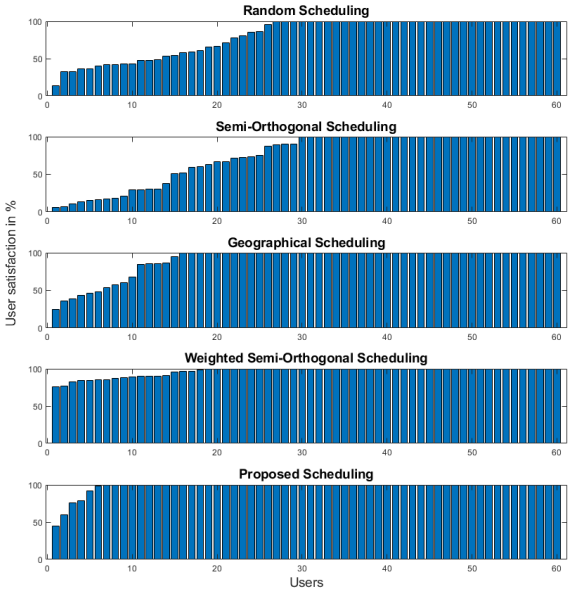

(b) Demand Satisfaction at User Level

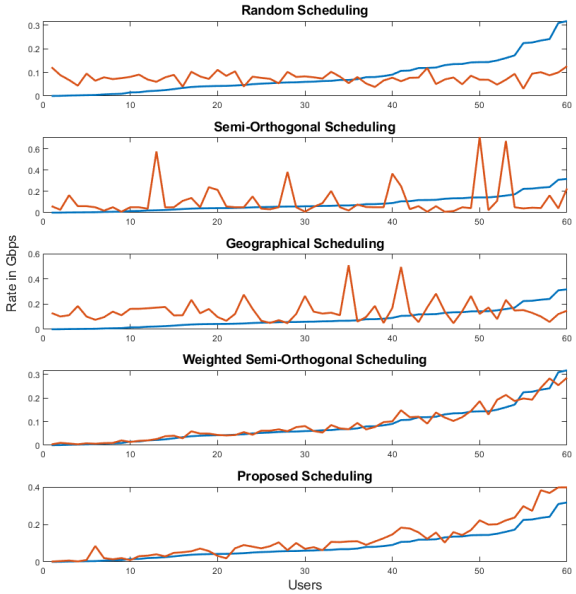

(c) The offered throughput(red) following the demand(blue) trend for moderately uniform demand distribution

Figure 4.17: Results for moderately uniform demand distribution

design proposed in [186] is not able to cope with strongly uneven demand distributions. On the other hand, as shown in Figure 4.18.a and 4.18.b, the proposed interference-aware demand-based scheduling performs best both at beam and user level. Also, as shown in the Figure 4.18.c, the offered throughput of the interference-aware demand-based scheduling algorithm follows the demand trend most effectively. Hence, interference-aware demand-based scheduling algorithm performs well with different demand distribution profiles whereas weighted semi-orthogonal scheduling can only perform well in uniform or moderately uniform demand distribution.

Furthermore, random scheduling and semi-orthogonal scheduling fails to provide demand satisfaction both at user and beam level. Geographical scheduling maximizes the offered capacity for multiple users, but fails to perform well for all the users. Also, the offered throughput of the geographical scheduling is out of sync with the demand curve, which means offered throughput is guaranteed based on the geographical position of the user and not by the demand.

Monte Carlo simulation with different demand distribution profiles

Figure 4.19 shows the user demand satisfaction using Empirical Cumulative Distribution Function (eCDF) for Monte Carlo simulations performed over 100 different randomly generated demand distribution profiles. The value of the eCDF, at any specified value of the measured variable is the fraction of observations of the measured variable that are less than or equal to the specified value. Hence, from Figure 4.19, it is evident that non demand based scheduling algorithms such as random, semi-orthogonal and geographical scheduling algorithms perform the worst. Furthermore, even though the demand based weighted semi-orthogonal scheduling algorithm performs well with higher probable values for higher demand satisfaction, the probability to have lower demand satisfaction is also high. However, the proposed interference-aware demand-based scheduling algorithm performs the best in having most probable values of eCDF for most of the higher user demand satisfaction.

Complexity Analysis

User scheduling is known to be a complex task. Herein, the computational complexity of the proposed interference-aware demand-based scheduling algorithm and the conventional benchmark algorithms are analysed using run-time analysis, where the amount of time taken by

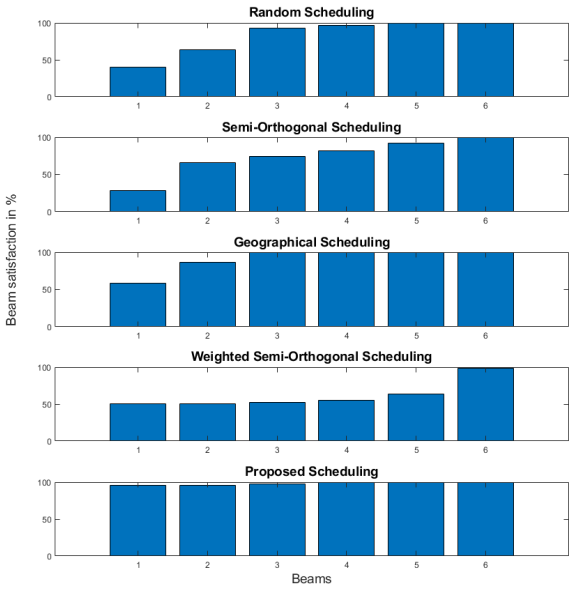

(a) Demand Satisfaction at Beam Level

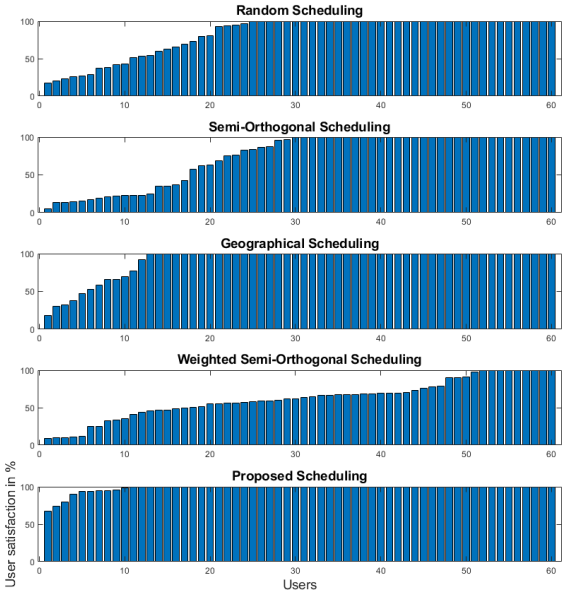

(b) Demand Satisfaction at User Level

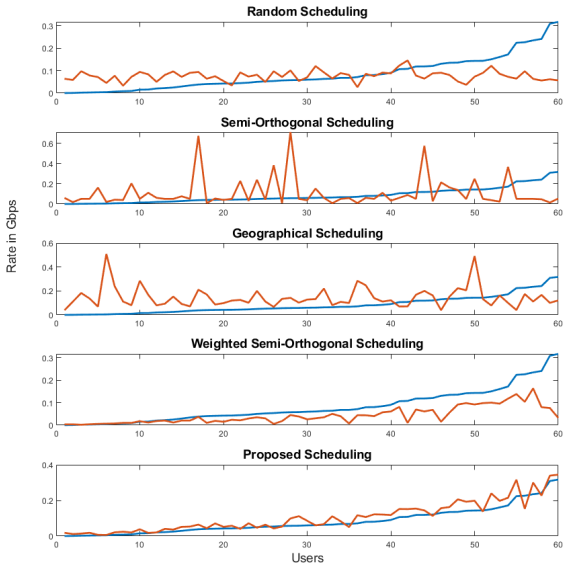

(c) The offered throughput(red) following the demand(blue) trend

Figure 4.18: Results for nonuniform demand distribution

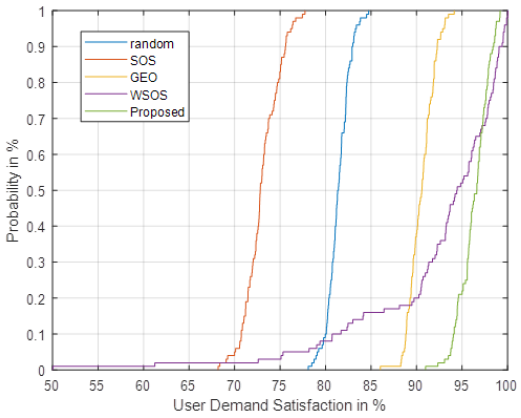

Figure 4.19: Empirical Cumulative Distribution Function (eCDF) for 100 different demand distribution profiles

the algorithm to complete is considered as metric of analysis. The run-time analysis of all the scheduling techniques are as shown in Figure 4.20 for scheduling users in $T = 100$ scheduling periods. The random scheduling has least complexity and takes very less computational time, as expected. Furthermore, the semi-orthogonal scheduling, weighted semi-orthogonal scheduling and geographical scheduling performs quite similarly and hence have similar complexities. Note that in both cases, semi-orthogonal and geographical scheduling, require a user-pair analysis of channel orthogonality and/or distance. On the other hand, the complexity of the proposed scheme is split into proposed class scheduling mentioned in 16 and proposed user scheduling mentioned in 16.

The complexity of proposed class scheduling is high because it involves in solving an integer programming problem. However, the proposed class scheduling is only performed when demand profile changes i.e, only when the demands of a sector, classes or beams changes considerably. Furthermore, the proposed user scheduling which has to be performed for every T scheduling period performs better than the other benchmarks except random scheduling.

Performance evaluation for different Beam-User Set ($\mathfrak{G}_k$)

In this section, we study the impact of Beam-User Set ($\mathfrak{G}_k$) of section 4.2.2. Figure 4.21 shows the simulation setup of 6 beams with 60 users, where 3 users have high demand (around 195 Mbps) and the remaining 57 users have low demand (around 50 Mbps). Accordingly, we formulated the Beam-User Set and computed user satisfaction for two cases, once with no user sharing and again by sharing the high demand users between two adjacent beams. When

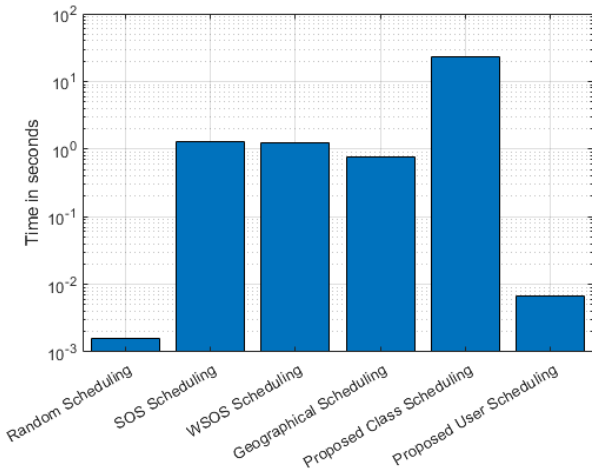

Figure 4.20: Run-time complexity Analysis.

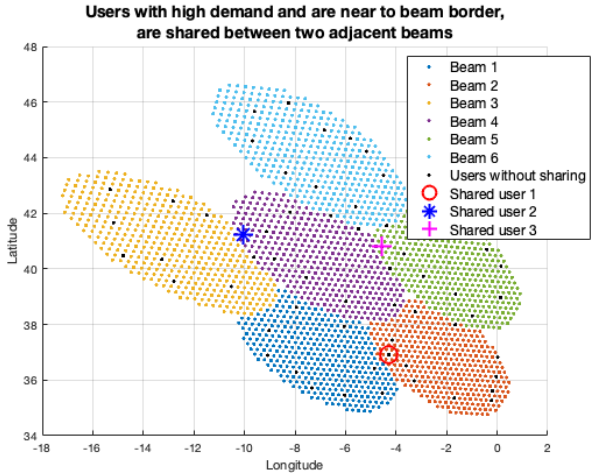

Figure 4.21: Shared user positions.

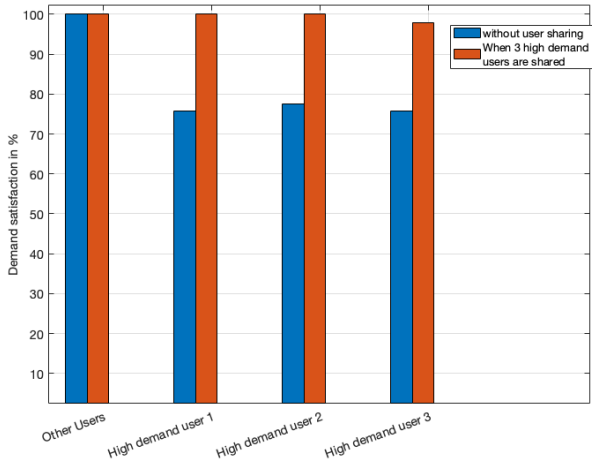

Figure 4.22: Improved demand satisfaction of shared users.

users are shared between two beams, shared-user-1 is shared between beam-1 and beam-2; Shared-user-2 is shared between beam-3 and beam-4; Shared-user-3 is shared between beam-4 and beam-5.

Figure 4.22 shows the benefits of formulating Beam-User Set with user sharing over formulating Beam-User Set without user sharing. The average demand satisfaction for low demand 57 users is 100% in both cases. However, demand satisfaction of high demand users have considerably increased when the users are shared between two beams. Thus by sharing high demand users with adjacent beams, the demand satisfaction of all the users can be met.

4.2.6 Conclusion

In this work, we first discuss the demand based adaptable multibeam high throughput satellite systems and express the need for demand based scheduling algorithm with focus on user demand matching and not on sum rate maximization. Furthermore, we propose a heuristic interference-aware demand-based user scheduling algorithm that reduces inter-beam interference by carefully scheduling non interfering classes while also ensuring that all the users demand is satisfied by the end of T scheduling periods. Numerical simulations have evidenced significantly better performance of the proposed interference-aware demand-based scheduling algorithm with respect to benchmark schemes such as random scheduling, semi-orthogonal scheduling, geographical scheduling and weighted semi-orthogonal scheduling both in terms of demand satisfaction at beam and user level. Furthermore, we also provide complexity analysis where when no major demand profile changes, the proposed interference-aware demand-based user scheduling has less complexity compared to most of the other benchmarks.

Chapter 5

Parallel implementation of beam design and user scheduling

5.1 Introduction

Motivated by its simple deployment, conventional multibeam GEO satellite systems operate with a static and fixed beam footprint, typically of the form of regular circular beams one next to each other, regardless of the actual user demands on Earth [15]. This naive approach typically leads to unbalanced situations, where some beams with high number of users (or with high-demand users) easily reach congestion while other beams have spare capacity [5]. A more optimal approach would explicitly consider the actual user traffic demands and design the beam footprint accordingly. Hence, beam footprint design that considers the actual spatial demand distribution on Earth, targets an evenly distributed demand among all the beams of a system [84]. Such approach has only recently become possible thanks to the advances in active antenna systems for satellite communications [99, 187].

On the other hand, the spectrum scarcity combined with the ever-growing demand for high-throughput satellite services has motivated many research works on full frequency reuse and the application of precoding to mitigate the resulting co-channel interference [89]. However, the potential benefits of precoding are limited by the user scheduling. This is because typical precoding methods rely on the channel matrix inversion [8], which is not straightforwards in case of rank-deficient matrices. Hence, while many research works focus on optimal user scheduling that selects users with orthogonal channel vectors to be served simultaneously [112], others focus on jointly addressing user scheduling and precoding [141]. However,

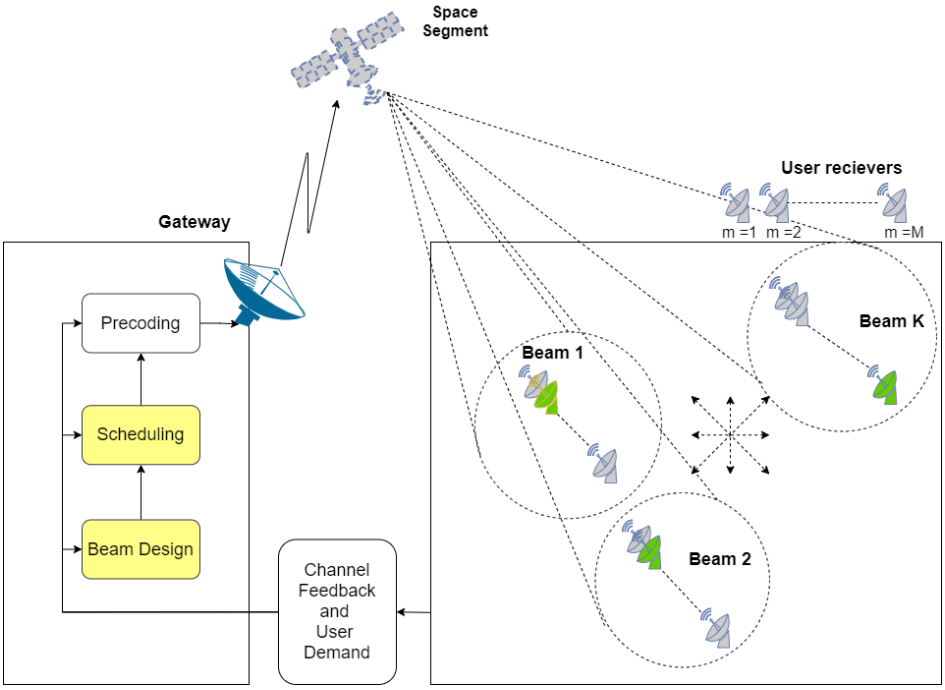

Figure 5.1: GEO multibeam system architecture including beam design, user scheduling and precoding.

considering demand satisfaction as an objective is a better approach to perform user scheduling which can be achieved by considering both user traffic demands and channel orthogonality of the scheduled users [186].

The contribution and novelty of this paper focuses on employing demand-driven system adaptability at multiple levels of the transmission chain and to evaluate the benefits of introducing demand considerations at these levels. Unlike previous techniques that focused on system throughput maximization [177], herein we focus on the user demand satisfaction objective. In particular, we apply demand-driven system adaptability and evaluate the demand satisfaction at beam design and user scheduling individually and jointly.

5.2 System Model

We consider a GEO multi-beam High Throughput Satellite (HTS) system as shown in Figure 5.1, employing multiple spot beams to provide the required coverage. Non-uniform spatially distributed broadband users, including mobile pedestrian users, aeronautical users and maritime users are considered. We assume that the optimization is carried out in the ground segment. While Channel State Information (CSI) is fed back for the precoding and schedul-

ing design, the user demand information is considered for beam and scheduling design. The space-segment consist of a programmable payload GEO satellite with Array-Fed Reflector (AFR) antennas with beamforming capabilities.

We consider N broadband users served by K-beam Satellite system. While CSI vector is expressed as $\mathbf{h}_n \in \mathbb{C}^{K\times 1}$, $\mathbf{x} \in \mathbb{C}^{K\times 1}$ represents the precoded signal and $\mathfrak{N}_n$ represent zero-mean Additive White Gaussian Noise (AWGN). Consequently, y_n is the received signal and is expressed as,

$$y_n = \mathbf{h}_n^T \mathbf{x} + \mathfrak{N}_n. \tag{5.1}$$

The above model can also be expressed as,

$$\mathbf{y} = \mathbf{H}\ \mathbf{x} + \mathfrak{N}, \tag{5.2}$$

by considering $\mathbf{H} = \Phi\mathbf{B}$, where $\mathbf{B} = [\mathbf{b}_1 \dots \mathbf{b}_N]^T$ is the system channel matrix whose the (n, k)th component is given by,

$$[\mathbf{b}]_{n,k} = \frac{\sqrt{G_{Rn}G_{kn}}}{(4\pi\frac{\mathfrak{D}_{nk}}{\lambda})}, \tag{5.3}$$

where λ is the wavelength of transmission, G_{kn} are the gains defined by satellite radiation pattern, G_{Rn} is the receiver antenna gain and $\mathfrak{D}_{nk}$ is the distance between the satellite transmit antenna and user's receiving antenna. The phase matrix $\Phi \in \mathbb{R}^{K\times K}$ is expressed as,

$$[\Phi]_{xx} = e^{i\phi_x}, \forall x = 1...K \tag{5.4}$$

where Φ_x is a uniform random variable in $[2\pi, 0]$ and $[\phi]_{xy} = 0, \forall x \neq y$. Then, the precoded signal is given by,

$$\mathbf{x} = \mathbf{W}\ \mathbf{s}. \tag{5.5}$$

where $\mathbf{W}$ is the precoding matrix and $\mathbf{s}$ is the transmit symbols that satisfies $[\mathbf{s}\mathbf{s}^H] = \mathbf{I}$. The precoding matrix $\mathbf{W}$ is the MMSE precoder [144] and is expressed as,

$$\mathbf{W}_{RZF} = \eta' \boldsymbol{H^H(HH^H + \alpha I)^{-1}}, \tag{5.6}$$

where α is a predefined regularisation factor [150] and η is the power allocation factor defined in (5.7) with P_{tot} being the total available power.

$$\eta = \sqrt{\frac{P_{tot}}{\text{Trace}(\mathbf{W}\mathbf{W}^{\dagger})}} \tag{5.7}$$

5.3 Problem Statement and Proposed Solution

5.3.1 Demand-Aware Beam Design

The benchmark fixed beam footprint [15] provided by European Space Agency (ESA) [89] consists of fixed number of beams (71 beams) with predetermined beam shape for a GEO 0°E satellite operating at the Ka exclusive band 19.7 to 20.2 GHz. As shown in Figure 5.2, we selected 6 adjacent beams out of the available 71 beams for our simulation where the blue asterisks represent the user positions. The predetermined beam shape or the beam footprint is fixed irrespective of the dynamic user profiles. Apparently, mobile users are not uniformly distributed and have different QoS requirements. Also, their position is a function of time. But, in the conventional beam footprint design shown in Figure 5.2, the offered throughput remains relatively similar across all the beams. Therefore, fixed beam plans will fail to distribute broadband traffic demand across all the beams evenly and result in either under-use the offered throughput (beam capacity is unused) or overload the beam (beam capacity is unmet).

Hence, the beam footprint has to be designed such that the occurrence of unbalanced aggregated-beam demand is avoided. To do so, we use demand-Aware adaptive beam footprint design [84]. Accordingly, we first need to find the best partition of all the users into sets of adjacent users in an euclidean distance sense such that total system demand is evenly distributed among all the sets and then, plan a beam which is suitable to serve each user set.

We define d_m as the requested traffic demand of user m, and $D_k = \sum_{m \in \mathcal{S}^k} d_m$ as the demand of beam k, where $\mathcal{S}^k$ represents the set of users belonging to beam k. Then, we define the problem using clustering approach and consider metric spaces where we endow universe $\mathcal{N}$ with a metric space $(\mathcal{X}, r)$ such that $\mathcal{N} \subseteq \mathcal{X}$, where $\mathcal{X}$ is a set of all points in a 2D Euclidean space and r is a distance metric on $\mathcal{X}$. Then to obtain the cluster sets $\{\mathcal{T}^1, \mathcal{T}^2, \ldots, \mathcal{T}^K\}$ that are optimized for even demand distribution, we can define the partitioning problem using clustering as formulated in (5.8a).

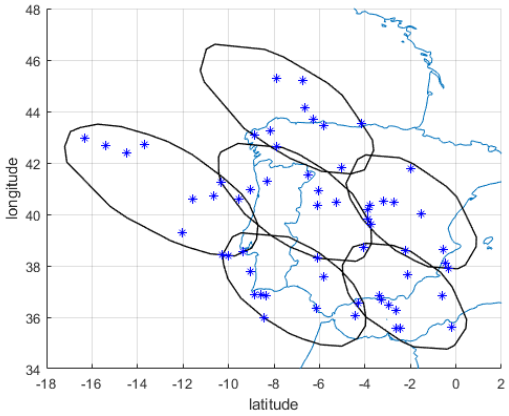

Figure 5.2: Fixed Beam Footprint

The first constraint in (5.8b) ensures that all the users are under the coverage region. The second constraint in (5.8c) assures that any user will be served by only one beam. The third constraint mentioned in (5.8d) ensures that the beams have at least one user and to avoid planning beams with zero demand. In the constraint (5.8e), $\boldsymbol{c}_{\mathcal{T}^k}$ is two element vector in the 2D Euclidean space representing the weighted cluster centroid of the cluster k.

$$\min_{\{\mathcal{T}^1,\mathcal{T}^2\ldots\mathcal{T}^K\}} \quad \sum_{k=1}^{K}\sum_{m\in\mathcal{T}^k} r(\mathbf{x}_m,\boldsymbol{c}_{\mathcal{T}^k})\left(\frac{\sum\limits_{m\in\mathcal{T}^k}(d_m)}{\sum\limits_{m=1}^{M}(d_m)}\right) \tag{5.8a}$$

$$\text{subject to} \quad \bigcup_{k=1}^{K}\mathcal{T}^k = \mathcal{N} \tag{5.8b}$$

$$\mathcal{T}^i \cap \mathcal{T}^j = \emptyset, \forall i \neq j \tag{5.8c}$$

$$\mathcal{T}^i \neq \emptyset, \forall i \tag{5.8d}$$

$$\boldsymbol{c}_{\mathcal{T}^k} = \frac{1}{\sum\limits_{m\in\mathcal{T}^k} d_m}\sum_{m\in\mathcal{T}^k} d_m\mathbf{x}_m \tag{5.8e}$$

To solve for (5.8a), we employ weighted k-means clustering using iterative Lloyd's algorithm [128] approach. Since the beam center is likely to point in the direction of the dominant group of users, centroid tessellation approach such as Lloyd's algorithm is beneficial for the beam design and the user demands can be better satisfied. The steps of Lloyd's Iteration Partition Clustering is shown in Algorithm 6. Upon termination, the Algorithm 6 provides K clusters $(\mathcal{T}^1,\mathcal{T}^2\ldots\mathcal{T}^K)$ with cluster centroids at $\boldsymbol{c}_{\mathcal{T}^1},\boldsymbol{c}_{\mathcal{T}^2}\ldots\boldsymbol{c}_{\mathcal{T}^k}$ such that D_k is more evenly

distributed among all the K beams.

Algorithm 6: Loyd's Iteration Partition Clustering Algorithm

[Step 1] Choose cluster centres $\{\boldsymbol{c}_{\mathcal{T}^1}, \boldsymbol{c}_{\mathcal{T}^2}...c_{\mathcal{T}^k}\}$ defined by C_s selected as per $k-means++$ Algorithm [129].

while *(Cluster assignments do not change) OR (Maximum number of iterations are not reached)* **do**

  [Step 2] Compute distance $\mathfrak{R}_{K\times N}$ between each of $\{\boldsymbol{c}_{\mathcal{T}^1}, \boldsymbol{c}_{\mathcal{T}^2}...\boldsymbol{c}_{\mathcal{T}^k}\}$ and all of $\{\boldsymbol{x}_1, \boldsymbol{x}_2...\boldsymbol{x}_N\}$.

  Every element of $\mathfrak{R}_{K\times N}$ is computed using,

$$\mathfrak{R}(k,n) = ((\mathbf{x}_n - \boldsymbol{c}_{\mathcal{T}^k})(\mathbf{x}_n - \boldsymbol{c}_{\mathcal{T}^k})') \left(\frac{\sum\limits_{n\in\mathcal{T}^k}(d_n)}{\sum\limits_{n=1}^{N}(d_n)} \right), \tag{5.9}$$

  [Step 3] Assign $\{\boldsymbol{x}_1, \boldsymbol{x}_2...\boldsymbol{x}_N\}$ users to K clusters $\{\mathcal{T}^1, \mathcal{T}^2...\mathcal{T}^K\}$ based on the minimum distance between the users and cluster centre using $\mathfrak{R}_{K\times N}$.

  [Step 4] Compute new cluster centres $\{\boldsymbol{c}_{\mathcal{T}^1}, \boldsymbol{c}_{\mathcal{T}^2}...\boldsymbol{c}_{\mathcal{T}^k}\}$ by using,

$$\boldsymbol{c}_{\mathcal{T}^k} = \frac{1}{\sum\limits_{n\in\mathcal{T}^k} d_n} \sum_{n\in\mathcal{T}^k} d_n \mathbf{x}_n. \tag{5.10}$$

end

To have a fair comparison between the conventional 6 beams of fixed beam design, we use Voronoi Tessellation [130] and generate convex polygons around the previously obtained clusters, such that, all the area covered by the benchmark design is covered by the proposed adaptive scheme. Any centre $\boldsymbol{c}_{\mathcal{T}^k}$ is simply a point in the Euclidean plane, and its corresponding Voronoi cell V_u consists of every point in the Euclidean plane whose Euclidean distance to $\boldsymbol{c}_{\mathcal{T}^u}$ is less than or equal to its Euclidean distance to any other centre $\boldsymbol{c}_{\mathcal{T}^{v\neq u}}$.

The Voronoi cells are convex polygons because each cell is obtained from the intersection of geometric half-spaces. The collection of such convex Voronoi polygons of the 6 reference beams is shown by red convex polygons in Figure 5.3. We approximate the boundary of Voronoi polygons as beam contour and the geographic centres $\{\boldsymbol{c}'_1, \boldsymbol{c}'_2...\boldsymbol{c}'_K\}$ of Voronoi polygons as beam centres.

Furthermore, from the perspective of antenna pattern design, the irregular Voronoi polygons cannot be approximated as beam footprints. Also, considering the mathematical tractability and topological packing, we approximate the convex polygons into ellipses as shown in [188]. The centres of the thus obtained ellipses $(\boldsymbol{c}_1, \boldsymbol{c}_2...\boldsymbol{c}_k)$ will represent the proposed

adaptive beams centres. The semi-major and semi-minor axis of the approximated ellipses defines the boundary of the proposed adaptive beams. The angle of rotation of approximated ellipses represents the orientation of the proposed adaptive beams. The approximated beams are denoted using green ellipses in Figure 5.3.

Finally, for comparison with the benchmark, the elliptical beam pattern is obtained by approximating the antenna gains using two-dimensional Gaussian elliptical function. The antenna gain at any point of the elliptical beam could be modelled using,

$$f(x,y) = A\exp(-(m_1(x-x_o)^2 + 2m_2(x-x_o)(y-y_o) + m_3(y-y_o)^2)), \quad (5.11)$$

where the matrix $\begin{bmatrix} m_1 & m_2 \\ m_2 & m_3 \end{bmatrix}$ is positive-definite matrix [133].

The semi-major and semi-minor axis of the ellipses are fitted with σ_X and σ_Y of elliptical Gaussian function. The Gaussian function is phase rotated with angle φ to fit the orientation of the ellipse. The coefficient A is the maximum antenna gain or the amplitude of boresight point which is chosen inline with the boresight antenna gain of the benchmark. The centre of the Gaussian function (intersection point of σ_x and σ_y) is the centre $(c_k = x_0, y_0)$ of the ellipse. The values of $m1, m2$ and $m3$ are defined using,

$$m_1 = \frac{\cos^2\varphi}{2\sigma_X^2} + \frac{\sin^2\varphi}{2\sigma_Y^2}, \quad (5.12a)$$

$$m_2 = -\frac{\sin 2\varphi}{4\sigma_X^2} + \frac{\sin 2\varphi}{4\sigma_Y^2}, \quad (5.12b)$$

$$m_3 = \frac{\sin^2\varphi}{2\sigma_X^2} + \frac{\cos^2\varphi}{2\sigma_Y^2}. \quad (5.12c)$$

5.3.2 Demand-Aware User Scheduling

Conventional scheduling techniques such as [173,177] focus on selecting users with orthogonal channel vectors at any time t. Even though such approach will help precoding to successfully mitigate interference, it might fail to satisfy the individual user demand request. To overcome this, we use a demand-Aware user scheduling, which essentially targets the selection of a set $\mathcal{U} = \{U_1, U_2 ... U_k\}$, containing K users from the pool of M users at each scheduling

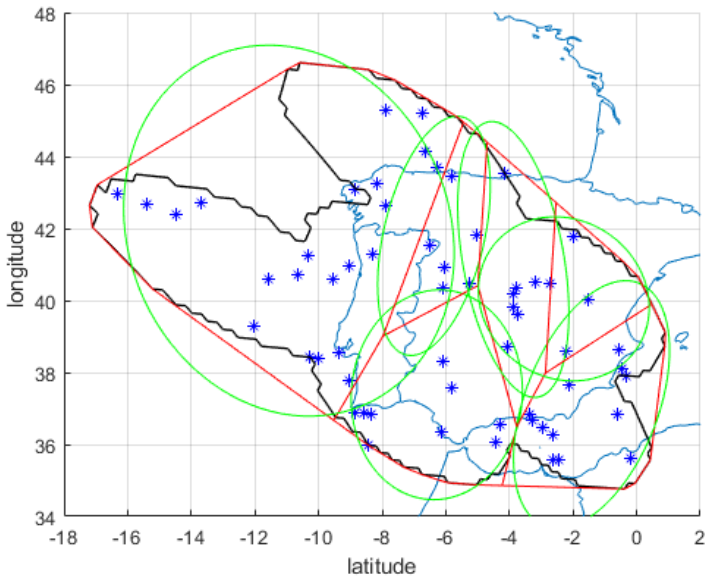

Figure 5.3: Demand-Aware Adaptive Beam Footprint

time, $t = 1, ..., T$ for all the K beams such that d_m, $\forall m$, is met at the end of T time period. Furthermore, to make sure that precoding still provide meaningful gains, the proposed demand-Aware scheduling also considers the channel orthogonality.

However, obtaining the optimal scheduling solution is a combinational problem and requires an exhaustive search-based user grouping and scheduling, which quickly become impractical due to exponential complexity. Hence, we use weighted semi-orthogonal scheduling [186] which is a sub-optimal heuristic method that uses both user demand and channel orthogonality. The Demand-Aware User Scheduling as shown in Algorithm 7, produces a schedule user set ($\mathcal{U} = \{U_1, U_2...U_k\}$) such that the channel vectors of the users in $\mathcal{U}$ are as orthogonal as possible using cosine similarity as,

$$\frac{|\ \mathbf{h}_1^H \mathbf{h}_2\ |}{\|\mathbf{h}_1\|\|\mathbf{h}_2\|} = \begin{cases} 1 & \text{Similar channel vectors} \\ 0 & \text{Orthogonal channel vectors} \end{cases} \tag{5.13}$$

and also ensures that the demand d_m of every user m is lesser or equal to the offered throughput using demand priority coefficient α_m. Furthermore, we consider unicast scheduling and hence one user per beam is selected.

Algorithm 7: Demand-Aware User Scheduling

Input : M, d_m, K, T
Output : U_k

[Step 1] Compute the initial demand priority coefficient at $t = 1$ for every user m using, $\alpha_m(t=1) = \frac{d_m(t=1)}{max_m(d_m(t=1))} \leftarrow \forall m$ where $\alpha_m \in [0, 1]$
[Step 2] Initialize the set of indexes of the previously scheduled users using, $\Lambda = \emptyset$
[Step 3] Perform user scheduling. For every value of t, select K users.
for $t = 1$ **to** T **do**
    [Step 3.A] Select first user using,
    for $m = 1$ **to** M **do**
        $U_1 = \max(\alpha_m(t).\|\mathbf{h}_m\|)$
    end
    Update Λ to avoid reselection of already scheduled user using, $\Lambda = \Lambda \in U_1$
    [Step 3.B] Select the remaining $(K - 1)$ users using,
    for $k = 2$ **to** K **do**
        for $m = 1$ **to** M **do**
            $w_m = \max(\alpha_m(t).(1 - \sum_{j \in \Lambda} \frac{|\mathbf{h}_j \mathbf{h}_m^H|}{\|\mathbf{h}_j\| \|\mathbf{h}_m\|}))$
        end
        U_k is the user m of w_m.
        set: $\Lambda = \Lambda \in U_k$
    end
    [Step 4] Update demand priority coefficient based on the average offered rate using α_m such that $\alpha_m(t) = \frac{d_m(t)}{E_m[R_m(t)]}$
end

Table 5.1: Cases evaluated

	Case 1	Case 2	Case 3	Case 4
Conventional Fixed Beam Design	✓	✓		
Demand-Aware Beam Design			✓	✓
Conventional Fixed Scheduling	✓		✓	
Demand-Aware Scheduling		✓		✓

5.4 Numerical Evaluation

In this section, we evaluate the proposed demand-Aware approaches with respect to conventional fixed approaches. Accordingly, the results are evaluated using four cases mentioned in Table 5.1.

In the first case, we consider 6 beams of conventional fixed beam design provided by European Space Agency (ESA) [111, 144] and a well known semi-orthogonal scheduling as a benchmark [177]. In case 2, we introduce demand driven adaptability at only user scheduling level. In case 3, we use demand driven adaptability only for beam designing. In case 4, we use demand-Aware adaptability at both beam design and user scheduling.

5.4.1 Simulation Parameters

The simulation parameters and the link budget are as shown in Table 5.2 we consider a total number of $M = 60$ users distributed across $K = 6$ beams. Users locations and demands have been extracted from the SnT traffic simulator [5]. Furthermore, we consider a sum power-constrained system with a per-beam power of 20 dBW and a bandwidth of 500 MHz.

Table 5.2: Simulation Parameters

Satellite longitude	13 degree East (GEO)
Satellite total radiated power, P_T	6000 W
Total Number of Beams, N_B	71 (Only 6 beams are considered)
Number of HPA, N_{HPA}	36 (2 beams per HPA)
Beam Radiation Pattern	Provided by ESA
Downlink carrier Frequency	19.5 GHz
User link bandwidth, B_W	500 MHz
Roll-off Factor	20%
Duration of time slot. T_{slot}	1.3 ms
Number of time slots	100
Antenna Diameter	0.6
Terminal antenna efficiency	60%
DL wavelength	0.01538 m

5.4.2 Beam level Demand Satisfaction

Demand satisfaction at beam level can be defined as the difference between the average beam demand and average beam offered throughput. Accordingly, Figure 5.4 provides demand

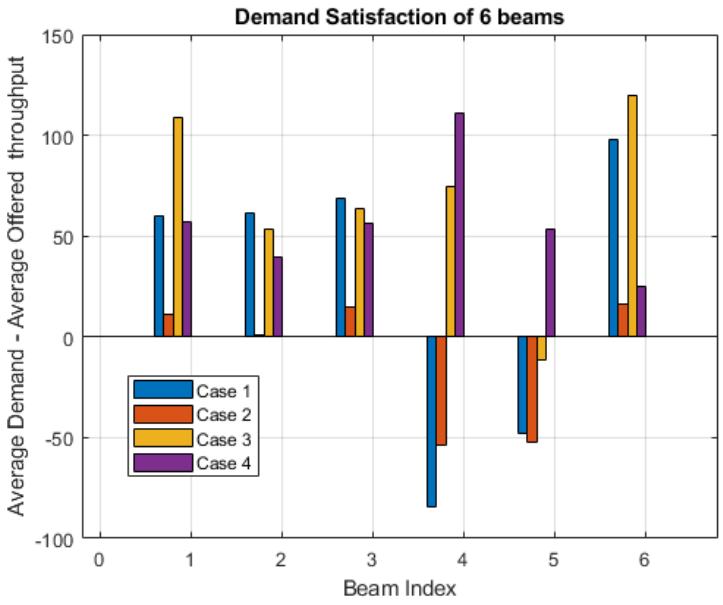

Figure 5.4: Beam-level Demand Satisfaction

satisfaction of 6 beams for the previously defined four cases. In case 1, where demand is not considered during beam design and user scheduling, demand satisfaction is not achieved for beam 4 and beam 5. In case 2, when demand awareness is considered for only user scheduling, beam demand is again not met for beams 4 and 5. This is because, due to uneven demand distribution among the 6 beams, the beam 4 and 5 have high demand to be met and demand-Aware user scheduling fails to meet demand of such beams. This can be verified in Figure 5.5 which shows the distribution of total system demand across the 6 beams. The conventional fixed beam design will result in some beams overload with high demand to meet and leave some beams underused. Also, the demand-Aware beam design will distribute the beam demand more equally among all the beams. Hence all the beams will have similar demand to be met. This can be verified by the Case 3 plots in Figure 5.4. The demand satisfaction is considerably improved as only beam 5 not been satisfied with a very small margin. However, in case 4, when we use demand awareness in both beam design and user scheduling, the demand of all the beams are satisfied.

5.4.3 User level Demand Satisfaction

Demand satisfaction at user level can be defined as the difference between the average user demand and average user offered throughput. Accordingly, Figure 5.6 provides demand

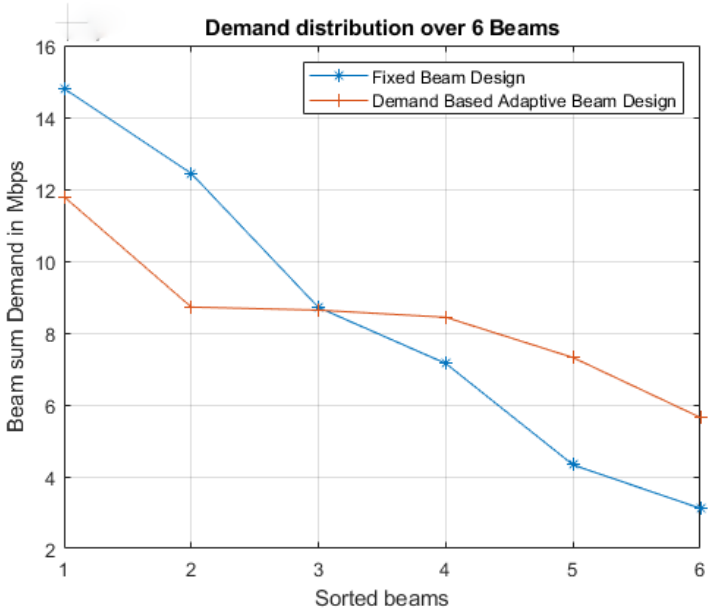

Figure 5.5: Demand Distribution across all 6 beams

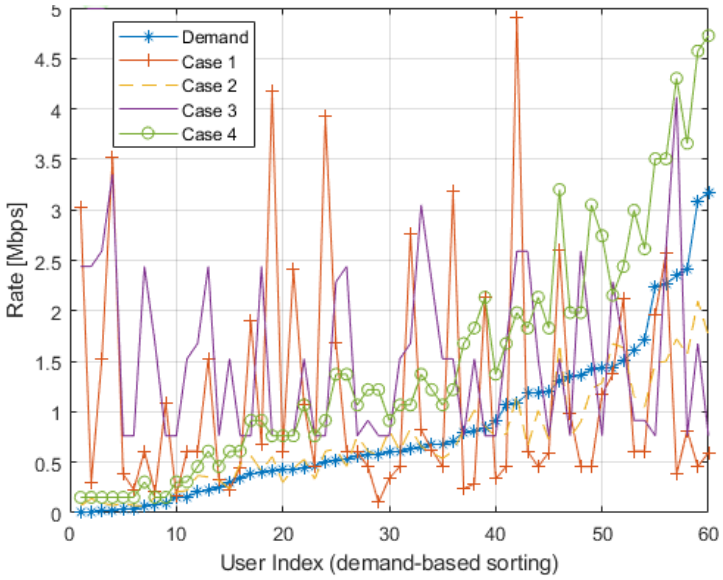

Figure 5.6: User-level Demand Satisfaction

satisfaction of 60 users. Clearly, the conventional Case 1 that does not consider demand for either beam design and user scheduling performs worst. In Case 2, when demand is considered only at user scheduling, the average offered throughput follows the demand curve. However, Many users with high demand are not satisfied. In Case 3, where demand is considered only for beam footprint planning, the user level demand satisfaction is poor but better than the Case 1. Finally, the Case 4 which uses demand at both beam design and scheduling performs best by both following the demand curve and satisfying the user demand at all cases.

5.5 Conclusion

Contrary to the current state-of-the-art solutions, we consider the actual user demand requirements in both beam planning and user scheduling. In this work, we show the benefits in terms of user demand satisfaction and beam demand satisfaction of the proposed beam design and user scheduling. In particular, the conventional systems face unbalanced situations with significant amounts of unmet capacity, while in our case, the users' demand requests and beams' demand requests have been met.

Chapter 6

Conclusion and Further Work

6.1 Conclusion

Due to increased mobile broadband users, the demand profiles are dynamically evolving and changing with time. Furthermore, for every demand profile, the user distribution and the demand distribution is nonuniform. While rural regions have low demand, urban regions have high demand hot-spots. Such dynamically changing nonuniform demand profiles are forcing the future multibeam satellite systems to adapt to the demand profile changes. Furthermore, recent advancements in the key enabling technologies such as precoding, digital beamforming networks and digital transparent payload have enabled the implementation of optimization modules to adapt the different radio resources in the satellite dynamic resource management system. As there are multiple degrees of freedom to implement such flexibility, in this thesis, we attempt to address two major radio resource adaptation in multibeam satellite systems. Firstly, the beam design and then, packet user scheduling.

Accordingly, we use two different approaches in beam design. Firstly, to achieve demand satisfaction at the high demand hot-spot regions, we explore opportunistic regular beam densification as the preliminary solution. Later, to further enhance the demand driven adaptability, we propose a novel dynamic beam densification methodology to choose ideal number of beams and their positions based on beam demand. Furthermore, as beam densification increases the interbeam interference, we propose a novel graph theory based dynamic frequency allocation strategy which on one hand helps to reduce interbeam interference and on the other ensures maximum bandwidth availability per beam. In the second approach of beam design, we propose an Adaptive Multi-beam Pattern and Footprint (AMPF) plan to

distribute the total system demand across all the beams evenly.

Furthermore, we propose two different approaches for user scheduling. Firstly, we propose a Weighted Semi-Orthogonal Scheme (WSOS) that provides a trade-off between the channel orthogonality needed for effective precoding performance and the user demand requirement for demand satisfaction. In the later part, we also propose a heuristic interference-aware demand-based user scheduling algorithm that reduces inter-beam interference by carefully scheduling non interfering classes while also ensuring that all the users demand is satisfied. Lastly, we verified a parallel implementation of beam design and user scheduling.

Conclusively, while any stand-alone demand driven real time optimization modules (verified in the scope of this thesis) ensure that the offered capacity to be inline with the spatio-temporal user demand, parallel implementation of multiple demand driven radio resource optimization techniques (case of beam design and user scheduling verified in the scope of this thesis) further enhance the demand satisfaction.

6.2 Future work

In this section, we discuss the extensions of the thesis and potential future work, which either focus on addressing some of the unsolved difficulties or explore the new directions following the current research trends.

1. **Optimization feasibility study:** Radio resource optimization is very well studied not only in the scope of this thesis but also by various authors in academia. While most of the works concentrate on capacity maximization, more recent works are towards maximizing the demand satisfaction (minimizing the error between the demand and offered capacity) at beam and user level. However, in most of the works, the capacity expression appears in the objective function and is in most cases non-linear and non-convex due to the logarithm function as well as non-linear dependencies on the optimization parameters. Accordingly, well-known methods of convex optimization might not be ideal in solving these problems. Hence, suboptimal methods that are typically proposed in this thesis and by other authors in literature, which either tackle parts of the problem separately and then iteratively tune the parameters, or convexify the problem by making some approximations, are typically impractical for realistic systems. Therefore, one direction of future work could be perform a feasibility study

on these heuristic suboptimal solutions under practical constraints keeping in mind the parameters that should be optimized, the complexity of the procedures and the required computational time. In this direction, the authors of [48] have already made the first step to consider limited on-board power budget, payload mass and size, and signaling regulations in the K-band as practical constraints for AMPF design. However, such feasibility studies have to performed for other degrees of freedom.

2. **Multiple degrees of freedom:** In recent years, there has been a lot of research on beamforming, user scheduling, and radio resource optimization for multi-beam satellite systems in an effort to build systematic design techniques and utilize all degrees of freedom. In this thesis, we have discussed multiple degrees of freedom where demand driven flexibility using scheduling, bandwidth, time, power and beam-design have been promising solutions individually (Chapter 2,3 and 4). Some parallel implementation of beam-design and scheduling have shown promising results (Chapter 5). Furthermore, many works in literature have tried to jointly optimize any two radio resources (power and bandwidth) and are quite successful [63]. However, this naturally raises the question whether all of them are needed. If yes, should they be implemented in standalone? or in parallel? or optimized jointly? This is a critical question, since its type of flexibility comes with an additional layer of complexity which could eventually be a point of failure. However, from this point, a better approach for future work is to establish systematic design methodologies and exploit all available degrees of freedom for demand satisfaction.

3. **Machine Learning for radio resource optimization:** The heuristic sub-optimal optimization solutions for radio resource management, either standalone or joint designs require solving optimization problems with significant complexity, which is unreasonable for practical systems. Hence, to achieve a trade-off between performance and complexity, we can explore the applicability of Machine Learning (ML) algorithms in radio resource optimization. Accordingly, for joint designs, metaheuristics ML methods can be applied to determine the optimal usage of the degrees of freedom. In that direction, the works of [189] have already shown promising results using unsupervised learning for user scheduling. Furthermore, the authors of [190] have also seen promising results in terms of computational complexity for bandwidth and power allocation

where conventional optimization allocates the radio resources, while ML accelerates the computation. Nevertheless, while optimizing using one degree of freedom, at least for conventional deep learning solutions, the trained networks will again result in suboptimal solutions, especially when the input-output correlation is difficult to learn due to problem non-convexity. Also, determining a proper ML model and handling the feasibility study of ML outputs, to determine optimal usage of all the available degrees freedom is an open and debatable question.

4. **GEO satellite multicast user scheduling:** This thesis considers scheduling in unicast fashion. However, in multicast GEO satellites, multiple users share a frame and are typically grouped based on similar SINR. These grouped users are scheduled at the physical frame defined by the standard DVB-S2X [11]. Hence, as a possible extension of this work, the scheduling algorithms proposed in this thesis can be to be verified in muticast systems. The challenge now breaks down to two steps, firstly to group users that can share DVB XFECFRAME, and then to schedule these groups in time. Furthermore, following the demand driven approach, user demands can be considered both while grouping and user scheduling. Nevertheless, the challenge is to ensure that all the users sharing the XFECFRAME decode the frame correctly. Hence, the modulation and coding scheme will be selected based on the SINR of the weakest user. Therefore, users have to be carefully chosen considering both user demand and channel orthogonality.

5. **Radio resource optimization for LEO satellites:** The optimization techniques discussed in this thesis considers GEO satellites, which appears nearly stationary in the sky as seen by a ground stations or user terminals. However, dynamic low latency requirements (15 to 30 ms) for direct to handheld and cars, have pushed to advancements of LEO satellites. The radio resource optimization techniques discussed in this thesis are limited to GEO satellites and have to be updated with additional constraints for LEO satellites. For example, in beam design, we consider the satellite to be fixed and users to be mobile to design adaptive and dynamic beams. However, in LEO constellation, satellites, user terminals and hence beams move dynamically. Also, with more narrow beams and LEO user tracking features, unicast scheduling and beam placement techniques overlap. This will raise to multiple new challenges that have to be addressed

in future works.

6. **Non-Terrestrial-Networks(NTN) and 3GPP:** In the latest technical specification release of 3GPP (release 17), it is evident that satellites are making there way into terrestrial cellular communication ecosystem. With possible global coverage where terrestrial coverage is absent, NTN complements terrestrial networks in remote areas over sea and land. This has opened a new path of research opportunities, especially for direct-to-handheld concept of 3GPP NTN. Accordingly, the future works can include NTN radio resource optimization techniques for all the degrees of freedom which has to consider NTN associated propagation delays, Doppler effects and moving cells.

Bibliography

[1] E. Tweedie, "The broadcast market for satellite services." [Online]. Available: http://satellitemarkets.com/news-analysis/broadcast-market-satellite-services

[2] "Ads-b exchange - world's largest co-op of unfiltered flight data," 2021. [Online]. Available: https://www.adsbexchange.com/data/

[3] "Ais ship tracking of marine traffic," 2021. [Online]. Available: https://www.vesselfinder.com/.

[4] NASA, "Nasa, socioeconomic data and applications center (sedac)," 2021. [Online]. Available: http://sedac.ciesin.columbia.edu.

[5] H. Al-Hraishawi, E. Lagunas, and S. Chatzinotas, "Traffic simulator for multibeam satellite communication systems," in *2020 10th Advanced Satellite Multimedia Systems Conference and the 16th Signal Processing for Space Communications Workshop (ASMS/SPSC)*, 2020, pp. 1–8.

[6] V. Pascale, D. Maiarelli, L. D'Agristina, and N. Gatti, "Design and qualification of ku-band radiating chains for receive active array antenna of flexible telecommunication satellites," in *2019 13th European Conference on Antennas and Propagation (EuCAP)*, 2019, pp. 1–5.

[7] C. Forrester, "Ses adopts digital satellite payloads," Jun 2016. [Online]. Available: https://advanced-television.com/2016/06/29/ses-adopts-digital-satellite-payloads/

[8] M. Vázquez, A. Pérez-Neira, D. Christopoulos, S. Chatzinotas, B. Ottersten, P.-D. Arapoglou, A. Ginesi, and G. Taricco, "Precoding in multibeam satellite communications: Present and future challenges," *IEEE Wireless Communications*, vol. 23, no. 6, pp. 88–95, 2016.

[9] R. Cochetti, *Origins of Communications Satellite Technology.* John Wiley amp; Sons Inc, 2015.

[10] T. M. Braun and W. R. Braun, *End to end satellite communication systems.* Wiley-IEEE Press, 2022.

[11] ETSI, "Digital video broadcasting (dvb); second generation framing structure, channel coding and modulation systems for broadcasting, interactive services, news gathering and other broadband satellite applications; part 2: DVB-S2 extensions (DVB-S2X)," *Digital Video Broadcasting (DVB)*, vol. ETSI EN 302 307-2 V1.1.1, 2014-10. [Online]. Available: https://www.etsi.org/deliver/etsi_en/302300_302399/30230702/\01.01.01_20/en_30230702v010101a.pdf

[12] "Satellite frequency bands." [Online]. Available: https://www.esa.int/Applications/Telecommunications_Integrated_Applications/Satellite_frequency_bands

[13] "Us5550831a - tdma satellite communication system for transmitting serial subsignal data." [Online]. Available: https://patents.google.com/patent/US5550831A/en

[14] "Cn102916738b - data reliable multicast method based on fdma (frequency division multiple access)/dama (demand assigned multiple access) satellite communication system." [Online]. Available: https://patents.google.com/patent/CN102916738B/en

[15] K. S. Rao, M. Cuchanski, and M. Q. Tang, "Multiple beam antenna concepts for satellite communications," in *Symposium on Antenna Technology and Applied Electromagnetics [ANTEM 1994]*, C. . Ottawa, Ed., 1994, pp. 289–292.

[16] S. Rao, M. Tang, and C.-C. Hsu, "Multiple beam antenna technology for satellite communications payloads," *The Applied Computational Electromagnetics Society Journal (ACES)*, pp. 353–364, 2006.

[17] S. K. Rao, "Advanced antenna technologies for satellite communications payloads," *in IEEE Transactions on Antennas and Propagation*, vol. 63, no. 4, pp. 1205–1217, April 2015.

[18] "The state of broadband - international telecommunication union (itu): People-centred approaches for universal broadband," Sep 2021. [Online]. Available: https://www.itu.int/dms_pub/itu-s/opb/pol/S-POL-BROADBAND.19-2018-PDF-E.pdf

[19] "Revolve: Radio technologies for broadband connectivity in a rapidly evolving space ecosystem: Innovating agility, throughput, power, size and cost." [Online]. Available: https://ec.europa.eu/research/participants/documents/downloadPublic?documentIds=080166e5b87884ea&appId=PPGMS

[20] G. Zheng, S. Chatzinotas, and B. Ottersten, "Generic optimization of linear precoding in multibeam satellite systems," *IEEE Transactions on Wireless Communications*, vol. 11, no. 6, pp. 2308–2320, 2012.

[21] P. M. Arapoglou, A. Ginesi, S. Cioni, S. Erl, F. Clazzer, S. Andrenacci, and A. Vanelli-Coralli, "Dvb-s2x enabled precoding for high throughput satellite systems," *CoRR*, vol. abs/1504.03109, 2015. [Online]. Available: http://arxiv.org/abs/1504.03109

[22] K.-U. Storek, R. T. Schwarz, and A. Knopp, "Multi-satellite multi-user mimo precoding: Testbed and field trial," in *ICC 2020 - 2020 IEEE International Conference on Communications (ICC)*, 2020, pp. 1–7.

[23] P. Angeletti and R. De Gaudenzi, "A pragmatic approach to massive mimo for broadband communication satellites," *IEEE Access*, vol. 8, pp. 132 212–132 236, 2020.

[24] B. S. Mysore, E. Lagunas, S. Chatzinotas, and B. Ottersten, "Precoding for satellite communications: Why, how and what next?" *IEEE Communications Letters*, vol. 25, no. 8, pp. 2453–2457, 2021.

[25] W. Li, X. Huang, and H. Leung, "Performance evaluation of digital beamforming strategies for satellite communications," *IEEE Transactions on Aerospace and Electronic systems*, vol. 40, no. 1, pp. 12–26, 2004.

[26] P. Angeletti, G. Gallinaro, M. Lisi, and A. Vernucci, "On-ground digital beamforming techniques for satellite smart antennas," *Proc. 19th AIAA, Toulouse, France*, pp. 1–8, 2001.

[27] M. Barrett and F. Coromina, "Development and implementation of an adaptive digital beamforming network for satellite communication systems," in *1991 Sixth International Conference on Digital Processing of Signals in Communications*. IET, 1991, pp. 10–15.

[28] D. Sikri and R. M. Jayasuriya, "Multi-beam phased array with full digital beamforming for satcom and 5g," *5G Phased Array Technologies*, p. 30, 2019.

[29] N. Mazzali, M. R. Bhavani Shankar, and B. Ottersten, "On-board signal predistortion for digital transparent satellites," in *2015 IEEE 16th International Workshop on Signal Processing Advances in Wireless Communications (SPAWC)*, 2015, pp. 535–539.

[30] U. du Luxembourg, "Prosat: On-board processing techniques for high throughput satellites." [Online]. Available: https://wwwfr.uni.lu/snt/research/sigcom/projects/prosat_on_board_processing_techniques_for_high_throughput_satellites

[31] V. Sulli, F. Santucci, M. Faccio, and D. Giancristofaro, "Performance of satellite digital transparent processors through equivalent noise," *IEEE Transactions on Aerospace and Electronic Systems*, vol. 54, no. 6, pp. 2643–2661, 2018.

[32] O. Kodheli, E. Lagunas, N. Maturo, S. K. Sharma, B. Shankar, J. F. M. Montoya, J. C. M. Duncan, D. Spano, S. Chatzinotas, S. Kisseleff, J. Querol, L. Lei, T. X. Vu, and G. Goussetis, "Satellite communications in the new space era: A survey and future challenges," *IEEE Communications Surveys Tutorials*, vol. 23, no. 1, pp. 70–109, 2021.

[33] U. Park, H. W. Kim, D. S. Oh, and B. J. Ku, "Flexible bandwidth allocation scheme based on traffic demands and channel conditions for multi-beam satellite systems," in *2012 IEEE Vehicular Technology Conference (VTC Fall)*, 2012, pp. 1–5.

[34] U. Park, H. W. Kim, D. S. Oh, and B.-J. Ku, "A dynamic bandwidth allocation scheme for a multi-spot-beam satellite system," *Etri Journal*, vol. 34, no. 4, pp. 613–616, 2012.

[35] J. Ha, J.-u. Kim, and S.-H. Kim, "Performance analysis of dynamic spectrum allocation in heterogeneous wireless networks," *ETRI journal*, vol. 32, no. 2, pp. 292–301, 2010.

[36] T. S. Abdu, S. Kisseleff, E. Lagunas, and S. Chatzinotas, "Power and bandwidth minimization for demand-aware geo satellite systems," in *2021 IEEE Global Communications Conference (GLOBECOM)*, 2021, pp. 1–6.

[37] T. S. Abdu, E. Lagunas, S. Kisseleff, and S. Chatzinotas, "Carrier and power assignment for flexible broadband geo satellite communications system," in *2020 IEEE 31st Annual International Symposium on Personal, Indoor and Mobile Radio Communications*, 2020, pp. 1–7.

[38] P. Angeletti, D. Fernandez Prim, and R. Rinaldo, "Beam hopping in multi-beam broadband satellite systems: System performance and payload architecture analysis," in *24th AIAA International Communications Satellite Systems Conference*, 2006, p. 5376.

[39] J. Lei and M. A. Vazquez-Castro, "Multibeam satellite frequency/time duality study and capacity optimization," *Journal of Communications and Networks*, vol. 13, no. 5, pp. 472–480, 2011.

[40] L. Lei, E. Lagunas, Y. Yuan, M. G. Kibria, S. Chatzinotas, and B. Ottersten, "Beam illumination pattern design in satellite networks: Learning and optimization for efficient beam hopping," *IEEE Access*, vol. 8, pp. 136 655–136 667, 2020.

[41] X. Alberti, J. Cebrian, A. Del Bianco, Z. Katona, J. Lei, M. Vazquez-Castro, A. Zanus, L. Gilbert, and N. Alagha, "System capacity optimization in time and frequency for multibeam multi-media satellite systems," in *2010 5th Advanced Satellite Multimedia Systems Conference and the 11th Signal Processing for Space Communications Workshop*. IEEE, 2010, pp. 226–233.

[42] R. Alegre-Godoy, N. Alagha, and M. A. Vázquez-Castro, "Offered capacity optimization mechanisms for multi-beam satellite systems," in *2012 IEEE International Conference on Communications (ICC)*. IEEE, 2012, pp. 3180–3184.

[43] A. Destounis and A. D. Panagopoulos, "Dynamic power allocation for broadband multi-beam satellite communication networks," *IEEE Communications Letters*, vol. 15, no. 4, pp. 380–382, 2011.

[44] N. K. Srivastava and A. K. Chaturvedi, "Flexible and dynamic power allocation in broadband multi-beam satellites," *IEEE Communications Letters*, vol. 17, no. 9, pp. 1722–1725, 2013.

[45] F. R. Durand and T. AbrÃ£o, "Power allocation in multibeam satellites based on particle swarm optimization," *AEU - International Journal of Electronics and Communications*, vol. 78, pp. 124–133, 2017. [Online]. Available: https://www.sciencedirect.com/science/article/pii/S1434841116303739

[46] J. P. Choi and V. W. Chan, "Optimum power and beam allocation based on traffic demands and channel conditions over satellite downlinks," *IEEE Transactions on Wireless Communications*, vol. 4, no. 6, pp. 2983–2993, 2005.

[47] J. Lei and M. A. Vazquez-Castro, "Joint power and carrier allocation for the multibeam satellite downlink with individual sinr constraints," in *2010 IEEE International Conference on Communications*. IEEE, 2010, pp. 1–5.

[48] H. Chaker, H. Chougrani, W. A. Martins, S. Chatzinotas, and J. Grotz, "Matching traffic demand in geo multibeam satellites: The joint use of dynamic beamforming and precoding under practical constraints," *IEEE Transactions on Broadcasting*, pp. 1–15, 2022.

[49] C. P. Niebla, C. Kissling, and E. Lutz, "Design and performance evaluation of efficient scheduling techniques for second generation dvb-s systems," 2005.

[50] M. Tropea, F. Veltri, F. De Rango, A.-F. Santamaria, and L. Belcastro, "Two step based qos scheduler for dvb-s2 satellite system," in *2011 IEEE International Conference on Communications (ICC)*, 2011, pp. 1–5.

[51] E. Rendon-Morales, J. Mata-Díaz, J. Alins, J. L. Muñoz, and O. Esparza, "Adaptive packet scheduling for the support of qos over dvb-s2 satellite systems," in *Wired/Wireless Internet Communications*, X. Masip-Bruin, D. Verchere, V. Tsaoussidis, and M. Yannuzzi, Eds. Berlin, Heidelberg: Springer Berlin Heidelberg, 2011, pp. 15–26.

[52] L. Cottatellucci, M. Debbah, G. Gallinaro, R. Müller, M. Neri, and R. Rinaldo, "Interference mitigation techniques for broadband satellite systems," *24th AIAA International Communications Satellite Systems Conference (ICSSC), San Diego (California), USA*, pp. 11–14, June 2006.

[53] Y. Couble, C. Rosenberg, E. Chaput, J.-B. Dupé, C. Baudoin, and A.-L. Beylot, "Two-color scheme for a multi-beam satellite return link: Impact of interference coordination," *IEEE Journal on Selected Areas in Communications*, vol. 36, no. 5, pp. 993–1003, 2018.

[54] O. Kilic and A. I. Zaghloul, "Interference in cellular satellite systems," in *Satellite Communications*, N. Diodato, Ed. Rijeka: IntechOpen, 2010, ch. 15. [Online]. Available: https://doi.org/10.5772/9997

[55] A. Mehrotra, "Cellular radio performance engineering," Boston, 1994.

[56] E. Lier and D. Purdy, "Techniques to maximize communication traffic capacity in multi-beam satellite active phased array antennas for non-uniform traffic model," in *Proceedings 2000 IEEE International Conference on Phased Array Systems and Technology (Cat. No.00TH8510)*, 2000, pp. 505–508.

[57] "Satellite traffic emulator," *SnT, University of Luxembourg*, 2021. [Online]. Available: https://wwwfr.uni.lu/snt/research/sigcom/\sw_simulators/satellite_traffic_emulator

[58] R. De Gaudenzi, M. Luise, and L. Sanguinetti, "The open challenge of integrating satellites into (beyond-) 5g cellular networks," *IEEE Network*, vol. 36, no. 2, pp. 168–174, 2022.

[59] F. Vidal, H. Legay, G. Goussetis, M. Vigueras, S. Tubau, and J. Gayrard, "A methodology to benchmark flexible payload architectures in a megaconstellation use case," *International Journal of Satellite Communications and Networking*, vol. 39, 03 2020.

[60] L. Chen, E. Lagunas, S. Chatzinotas, and B. Ottersten, "Satellite broadband capacity-on-demand: Dynamic beam illumination with selective precoding," in *2021 29th European Signal Processing Conference (EUSIPCO)*, 2021, pp. 900–904.

[61] Z. Lin, Z. Ni, L. Kuang, C. Jiang, and Z. Huang, "Dynamic beam pattern and bandwidth allocation based on multi-agent deep reinforcement learning for beam hopping satellite systems," *IEEE Transactions on Vehicular Technology*, vol. 71, no. 4, pp. 3917–3930, 2022.

[62] F. G. Ortiz-Gomez, L. Lei, E. Lagunas, R. Martinez, D. Tarchi, J. Querol, M. A. Salas-Natera, and S. Chatzinotas, "Machine learning for radio resource management in multibeam geo satellite systems," *Electronics*, vol. 11, no. 7, 2022. [Online]. Available: https://www.mdpi.com/2079-9292/11/7/992

[63] T. S. Abdu, S. Kisseleff, E. Lagunas, and S. Chatzinotas, "Flexible resource optimization for geo multibeam satellite communication system," *IEEE Transactions on Wireless Communications*, vol. 20, no. 12, pp. 7888–7902, 2021.

[64] G. Cocco, T. de Cola, M. Angelone, Z. Katona, and S. Erl, "Radio Resource Management Optimization of Flexible Satellite Payloads for DVB-S2 Systems," *IEEE Transactions on Broadcasting*, vol. 64, no. 2, pp. 266–280, Jun. 2018.

[65] A. Freedman, D. Rainish, and Y. Gat, "Beam Hopping – How To Make it Possible," in *Proc. of Ka and Broadband Communication Conference*, Oct. 2015.

[66] C. N. Efrem and A. D. Panagopoulos, "Dynamic Energy-Efficient Power Allocation in Multibeam Satellite Systems," *IEEE Wireless Communications Letters*, vol. 9, no. 2, pp. 228–231, 2020.

[67] A. I. Aravanis, B. Shankar M. R., P. Arapoglou, G. Danoy, P. G. Cottis, and B. Ottersten, "Power Allocation in Multibeam Satellite Systems: A Two-Stage Multi-Objective Optimization," *IEEE Transactions on Wireless Communications*, vol. 14, no. 6, pp. 3171–3182, June 2015.

[68] P. Angeletti and J. Lizarraga Cubillos, "Traffic balancing multibeam antennas for communication satellites," *IEEE Transactions on Antennas and Propagation*, vol. 69, no. 12, pp. 8291–8303, 2021.

[69] R. De Gaudenzi, P. Angeletti, D. Petrolati, and E. Re, "Future technologies for very high throughput satellite systems," *International Journal of Satellite Communications and Networking*, vol. 38, no. 2, pp. 141–161, 2020. [Online]. Available: https://onlinelibrary.wiley.com/doi/abs/10.1002/sat.1327

[70] G. Toso, P. Angeletti, and C. Mangenot, "Multibeam antennas based on phased arrays: An overview on recent esa developments," in *The 8th European Conference on Antennas and Propagation (EuCAP 2014)*, 2014, pp. 178–181.

[71] G. Gallinaro, G. Caire, M. Debbah, L. Cottatellucci, R. Mueller, and R. Rinaldo, "Perspectives of adopting inteference mitigation techniques in the context of broadband multimedia satellite systems," in *Proc. ICSC*. Citeseer, 2005.

[72] M. Schneider, C. Hartwanger, and H. Wolf, "Antennas for Multiple Spot Beam Satellites," *CEAS Space Journal*, vol. 2, pp. 59–66, Aug. 2011.

[73] C. Leclerc, M. Romier, A. Annabi, and H. Aubert, "Ka-band multiple feed per beam antenna architecture based on interleaved 3-d directional couplers," in *2013 IEEE-APS Topical Conference on Antennas and Propagation in Wireless Communications (APWC)*, 2013, pp. 367–369.

[74] P. Bosshard *et al.*, "Space HTS/V-HTS Multiple Beam Antennas sub-systems on the right track," *Proc. European Conference on Antennas and Propag. (EuCAP), Davos, Switzerland*, vol. 2, pp. 1–5, 2016.

[75] W. M. Abdel-Wahab, H. Al-Saedi, M. Raeis-Zadeh, E. H. Mirza Alian, A. Ehsandar, G. Chen, A. Palizban, N. Ghafarian, H. El-Sawaf, M. R. Nezhad-Ahmadi, and S. Safavi Naeini, "Affordable large scale active-phased array antenna for ka-band mobile satcom applications," in *2019 13th European Conference on Antennas and Propagation (EuCAP)*, 2019, pp. 1–4.

[76] M. Cooley, "Phased Array-Fed Reflector (PAFR) Antenna Architectures for Space-Based Sensors ," *IEEE Aerospace Conference*, pp. 1–11, 2015.

[77] J. Liu, M. Sheng, L. Liu, and J. Li, "Network densification in 5g: From the short-range communications perspective," *IEEE Communications Magazine*, vol. 55, no. 12, pp. 96–102, 2017.

[78] D. López-Pérez, M. Ding, H. Claussen, and A. H. Jafari, "Towards 1 Gbps/UE in Cellular Systems: Understanding Ultra-Dense Small Cell Deployments," *IEEE Communications Surveys Tutorials*, vol. 17, no. 4, pp. 2078–2101, 2015.

[79] J. Hoadley and P. Maveddat, "Enabling small cell deployment with hetnet," *IEEE Wireless Communications*, vol. 19, no. 2, pp. 4–5, 2012.

[80] N. Bhushan, J. Li, D. Malladi, R. Gilmore, D. Brenner, A. Damnjanovic, R. T. Sukhavasi, C. Patel, and S. Geirhofer, "Network densification: the dominant theme for wireless evolution into 5g," *IEEE Communications Magazine*, vol. 52, no. 2, pp. 82–89, 2014.

[81] S. Seewald and D. Manteuffel, "Design approach for modular millimeter wave beamforming antenna arrays for 5g pico-cells," in *2019 IEEE-APS Topical Conference on Antennas and Propagation in Wireless Communications (APWC)*, 2019, pp. 174–177.

[82] W.-S. Chen and H.-J. Lin, "Dual-polarization slot antenna array with resonant cavities for small-cell base station applications," in *2015 IEEE 4th Asia-Pacific Conference on Antennas and Propagation (APCAP)*, 2015, pp. 58–59.

[83] Z. N. Chen, X. Qing, X. Tang, W. E. Liu, and R. Xu, "Phased array metantennas for satellite communications," *IEEE Communications Magazine*, vol. 60, no. 1, pp. 46–50, 2022.

[84] P. J. Honnaiah, N. Maturo, S. Chatzinotas, S. Kisseleff, and J. Krause, "Demand-based adaptive multi-beam pattern and footprint planning for high throughput GEO satellite systems," *IEEE Open Journal of the Communications Society*, vol. 2, pp. 1526–1540, 2021.

[85] H. Chaker, N. Maturo, S. Chatzinotas, H. Chougrani, W. A. Martins, and J. Grotz, "Enablers for matching demand in geo multi-beam satellites: dynamic beamforming, precoding, or both?" in *38th International Communications Satellite Systems Conference (ICSSC 2021)*, vol. 2021, 2021, pp. 104–111.

[86] A. Guidotti and A. Vanelli-Coralli, "Design trade-off analysis of precoding multi-beam satellite communication systems," in *2021 IEEE Aerospace Conference (50100)*, 2021, pp. 1–12.

[87] S. Kisseleff, E. Lagunas, J. Krivochiza, J. Querol, N. Maturo, L. Martinez Marrero, J. C. Merlano Duncan, and S. Chatzinotas, "Centralized gateway concept for precoded multi-beam GEO satellite networks," in *VTC2021-Fall Workshop on Evolution of Non-Terrestrial Networks Toward 6G,*, 2021.

[88] A. I. Perez-Neira, M. A. Vazquez, M. B. Shankar, S. Maleki, and S. Chatzinotas, "Signal processing for high-throughput satellites: Challenges in new interference-limited scenarios," *IEEE Signal Processing Magazine*, vol. 36, no. 4, pp. 112–131, 2019.

[89] J. Krivochiza, J. C. M. Duncan, J. Querol, N. Maturo, L. M. Marrero, S. Andrenacci, J. Krause, and S. Chatzinotas, "End-to-end precoding validation over a live GEO satellite forward link," *IEEE Access*, pp. 1–1, 2021.

[90] T. Iguchi, D. G. Mixon, J. Peterson, and S. Villar, "On the tightness of an SDP relaxation of k-means," *CoRR*, vol. abs/1505.04778, 2015. [Online]. Available: http://arxiv.org/abs/1505.04778

[91] Q. Du, V. Faber, and M. Gunzburger, "Centroidal voronoi tessellations: Applications and algorithms," *SIAM Review*, vol. 41, no. 4, pp. 637–676, Jan. 1999. [Online]. Available: https://doi.org/10.1137/s0036144599352836

[92] P. J. Rousseeuw, "Silhouettes: A graphical aid to the interpretation and validation of cluster analysis," *Journal of Computational and Applied Mathematics*, vol. 20, pp. 53–65, Nov. 1987. [Online]. Available: https://doi.org/10.1016/0377-0427(87)90125-7

[93] R. Tibshirani, G. Walther, and T. Hastie, "Estimating the number of clusters in a data set via the gap statistic," *Journal of the Royal Statistical Society: Series B (Statistical Methodology)*, vol. 63, no. 2, pp. 411–423, 2001. [Online]. Available: https://doi.org/10.1111/1467-9868.00293

[94] D. L. Davies and D. W. Bouldin, "A cluster separation measure," *IEEE Transactions on Pattern Analysis and Machine Intelligence*, vol. PAMI-1, no. 2, pp. 224–227, 1979.

[95] S. Maher, M. Miltenberger, J. P. Pedroso, D. Rehfeldt, R. Schwarz, and F. Serrano, "PySCIPOpt: Mathematical programming in python with the SCIP optimization suite," in *Mathematical Software – ICMS 2016*. Springer International Publishing, 2016, pp. 301–307.

[96] K. Bestuzheva, M. Besançon, W.-K. Chen, A. Chmiela, T. Donkiewicz, J. van Doornmalen, L. Eifler, O. Gaul, G. Gamrath, A. Gleixner, L. Gottwald, C. Graczyk, K. Halbig, A. Hoen, C. Hojny, R. van der Hulst, T. Koch, M. Lübbecke, S. J. Maher, F. Matter, E. Mühmer, B. Müller, M. E. Pfetsch, D. Rehfeldt, S. Schlein, F. Schlösser, F. Serrano, Y. Shinano, B. Sofranac, M. Turner, S. Vigerske, F. Wegscheider, P. Wellner, D. Weninger, and J. Witzig, "The SCIP Optimization Suite 8.0," Optimization Online, Technical Report, December 2021. [Online]. Available: http://www.optimization-online.org/DB_HTML/2021/12/8728.html

[97] "Esa cgd - prototype of a centralized broadband gateway for precoded multi-beam networks," *SnT, University of Luxembourg*, 2021. [Online]. Available: https://wwwfr.uni.lu/snt/research/sigcom/projects/esa_cgd

[98] A. Kyrgiazos, B. Evans, P. Thompson, P. T. Mathiopoulos, and S. Papaharalabos, "A terabit/second satellite system for european broadband access: a feasibility study," *International Journal of Satellite Communications and Networking*, vol. 32, no. 2, pp. 63–92, 2014. [Online]. Available: https://onlinelibrary.wiley.com/doi/abs/10.1002/sat.1067

[99] M. Gerard, M. Bousquet, and Z. Sun, *Satellite communications systems: Systems, Techniques and Technology.* John Wiley amp; Sons, Inc., 2020.

[100] D. Digdarsini, M. Kumar, and T. V. S. Ram, "Design hardware realization of fpga based digital beam forming system," in *2016 3rd International Conference on Signal Processing and Integrated Networks (SPIN).* Noida, 2016, pp. 275–278.

[101] C. Balanis, *Antenna Theory : Analysis and Design*, 4th ed., 2016.

[102] K. Y. Jo, *Satellite Communications Network Design and Analysis.* Artech House, 2011.

[103] Y. Su, Y. Liu, Y. Zhou, J. Yuan, H. Cao, and J. Shi, "Broadband leo satellite communications: Architectures and key technologies," *IEEE Wireless Communications*, vol. 26, no. 2, pp. 55–61, April 2019.

[104] M. Takahashi, Y. Kawamoto, N. Kato, A. Miura, and M. Toyoshima, ""adaptive power resource allocation with multi-beam directivity control in high-throughput satellite communication systems,"," *IEEE Wireless Communications Letters*, vol. 8, no. 4, pp. 1248–1251, August 2019.

[105] S. Tani, K. Motoyoshi, H. Sano, A. Okamura, H. Nishiyama, and N. Kato, ""an adaptive beam control technique for q band satellite to maximize diversity gain and mitigate interference to terrestrial networks,"," *IEEE Transactions on Emerging Topics in Computing*, vol. 7, no. 1, p. 1, 2019.

[106] S. Kisseleff, M. R. B. Shankar, D. Spano, and J. D. Gayrard, ""a new optimization tool for mega-constellation design and its application to trunking systems."," in *37th*

International Communications Satellite Systems Conference (ICSSC). Japan, October 2019.

[107] M. Takahashi, Y. Kawamoto, N. Kato, A. Miura, and M. Toyoshima, "Adaptive multi-beam arrangement for improving throughput in an hts communication system," *ICC - 2020 IEEE International Conference on Communications (ICC), Dublin, Ireland*, vol. 2020, pp. 1–6, 2020.

[108] D. Christopoulos, S. Chatzinotas, G. Zheng, J. Grotz, and B. Ottersten, "Linear and nonlinear techniques for multibeam joint processing in satellite communications," *EURASIP Journal of Wireless Communications and Networking*, p. 1–13, 2012.

[109] C. A. Siocos, "Broadcasting-satellite coverage-geometrical considerations," *IEEE Transactions on Broadcasting*, vol. 19, no. 4, pp. 84–87, December 1973.

[110] M. A. Diaz, N. Courville, C. Mosquera, G. Liva, and G. E. Corazza, "Non-linear interference mitigation for broadband multimedia satellite systems," in *2007 International Workshop on Satellite and Space Communications*. Salzburg, 2007, pp. 61–65.

[111] "Flexpredem - demonstrator of precoding techniques for flexible broadband systems," *Activity Code: 3C.014*. [Online]. Available: https://artes.esa.int/projects/flexpredem

[112] G. Taricco and A. Ginesi, "Precoding for flexible high throughput satellites: Hot-spot scenario," *in IEEE Transactions on Broadcasting*, vol. 65, no. 1, pp. 65–72, March 2019.

[113] J. Duncan, J. Krivochiza, S. Andrenacci, S. Chatzinotas, and B. Ottersten, "Hardware demonstration of precoded communications in multi-beam UHTS systems," in *36th International Communications Satellite Systems Conference (ICSSC 2018)*, 2018, pp. 1–5.

[114] M. G. Kibria, E. Lagunas, N. Maturo, D. Spano, and S. Chatzinotas, "Precoded cluster hopping in multibeam high throughput satellite systems," *IEEE Global Communications Conference (GLOBECOM), Waikoloa, HI, USA*, pp. 1–6, 2019.

[115] C. Wu, E. Kamar, and E. Horvitz, "Clustering for set partitioning: A case study in carpooling," in *In Proceedings of the Workshop on Optimization for Machine Learning (OPT) at NIPS 2015.*, May 2015. [Online]. Available: https://www.microsoft.com/en-us/research/publication/clustering-set-partitioning-case-study-carpooling/

[116] R. M. Karp, "Reducibility among combinatorial problems," *In: Miller R.E., Thatcher J.W., Bohlinger J.D. (eds) Complexity of Computer Computations, The IBM Research Symposia Series. Springer, Boston, MA*.

[117] M. W. Padberg, "On the facial structure of set packing polyhedra," *Mathematical Programming 5*, vol. 199–215, 1973.

[118] X. Gandibleux, X. Delorme, and V. TKindt, *An ant colony optimisation algorithm for the set packing problem.* pages 49–60. Springer: In Ant Colony Optimization and Swarm Intelligence, 2004.

[119] L. Kaufman and P. J. Rousseeuw, *Finding Groups in Data : an Introduction to Cluster Analysis.* Wiley Interscience, 2005.

[120] "Relax, no need to round: integrality of clustering formulations," *Theoretical Computer Science (ITCS) conference*, 2015.

[121] W. V. Parker and J. E. Pryor, "Polygons of greatest area inscribed in an ellipse." *The American Mathematical Monthly*, vol. 51, p. 205–209, 1944.

[122] T. Wigren, "A polygon to ellipse transformation enabling fingerprinting and emergency localization in gsm," *in IEEE Transactions on Vehicular Technology*, vol. 60, no. 4, pp. 1971–1976, May 2011.

[123] D. Eberly, *Geometric Tools.* [Online]. Available: https://www.geometrictools.com/Documentation/InformationAboutEllipses.pdf

[124] H. Al-Hraishawi, E. Lagunas, and S. Chatzinotas, *"Traffic Simulator for Broadband Satellite Communication Systems".* ASMS/SPSC Virtual Conference, 2020.

[125] E. W. Weisstein, *Spherical Coordinates*, MathWorld-A Wolfram Web Resource. [Online]. Available: https://mathworld.wolfram.com/SphericalCoordinates.html

[126] U. Fayyad and R. Uthurusamy, ""data mining and knowledge discovery in databases.","
Communications of the ACM, vol. 39, p. 24–26, 1996.

[127] D. Xu and Y. Tian, "A comprehensive survey of clustering algorithms," *Annals of Data Science*, vol. 2, no. 2, pp. 165–193, Jun. 2015. [Online]. Available: https://doi.org/10.1007/s40745-015-0040-1

[128] S. Lloyd, "Least squares quantization in PCM," *IEEE Transactions on Information Theory*, vol. 28, no. 2, pp. 129–137, Mar. 1982. [Online]. Available: https://doi.org/10.1109/tit.1982.1056489

[129] D. Arthur and S. Vassilvitskii, "K-means++: The advantages of careful seeding," in *Proceedings of the Eighteenth Annual ACM-SIAM Symposium on Discrete Algorithms*, ser. SODA '07. USA: Society for Industrial and Applied Mathematics, 2007, p. 1027–1035.

[130] R. Apu and M. Gavrilova, *Generalized Voronoi Diagram: A Geometry-Based Approach to Computational Intelligence*. Berlin, Germany: Springer, pp. 109-129, 2009, vol. 158.

[131] D. Reem, "An algorithm for computing voronoi diagrams of general generators in general normed spaces," in *2009 Sixth International Symposium on Voronoi Diagrams*. Copenhagen, 2009, pp. 144–152.

[132] E. W. Weisstein, *Ellipse*, MathWorld-A Wolfram Web Resource. [Online]. Available: https://mathworld.wolfram.com/Ellipse.html

[133] N. Nawri, *Berechnung von Kovarianzellipsen, Web Resource*, [Online]. Available. [Online]. Available: http://imkbemu.physik.uni-karlsruhe.de/~eisatlas/covariance_ellipses.pdf

[134] R. Jain, D. Chiu, and W. R. Hawe, "A quantitative measure of fairness and discrimination for resource allocation in shared computer system,"," in *Eastern Research Laboratory, Digital Equipment Corporation*, 1984.

[135] "Ads-b exchange - world's largest co-op of unfiltered flight data," November 2020. [Online]. Available: https://www.adsbexchange.com/data/

[136] "Ais ship tracking of marine traffic," November 2020. [Online]. Available: https://www.vesselfinder.com/

[137] "Nasa, "nasa, socioeconomic data and applications center (sedac)," November 2020. [Online]. Available: http://sedac.ciesin.columbia.edu

[138] X. Artiga and M. A. Vazquez, ""effects of channel phase in multibeam multicast satellite precoding systems"," in *37th International Communications Satellite Systems Conference (ICSSC)*. Japan: November Okinawa, 2019, pp. 28–1.

[139] S. Kisseleff, E. Lagunas, T. S. Abdu, S. Chatzinotas, and B. Ottersten, "Radio resource management techniques for multibeam satellite systems," *in IEEE Communications Letters*.

[140] G. W. W. C. Swannack E. Uysal-Biyikoglu, "Low complexity multiuser scheduling for maximizing throughput in the mimo broadcast channel," in *Annual Allerton Conference on Communication, Control, and Computing*, October 2004.

[141] A. Bandi, M. R. B. Shankar, S. Chatzinotas, and B. Ottersten, "Joint user grouping, scheduling, and precoding for multicast energy efficiency in multigroup multicast systems," *IEEE Transactions on Wireless Communications*, vol. 19, no. 12, pp. 8195–8210, 2020.

[142] A. Bandi, B. S. Mysore R., S. Chatzinotas, and B. Ottersten, "Joint scheduling and precoding for frame-based multigroup multicasting in satellite communications," in *2019 IEEE Global Communications Conference (GLOBECOM)*, 2019, pp. 1–6.

[143] T. Yoo and A. Goldsmith, "On the optimality of multi-antenna broadcast scheduling using zero-forcing beamforming," *IEEE J. Sel. Areas Commun, 24(3)*, March 2006.

[144] D. Christopoulos, S. Chatzinotas, and B. Ottersten, "Multicast multigroup precoding and user scheduling for frame-based satellite communications," *IEEE Trans. Wireless Commun*, vol. 14, p. 9, September 2015.

[145] E. Lagunas, S. Andrenacci, S. Chatzinotas, and B. Ottersten, "Cross-layer forward packet scheduling for emerging precoded broadband multibeam satellite system," in *2018 9th Advanced Satellite Multimedia Systems Conference and the 15th Signal Processing for Space Communications Workshop (ASMS/SPSC)*, 2018, pp. 1–8.

[146] A. Guidotti and A. Vanelli-Coralli, "Geographical scheduling for multicast precoding in multi-beam satellite systems," in *2018 9th Advanced Satellite Multimedia Systems Conference and the 15th Signal Processing for Space Communications Workshop (ASMS/SPSC)*, 2018, pp. 1–8.

[147] ——, *Geographical Scheduling for Multicast Precoding in multibeam Satellite Systems*. ASMS/SPSC, 2018.

[148] V. Joroughi, M. A. Vázquez, and A. I. Pérez-Neira, "Generalized multicast multibeam precoding for satellite communications," *IEEE Transactions on Wireless Communications*, vol. 16, no. 2, pp. 952–966, 2016.

[149] E. Lagunas, M. Kibria, H. Al-Hraishawi, N. Maturo, and S. Chatzinotas, *"Dealing with Non-Uniform Demands in Flexible GEO Satellites: The Carrier Aggregation Perspectives"*. ASMS/SPSC Virtual Conference, 2020.

[150] C. Peel, B. Hochwald, and A. Swindlehurst, "vector-perturbation technique for near-capacity multiantenna multiuser communication—part i: Channel inversion and regularization,"," in *IEEE Transactions on Communications*. no. 1, pp. 195–202: vol. 53, January 2005.

[151] T. M. Braun and W. R. Braun, *Chapter in Book: HIGH-THROUGHPUT SATELLITES*, 2021, pp. 530–549.

[152] R. De Gaudenzi, P. Angeletti, D. Petrolati, and E. Re, "Future technologies for very high throughput satellite systems," *International Journal of Satellite Communications and Networking*, vol. 38, no. 2, pp. 141–161, 2020. [Online]. Available: https://onlinelibrary.wiley.com/doi/abs/10.1002/sat.1327

[153] P. Zetterberg and B. Ottersten, "The spectrum efficiency of a base station antenna array system for spatially selective transmission," in *Proceedings of IEEE Vehicular Technology Conference (VTC)*, 1994, pp. 1517–1521 vol.3.

[154] M. Á. Vázquez, A. Perez-Neira, D. Christopoulos, S. Chatzinotas, B. Ottersten, P.-D. Arapoglou, A. Ginesi, and G. Taricco, "Precoding in multibeam satellite communications: Present and future challenges," *IEEE Wireless Communications*, vol. 23, no. 6, pp. 88–95, 2016.

[155] E. Björnson, M. Bengtsson, and B. Ottersten, "Optimal multiuser transmit beamforming: A difficult problem with a simple solution structure [lecture notes]," *IEEE Signal Processing Magazine*, vol. 31, no. 4, pp. 142–148, 2014.

[156] M. Haardt, V. Stankovic, and G. Del Galdo, "Efficient multi-user mimo downlink precoding and scheduling," in *1st IEEE International Workshop on Computational Advances in Multi-Sensor Adaptive Processing, 2005.*, 2005, pp. 237–240.

[157] Y. D. Zhang and K. D. Pham, "Joint precoding and scheduling optimization in downlink multicell satellite communications," in *2020 54th Asilomar Conference on Signals, Systems, and Computers*, 2020, pp. 480–484.

[158] A. Bandi, B. Shankar M. R, S. Chatzinotas, and B. Ottersten, "A joint solution for scheduling and precoding in multiuser MISO downlink channels," *IEEE Transactions on Wireless Communications*, vol. 19, no. 1, pp. 475–490, 2020.

[159] T. Forum, "Sla management handbook," *Public Evaluation*, vol. Version 1.5, 2001. [Online]. Available: https://silo.tips/download/SLA-management-handbook#

[160] V. Joroughi, E. Lagunas, S. Andrenacci, N. Maturo, S. Chatzinotas, J. Grotz, and B. Ottersten, "Deploying joint beam hopping and precoding in multibeam satellite networks with time variant traffic," in *2018 IEEE Global Conference on Signal and Information Processing (GlobalSIP)*, 2018, pp. 1081–1085.

[161] M. Costa, "Writing on dirty paper (corresp.)," *IEEE Transactions on Information Theory*, vol. 29, no. 3, pp. 439–441, 1983.

[162] F. Boccardi and H. Huang, "Zero-forcing precoding for the MIMO broadcast channel under per-antenna power constraints," in *2006 IEEE 7th Workshop on Signal Processing Advances in Wireless Communications*, 2006, pp. 1–5.

[163] M. Joham, W. Utschick, and J. A. Nossek, "Linear transmit processing in MIMO communications systems," *IEEE Transactions on signal Processing*, vol. 53, no. 8, pp. 2700–2712, 2005.

[164] O. Simeone, U. Spagnolini, and Y. Bar-Ness, "Linear and non-linear precoding/decoding for mimo systems using the fading correlation at the transmitter," in *2003 4th IEEE Workshop on Signal Processing Advances in Wireless Communications-SPAWC 2003 (IEEE Cat. No. 03EX689)*. IEEE, 2003, pp. 6–10.

[165] Y. Chen, "Low complexity precoding schemes for massive MIMO systems," Ph.D. dissertation, Newcastle University, 2019.

[166] Y. Liu, J. Liu, Q. Wu, Y. Zhang, and M. Jin, "A near-optimal iterative linear precoding with low complexity for massive MIMO systems," *IEEE Communications Letters*, vol. 23, no. 6, pp. 1105–1108, 2019.

[167] X. Qiang, Y. Liu, Q. Feng, J. Liu, X. Ren, and M. Jin, "Approximative matrix inversion based linear precoding for massive MIMO systems," in *2020 International Conference on Computing, Networking and Communications (ICNC)*. IEEE, 2020, pp. 950–955.

[168] T. K. Lyu, "Capacity of multi-user MIMO systems with mmse and zf precoding," in *2016 IEEE Conference on Computer Communications Workshops (INFOCOM WKSHPS)*, 2016, pp. 1083–1084.

[169] "Predem - precoding demonstrator for broadband system forward links," *Activity Code: 14.1TT.60*. [Online]. Available: https://artes.esa.int/projects/predem

[170] W. Wang, A. Liu, Q. Zhang, L. You, X. Gao, and G. Zheng, "Robust multigroup multicast transmission for frame-based multi-beam satellite systems," *IEEE Access*, vol. 6, pp. 46 074–46 083, 2018.

[171] M. Vázquez, M. R. B. Shankar, C. I. Kourogiorgas, P.-D. Arapoglou, V. Icolari, S. Chatzinotas, A. D. Panagopoulos, and A. I. Pérez-Neira, "Precoding, scheduling, and link adaptation in mobile interactive multibeam satellite systems," *IEEE Journal on Selected Areas in Communications*, vol. 36, no. 5, pp. 971–980, 2018.

[172] E. Castañeda, A. Silva, A. Gameiro, and M. Kountouris, "An overview on resource allocation techniques for multi-user MIMO systems," *IEEE Communications Surveys Tutorials*, vol. 19, no. 1, pp. 239–284, 2017.

[173] G. Taricco, "Linear precoding methods for multi-beam broadband satellite systems," in *European Wireless 2014; 20th European Wireless Conference*, 2014, pp. 1–6.

[174] Z. Sha, Z. Wang, S. Chen, and L. Hanzo, "Graph theory based beam scheduling for inter-cell interference avoidance in mmwave cellular networks," *IEEE Transactions on Vehicular Technology*, vol. 69, no. 4, pp. 3929–3942, 2020.

[175] S. Dimitrov, S. Erl, B. Barth, S. Jaeckel, A. Kyrgiazos, and B. G. Evans, "Radio resource management techniques for high throughput satellite communication systems," in *2015 European Conference on Networks and Communications (EuCNC)*. IEEE, 2015, pp. 175–179.

[176] S. Zhang, M. Jia, Y. Wei, and Q. Guo, "User scheduling for multicast transmission in high throughput satellite systems," *EURASIP Journal on Wireless*

Communications and Networking, vol. 2020, no. 1, p. 133, Jun 2020. [Online]. Available: https://doi.org/10.1186/s13638-020-01749-7

[177] T. Yoo and A. Goldsmith, "On the optimality of multiantenna broadcast scheduling using zero-forcing beamforming," *IEEE Journal on Selected Areas in Communications*, vol. 24, no. 3, pp. 528–541, 2006.

[178] "SES and Thales Unveil Next Generation Capabilities On-Board SES-17, April 2017," https://www.ses.com/press-release/ses-and-thales-unveil-next-generation-capabilities-onboard-ses-17, accessed: 2020-02.

[179] "EUTELSAT 172b Satellite: On the Road to Kourou, March 2017," https://news.eutelsat.com/pressreleases/eutelsat-172b-satellite-on-the-road-to-kourou-1857558, accessed: 2019-12.

[180] H. Han, X. Zheng, Q. Huang *et al.*, "QoS-equilibrium slot allocation for beam hopping in broadband satellite communication systems," *SPRINGER Wireless Networks*, vol. 21, pp. 2617–2630, 2015.

[181] M. Vázquez and A. I. Pérez-Neira, "Spectral clustering for beam-free satellite communications," in *2018 IEEE Global Conference on Signal and Information Processing (GlobalSIP)*, 2018, pp. 1030–1034.

[182] M. ApS, *The MOSEK optimization toolbox for MATLAB manual. Version 9.0.*, 2019. [Online]. Available: http://docs.mosek.com/9.0/toolbox/index.html

[183] T. M. integer Conic Optimizer in MOSEK, *23rd International Symposium on Mathematical Programming*, 2021. [Online]. Available: https://docs.mosek.com/slides/2018/ismp2018/ismp-wiese.pdf

[184] M. Cookbook, *Mixed integer optimization*, 2021. [Online]. Available: https://docs.mosek.com/modeling-cookbook/mio.html

[185] X. Song, L. Qin, Y. Ni, and Z. Xie, "A user-qoe aware scheduling scheme in hetnets," in *2018 3rd International Conference on Mechanical, Control and Computer Engineering (ICMCCE)*, 2018, pp. 599–602.

[186] P. J. Honnaiah, E. Lagunas, D. Spano, N. Maturo, and S. Chatzinotas, "Demand-based scheduling for precoded multibeam high-throughput satellite systems," in *2021 IEEE Wireless Communications and Networking Conference (WCNC)*, 2021, pp. 1–6.

[187] D. Digdarsini, M. Kumar, and T. Ram, "Design amp; hardware realization of fpga based digital beam forming system," in *2016 3rd International Conference on Signal Processing and Integrated Networks (SPIN)*, 2016, pp. 275–278.

[188] E. W. Weisstein. Polygon to ellipse approximation, MathWorld: A Wolfram Web Resource. [Online]. Available: https://mathworld.wolfram.com/Ellipse.html

[189] F. Ortiz, E. Lagunas, and S. Chatzinotas, "Unsupervised learning for user scheduling in multibeam precoded geo satellite systems," in *2022 Joint European Conference on Networks and Communications 6G Summit (EuCNC/6G Summit)*, 2022, pp. 190–195.

[190] T. Abdu, S. Kisseleff, L. Lei, E. Lagunas, J. Grotz, and S. Chatzinotas, "A deep learning based acceleration of complex satellite resource management problem," 08 2022.